TSPE16900-077-13

극지 미생물유래 분해 효소를 이용한 퇴행성 뇌질환인 파킨슨병의 치료제 개발

Decomposition of neurodegenerative oligosome using microbial proteases engaged in biofim metabolism of polar microorganisms

숙명여자대학교

제 출 문

극지연구소장 귀하

본 보고서를 “국내 학 · 연 극지연구진흥프로그램(PAP사업)” “극지미생물유래 분해효소를 이용한 퇴행성 뇌질환인 파킨슨병의 치료제 개발”의 최종보고서로 제출합니다.

2017 . 6 . 28

연구기관명 : 숙명여자대학교

연구책임자 : 김 두헌

참여연구원 : 류 범한

참여연구원 : 유 완기

참여연구원 : 김 부영

참여연구원 : 권 세나

참여연구원 : 이 소정

요 약 문

Ⅰ. 제　　목

극지 미생물유래 분해효소를 이용한 퇴행성뇌질환인 파킨슨병의 치료제 개발

Ⅱ. 연구개발의 목적 및 필요성

본 연구과제는 1) 극지미생물의 chromosomal DNA 및 metagenomic pool을 이용하여 단백질 가수분해 효소 유전자를 탐색 확보하고, 이를 이용하여 유전자 라이브러리를 구축하고, 2) 가수분해유전자 라이브러리를 이용하여 극지미생물유래의 단백질 가수분해효소의 특성, 기능, 그리고 구조분석을 통하여 생화학/분자생물학적인 특성을 규명하며, 3) 극지미생물유래의 단백질가수분해효소를 이용하여 퇴행성뇌질환의 원인인 올리고솜의 분해 및 제어기작을 응용할 수 있는 시스템을 구축하는 것을 목표로 한다.

Ⅲ. 연구개발의 내용 및 범위

○ 극지미생물 유래의 단백질 가수분해효소의 탐색 및 라이브러리 구축
○ 단백질가수분해효소의 생산시스템 구축 및 특성분석
○ 퇴행성 뇌질환의 아밀로이드형성기작 및 올리고솜 형성
○ 가수분해효소의 결정화를 통하여 3차원 구조결정
○ 동물세포 및 마우스모델에서 신경세포의 작용기작 연구

Ⅳ. 연구개발결과의 활용계획

○ 연구 성과를 통한 추가연구 및 신규분야 활성화
○ 연구 성과 활용을 위한 데이터 베이스 구축
○ 국제 공동연구네트워크의 구성

목 차

제 1 장 서론

고령화 사회의 도래와 더불어 노인들에게서 주로 나타나는 알츠하이머 병, 파킨슨병, 그리고 헌팅턴병 등의 퇴행성 뇌질환들은 환자, 가족 및 보호자, 그리고 사회 전반에 걸쳐서 막대한 경제적 비용을 초래하고 있으며, 노년기 개인의 삶을 피폐하게 만드는 주요한 원인으로서 공동체의 파괴를 가져오는 커다란 사회불안요소중의 하나이다. 이러한 퇴행성 뇌질환들은 구체적으로 뇌에서 기억 및 운동을 담당하는 신경세포들의 사멸이나 기능저하에 의해 일어나게 되며, 우리나라뿐만 아니라 구미 각국에서도 가장 큰 사회적인 관심사항중의 하나로 부각되고 있으나, 현재까지 다양한 노력에도 불구하고 퇴행성 뇌질환을 효과적으로 예방하거나 치료할 수 있는 방법은 알려져 있지 않다. 따라서, 이러한 퇴행성 뇌질환에 대한 연구는 뇌신경계에 대한 생명과학적 이해를 가능하게 하는 기초과학의 성격을 가진 동시에, 보건의료 산업에서 고부가가치를 창출할 수 있는 미래기술의 중요한 방향이라고 할 수 있다.

제 2 장 국내외 기술개발 현황

1 절. 연구의 필요성

알츠하이머병, 파킨슨병, 헌팅턴병등 많은 종류의 퇴행성 뇌질환들은 공통적으로 환자의 뇌조직에서 아밀로이드 및 그 침착체(Amyloid plaue나 Lewy bodies 등)가 발견되는 특징을 가지고 있다. 즉, 뇌신경세포의 특정 단백질들(Amyloid beta, α-Synuclein, Tau, Huntington 등)이 비정상적인 집적화과정을 거쳐서 올리고솜(Oligosome)이라 불리는 단백질 복합체를 만들게 되고, 추가 단계를 거쳐서 최종적으로 아밀로이드 및 그 침착체를 형성되는 것으로 이해되고 있다. 흥미롭게도 이 과정에서 형성되는 올리고솜은 뇌신경세포의 사멸에 직접적인 영향을 미치는 퇴행성 뇌질환 유발원으로 알려져 있다. 즉, 병인 단백질이 침전과정을 통하여 올리고머(oligomer) 상태가 되었을 때 세포독성을 가지게 되며, 성숙된 아밀로이드로 성장하게 되면 더 이상 세포독성을 나타내지 않게 된다고 생각된다.

현재까지 퇴행성 뇌질환에 관한 치료제 개발 연구는 크게 두 가지 방향으로 진행되고 있는 데, 1) 올리고솜 및 아밀로이드의 형성을 억제할 수 있는 작은 유기분자화합물(small organic molecules)의 개발과, 2) 세포사멸에 직접적인 영향을 미치는 올리고솜에 효과적으로 결합할 수 있는 특정 항체의 개발에 집중되어 있다. 그러나, 이러한 연구방향은 1) 세포사멸기작의 원인인 올리고솜의 물리적/화학적 특성이 아직까지도 명확하게 밝혀지지 않은 상태이므로 특이성이 현저히 떨어지는 화합물의 탐색하는 결과를 가져오고 있으며, 2) 올리고솜 자체가 다양한 단백질중합체(Oligomer)들의 집합체로서 Heterogeneous한 성격을 가짐으로 말미암아 특정 항체의 개발이 어려운 근본적인 한계가 있다.

2 절. 관련 연구동향 및 독창성(창의성)

본 연구과제는 날로 중요성을 더해가는 퇴행성 뇌질환에 대한 치료제의 개발과정에서 기존의 유기화합물 및 항체 기반 연구전략에 한계가 있음을 인식하고, 이를 해결하기 위하여 뇌신경세포의 사멸의 원인이 된다고 생각되는 올리고솜(Oligosome)에 대해 특이적으로 작용하여 올리고솜의 분해를 촉진하고 세포의 사멸을 저해하는 단백질 가수분해효소를 극지미생물에서 탐색하고 이를 통하여 새로운 치료제의 가능성을 제시하고자 한다.

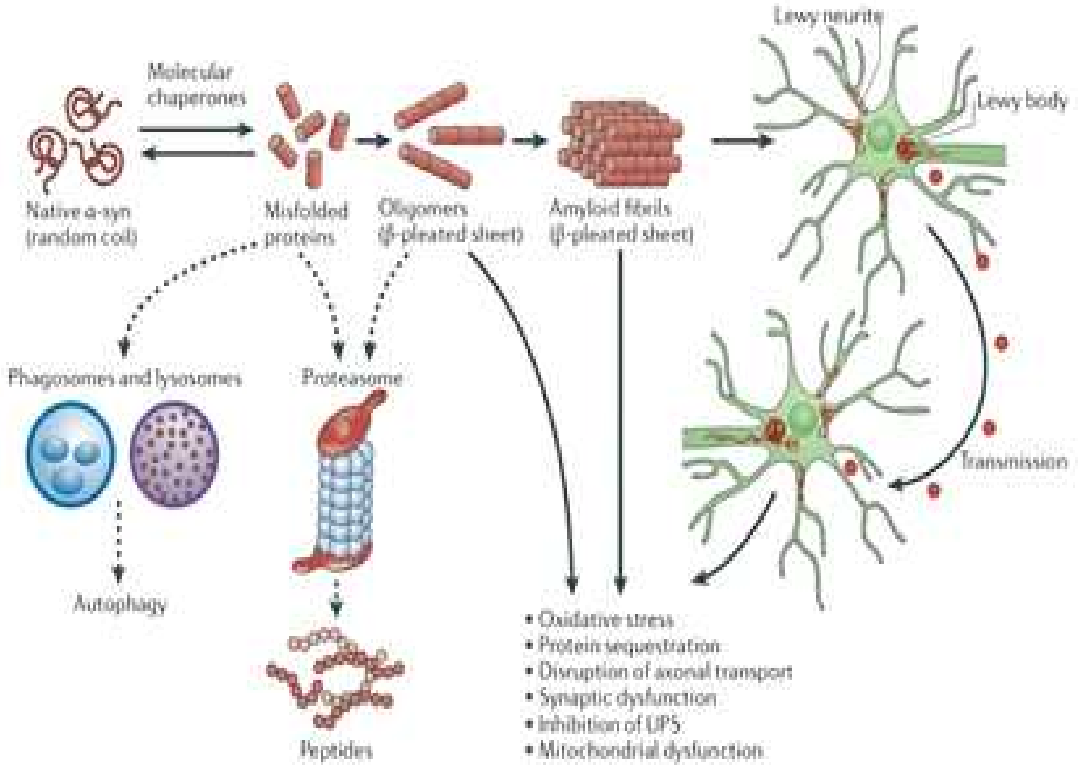

그림 1. alpha-synuclein의 구조변형에 의한 올리고솜의 형성 및 세포독성유발 메카니즘

퇴행성뇌질환인 원인 단백질들(Amyloid beta, alpha-Synuclein, Huntingtin등)이 올리고솜을 거쳐서 최종적으로 만들어지는 아밀로이드는 높은 물리화학적 안정성을 가지게 된다. 흥미롭게도, 몇 가지 병원성미생물들(Pseudomonas, Streptococcus, Staphylococcus 등)은 아밀로이드를 일부 함유하는 복합지지체를 가지는 것이 발견되었다. 이러한 미생물들은 아밀로이드의 안정성을 활용하여, 생존을 위한 군집의 형성을 촉진하거나 인체감염과정의 효율성을 증대시키는 것으로 추측된다. 본 연구진은 이에 착안하여 미생물들이 외부환경의 변화에 따라 형성된 복합지지체를 효과적으로 제어하는 정교한 조절체계로서 일련의 효소군을 가지고 있을 것으로 예상하였다. 또한, 이러한 효소들의 상당수는 안정성이 큰 아밀로이드에 직접적으로 작용하기보다는 중간체인 올리고솜의 구조나 기능을 효과적으로 조절하는 역할을 수행할 것으로 판단하였다. 이에 따라 본 연구진은 극지미생물유전체로부터 올리고솜을 분해하는 효소를 탐색하고자하며, 이를 바탕으로 기존의 퇴행성 뇌질환 연구가 가지는 단점을 극복하는 새로운 가능성을 제안하고자 한다. 또한 **퇴행성 뇌질환 치료를 주제로 하는 극지 미생물 연구는 연구의 중요성에 비해 매우 미흡**한 실정이다. 일반적인 환경이 아닌 극지환경에 서식하는 미생물을 대상으로 연구하면, 활성이 높으면서도 특정 질환으로 제한되지 않고 퇴행성 뇌질환 전반에 작용할 수 있는 새로운 효소의 발견 가능성을 높일 수 있다.

기존의 연구들과는 달리, **극지 미생물에 이미 존재하는 바이오필름 또는 아밀로이드 형성에 관여하는 효소를 응용하는 방식**이기 때문에, 찾고자 하는 단백질 분해효소가 가지는 올리고솜에 대한 표적화 수준이나 분해 활성이 높을 것으로 예상된다. 따라서 **많은 시간과 노력을 요구하는 시행착오방식의 소모적인 기존 연구방법론에서 탈피**할 수 있다. 또한, 실제 질환의 원인이나 진행 메커니즘을 완전히 이해하지 못하고 있는 현재 상황에서도, 퇴행성 뇌질환 예방 및 치료에 충분한 효과를 기대할 수 있고, 반대로 단백질 분해효소를 이용하여 질병의 직접적인 원인이 되는 병인 단백질종을 확인할 수 있게 되어 퇴행성 뇌질환의 병인 및 진행에 대한 이해에 기여할 수 있게 된다.

3 절. 연구 과제의 중요성

본 연구는 퇴행성 뇌질환에 대한 새로운 패러다임을 제시할 수 있는 연구로서, 연구가 성공적으로 진행되어 극지 미생물로부터 뇌신경세포의 사멸을 유도하는 올

리고솜을 표적화 및 선택적으로 분해하는 단백질 분해효소를 발견하게 되면, 퇴행성 뇌질환을 예방 및 치료할 수 있는 새로운 생물학적 치료제가 될 것으로 생각된다. 또한 과학계 전반에 걸쳐 극지생물 연구의 중요성 및 응용가능성을 환기시킬 수 있으며, 나아가 다가오는 글로벌 이슈인 고령화 사회 및 퇴행성 뇌질환 환자의 증가에 대비하고 의약 분야의 국가 원천기술 확보를 위해 매우 중요한 토대가 될 수 있다.

본 연구는 극지미생물의 바이오필름의 제어 및 조절에 관여하는 단백질 가수분해효소에 대한 연구로서, 본 연구를 통하여 이 효소군의 기능과 구조에 대한 자세한 정보를 얻게 되면, 극지미생물의 바이오필름형성에 대한 구체적인 생명과학적인 정보 및 이의 제어방법에 대한 기술을 확보할 수 있다. 현재 확실하게 규명되지 않은 극지미생물 유래의 단백질 가수분해효소의 구조-기능 상관관계를 규명하여 다학제간 연구를 활성화 할 수 있는 유용한 지식기반을 제공할 수 있을 것으로 생각된다.

많은 퇴행성 뇌질환의 병인단백질들의 생체 내 역할에서부터 병의 발생 원인과 메커니즘, 아밀로이드와 질병 사이의 연관성에 이르기 까지 많은 부분이 불명확한 상태로 남아 있어 퇴행성 뇌질환을 치료하거나 진행을 억제하고 미리 예방할 수 있는 방법은 여전히 발견되지 않고 있다. 따라서 이들 병인 단백질이 어떠한 과정을 거쳐 아밀로이드를 형성하게 되는지, 단량체에서 올리고솜을 거쳐서 아밀로이드가 형성되고 이 과정에서 퇴행성 뇌질환을 유발하는지를 밝히는 일은 병의 원인과 치료책을 찾는데 있어 매우 중요하다. 따라서 올리고솜의 형성 및 분해에 관한 본 연구과제가 퇴행성 뇌질환의 병인과 병의 진행을 규명하는데 크게 도움을 줄 수 있다.

제 3 장 연구개발수행내용 및 결과

1 절 연구개발목표

본 연구과제는 1) 극지미생물의 chromosomal DNA 및 metagenomic pool을 이용하여 단백질 가수분해 효소 유전자를 탐색 확보하고, 이를 이용하여 유전자 라이브러리를 구축하고, 2) 가수분해유전자 라이브러리를 이용하여 극지미생물유래의 단백질 가수분해효소의 특성, 기능, 그리고 구조분석을 통하여 생화학/분자생물학적인 특성을 규명하며, 3) 극지미생물유래의 단백질가수분해효소를 이용하여 퇴행성 뇌질환의 원인인 올리고솜의 분해 및 제어기작을 응용할 수 있는 시스템을 구축하는 것을 목표로 한다. 따라서, 본 연구과제는 극지생명과학으로서 학문적인 중요성뿐만 아니라 보건의료산업 및 생명공학산업에의 파급효과가 커다란 연구 주제라고 할 수 있다. 본 연구과제가 효과적으로 추진되면 1) 극지미생물유래의 다양한 단백질 가수분해효소의 구조와 기능에 대한 정보를 확보할 수 있으며, 2) 퇴행성 뇌질환의 위험효소인 올리고솜의 효과적인 분해와 제거기작에 극지미생물 유래의 가수분해효소를 활용하는 전략을 수립할 수 있을 것으로 예상되어 질병에 대한 효과적인 치료제의 개발에 중요한 역할을 할 것으로 생각되며, 3) 가수분해효소의 활성을 이용하여 다양한 생명공학적 응용 및 실용화에 이용할 수 있을 것이다.

2 절. 연구의 수월성

본 연구과제가 목표로 하는 연구는 학문적인 중요성과 더불어 연구성과의 파급효과가 아주 커다란 연구주제이므로 미생물학/생화학/유전공학등의 개별학문분야의 최신 기술과 지식을 접목하여 성과를 극대화하고자 한다. 따라서 본 과제의 수행이 성공적으로 완료되면 참여 연구원 연구능력을 극대화할 수 있으며, 본 연구진은 국내의 유수의 연구그룹으로 성장할뿐더러 국제적인 연구네트워크를 구축할 수 있을 것으로 기대된다. 현재까지 본 연구진은 다음과 같은 분야에서 장점을 가진 연구진이므로 본 연구 과제의 성공적인 수행이 가능할 것으로 생각된다.

본 연구진은 미생물 유전체 및 metagenome library로부터 genome-wide mining을 통하여 짧은 시간에 다량의 가수분해효소들의 유전자를 탐색/확보할 수 있는 시스템을 구축한 경험을 가지고 있다. 또한, 기질 특이성, 반응성 및 안정성이 확보된 효소를 얻기 위하여 본 연구진은 semi-high throughput assay를 구축하고 단 시간에 genome-wide mining을 통하여 대량의 유전자를 탐색/확보할 수 있다. 이러한

기술및 경험을 바탕으로 극지미생물에서 단백질가수분해유전자를 탐색하고 라이브러리의 구축을 효율적으로 진행할 것으로 생각된다.

본 연구진은 이미 선행연구를 통하여 미생물의 단백질가수분해효소에 대한 구조와 기능에 대한 연구경험을 축적하고 있기 때문에 본 연구과제의 목적을 효과적으로 달성할 수 있을 것으로 생각된다. 구체적으로, 본 연구진은 현재까지 Est25, Est-Y29, Sm23, LI22와 같은 단백질 가수분해효소들의 기능분석을 성공적으로 수행하였으며, 현재는 EstA, EstLI, Estcc의 특성분석을 진행하고 있다. 또한, Est25, Est-Y29, Sm23의 구조분석을 X-ray crystallography를 이용하여 성공적으로 수행하였다. 이러한 기능 및 구조연구를 기반으로 하여 방향적 진화(directed evolution) 및 정보기반형 설계(rational design)를 통하여 열 및 유기용매에 대한 안정성을 가지는 효소를 얻는 연구를 수행하고 있다.

본 연구진은 지난 수년간 파킨슨병과 관련한 퇴행성 뇌질환의 치료제의 개발을 위하여 아밀로이드의 생성을 저해(inhibition)하거나 생성된 아밀로이드를 분해(disaggregation)하기 위한 small molecule 혹은 분자 저해제(molecular inhibitor) 연구들이 활발히 진행하고 있다. 본 연구에서는 그리고 다양한 방법을 통해 생성된 여러 가지 타입의 아밀로이드들의 특성을 효과적으로 규명하고 있으며 세포의 독성과 밀접한 연관을 갖는 올리고솜의 형성원리와 특징을 규명하고 있다.

본 연구진은 유용한 생체화합물의 생산을 위하여 효소와 다양한 기질 들의 상호 작용 메카니즘을 다년간 심층적으로 연구하였으며, 효소반응에 대한 이해 및 반응 조건에 따른 효소의 구조적 안정성 등을 대한 선행 연구 경험 및 장비를 보유하고 있다. 또한, 효소의 고집적화및 고정화를 위하여 crosslinked enzyme aggregate(CLEA)방법을 구축하고 있으며, 효율성과 저장기능(storage)의 향상을 위하여 amyloid fibril을 비롯한 여러 종류의 polymorphic protein aggregates을 사용하여 효소의 고집적화및 저장효율을 지속적으로 유지시키는 방법을 연구하고 있다. 이러한 효소의 집적화및 효율향상에 대한 연구경험은 본 연구의 수행 과정및 실용화과정에 중요한 역할을 할 것이다.

3 절. 연구진의 우수성

본 연구책임자는 2013-2014년에 단백질의 구조와 기능에 관하여 12편의 논문을 발표하였으며 이중 Structural and Functional Analyses of a Bacterial Homolog of Hormone Sensitive Lipase from a Metagenomic Library의 논문은 국가생물학정보

센터인 BRIC에 소개가 되었습니다. 본 연구책임자는 2013-2014년에 걸쳐서 Acta Crystallographica Sec. D (IF 7.2), Bioresource Technology (IF 5.0), Applied Microbiology and Biotechnology (IF 3.8), International Journal of Biological Macromolecules (IF 3.0)등의 저널에 논문을 발표하였습니다.

본 연구책임자는 현재 퇴행성 뇌질환인 파킨슨병에 관한 alpha-synuclein에 관한 연구와 관련하여 서울대 화학과(남좌민교수), KIST(안대로 박사), 가톨릭대(신계정 교수), 한국해양연구원(차선신박사)등 국내의 다양한 연구그룹들과 공동연구를 진행하고 있으며 이러한 공동연구네트워크의 구성을 통하여 국제적인 수준의 연구결과를 산출하고 있습니다. 따라서, 이를 바탕으로 본 연구과제를 수행하기에 적절한 노하우 및 연구네트워크의구성을 통한 연구의 수월성을 확보하고 있다고 판단됩니다.

본 연구책임자는 서울대학교에서 박사학위논문으로 “Structure and functional studies of alpha-synuclein”을 파킨슨병의 원인단백질에 관한 연구를 진행하였으며 2001년 한국분자세포생물학회로부터 우수박사학위논문상을 수상하였으며, 관련된 연구로 Faculty of Biology 1000에 소개가 되었습니다. 본 연구책임자는 약 20년 가까이 퇴행성뇌질환의 원인 물질에 대한 구조와 기능연구에 매진하여 왔습니다. 따라서, 연구의 지속성 및 발전가능성 측면에서 장점이 있다고 할 수 있습니다. 본 연구책임자는 연구기자재 및 시설, 그리고 연구인력의 충분한 확보를 바탕으로 2013년에 아주대학교의 우수논문상을 수상하는 등 국제적인 수준의 연구를 진행하기에 충분한 연구기자재 및 시설을 갖추고 있습니다.

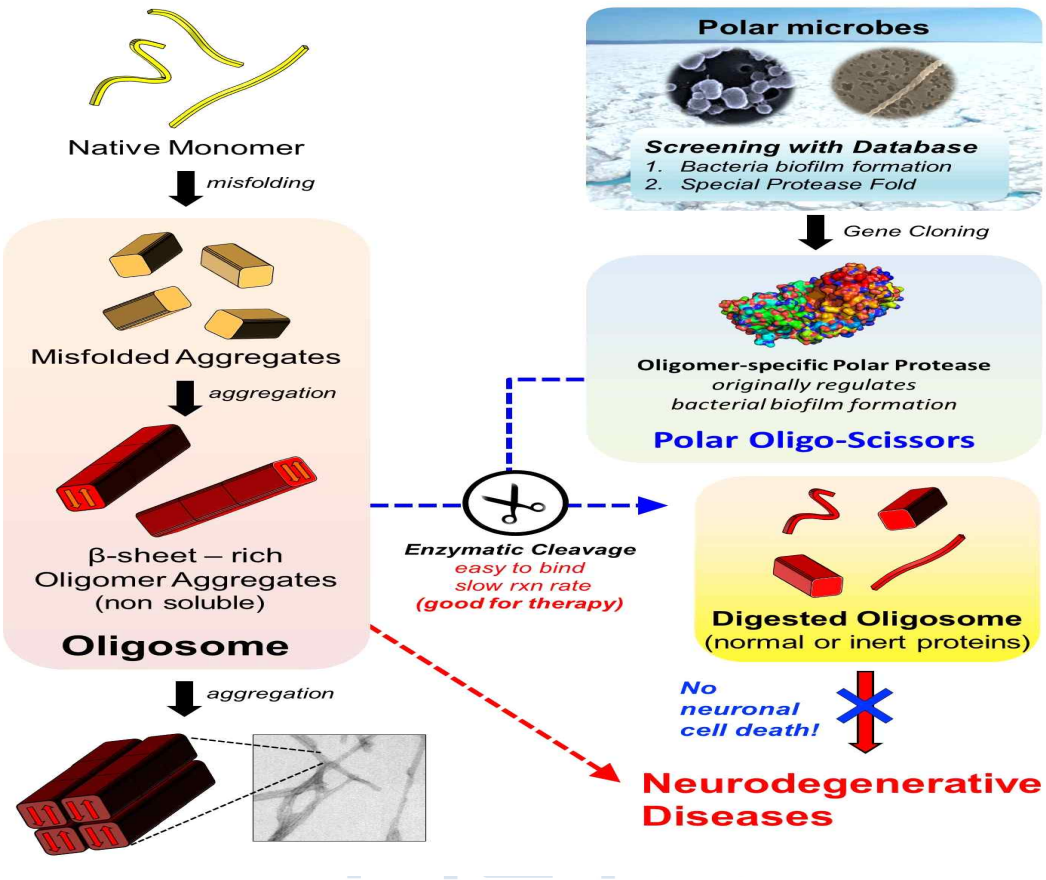

그림 2. 올리고솜의 분해에 극지미생물 유래의 가수분해효소의 활용에 대한 개념 및 내용

표 1. 올리고솜의 분해를 위한 극지미생물 유래의 가수분해효소의 활용에 대한 구체적인 연구내용

구분	년도	연구개발목표	연구개발내용
1차년도		극지미생물 유래의 단백질 가수분해효소의 탐색 및 라이브러리 구축	극지미생물 유전체 및 메타게놈으로부터 단백질 가수분해효소를 효과적으로 탐색/확인하고, 이를 이용하여 유전자 라이브러리를 구축한다.
		단백질가수분해효소의 생산시스템 구축 및 특성분석	단백질 가수분해효소들을 효율적으로 생산하기 위한 시스템을 구축하고, 이의 특성을 생화학, 미생물학, 그리고 세포생물학적인 방법으로 분석한다.
		퇴행성 뇌질환의 아밀로이드형성기작 및 올리고솜 형성에 대한 메카니즘 연구	알파-시누클린을 중심으로 단위체, 중합체, 아밀로이드복합체들의 형성과정을 체계적으로 이해하고 이를 모니터링할 수 있는 시스템을 구축한다.
2차년도		가수분해효소의 결정화를 통하여 3차원 구조결정을 통하여 효소의 특성 규명	얻어진 단백질가수분해효소를 이용하여 다양한 생화학방법(CD spectroscopy, FT-IR, X-ray crystallography, Molecular modeling)등을 이용하여 및 3차원 구조를 결정하고, 개별 효소의 기질특이성, 안정성, 반응속도론적인 특성을 규명한다.
		1년차에서 얻어진 가수분해효소를 이용하여 올리고솜 분해과정의 연구	파킨슨병에 관여하는 alpha-synuclein의 올리고솜 및 아밀로이드의 형성시스템을 구축하고 가수분해효소를 이용하는 활성분석 및 메카니즘 규명
		동물세포 및 마우스모델에서 신경세포의 작용기작 연구	뇌신경세포의 독성과 연관된 올리고솜을 특서오하 하고 이를 동물세포와 마우스모델에서 확인하고 효능분석

4 절. 연구개발 방법

연구방법 1. 극지미생물의 chromosomal DNAs및 metagenome pool을 이용하여 극지미생물유래의 단백질 가수분해효소의 유전자 라이브러리를 구축한다. 이때 가수분해효소의 유전자를 탐색하는 방법은 활성측정과정이 *p*-nitrophenol을 통하여 진행됨을 이용하여, pH indicator를 이용한 색 변화 반응을 이용한다. 우선, 기질로 150mM *p*-nitrophenol derivatives를 사용하여 페놀레드(1g/l)와 함께 20mM Tris-HCl에 1% Triton X-100을 이용하여 staining solution을 만들어 사용하게 되면, pH indicator는 *p*-nitrophenol이 생성됨에 따라 붉은색에서 노란색으로 변하게 된다. 따라서, 색깔변화에 사용된 *E. coli* 를 선별하여 내고 이들로부터 유전자 라이브러리를 구축하게 된다. 미생물 가수분해효소의 활성을 분석하기 위하여 다양한 기질과의 반응을 Biochemical assays, Fluorescence microscpe, Flow cytometer, Liquid Chromatography등을 이용한다. 이를 통해 극지미생물유래의 단백질가수분해효소의 반응 kinetics 및 효소-기질 친화상수, 열역학적인 탈피 및 엔트로피 측정 등을 통해 파악한다. 이를 통하여 효소와 기질의 인지 메카니즘 규명, 반응 site 분석, 열역학적 반응 포텐셜 측정, 반응 메카니즘을 분석한다.

연구방법 2. 유전자 라이브러리를 통하여 확보한 극지미생물 유래의 단백질가수분해효소를 E. coli를 통하여 단백질 발현과정을 진행하고, 단백질의 분리및 정제를 통하여 결정을 준비하게 되고, 이를 바탕으로 x-ray 회절실험을 진행하고 3차원 구조를 결정하게 된다. 단백질 결정과정을 위하여 polyethylene glycol, ammonium sulfate 등 다양한 침전제들을 사용하게 되며, crystal screen I/II 등을 이용하게 된다. 얻어진 결정은 포항의 가속기 연구소나 일본의 Photon Factory 등의 synchrotron radiation facilities를 이용하여 정밀한 회절데이터를 수집하게 된다. 이러한 데이터를 해석하여 단백질의 3차원 구조를 결정하고, active site environment에 대한 구체적인 정보를 얻게 된다. 단백질결정화 및 XRD를 통해 단백질 구조를 결정하고 PyMOL, CCP4 등의 컴퓨터 프로그램과 PISA, DALI server 등의 생물정보학 tool과 데이터베이스를 이용하여 구조의 구성요소를 분석하고 촉매 메커니즘을 확인한다. 단백질의 구조와 효소의 특성, 기질에 대한 활성 등 분석 결과를 유기적으로 종합 및 알려진 다른 구조나 정보와 비교를 통해, 구조-기능 상관관계를 도출한다.

연구방법 3. 유전자 라이브러리를 통하여 확보한 극지미생물 유래의 단백질 가수분해효소를 기반으로 퇴행성 뇌질환에서 세포독성을 나타내는 올리고솜의 분해과정을 확인한다. 이 과정에서 먼저 아밀로이드에 대한 효과를 검증하고 이를 바탕으로 올리고솜에 대한 분해를 확인하여 퇴행성 뇌질환에 대한 새로운 치료제로서의 가능성을 탐색한다. 본 연구진은 다양한 종류의 조건에서 아밀로이드 및 올리고솜의 형성기작에 대한 선행결과 및 연구정보를 확보하고 있으며, 이들을 바탕으로 가수분해효소에 의하여 제거되는 조건에 대한 연구를 진행하고자 한다. Transmission Electron Microscopy (TEM), Fluorescence microscopy, Fluorescence spectroscopy, SDS-PAGE등 다양한 방법을 활용하여 올리고솜의 분해과정을 측정하게 된다.

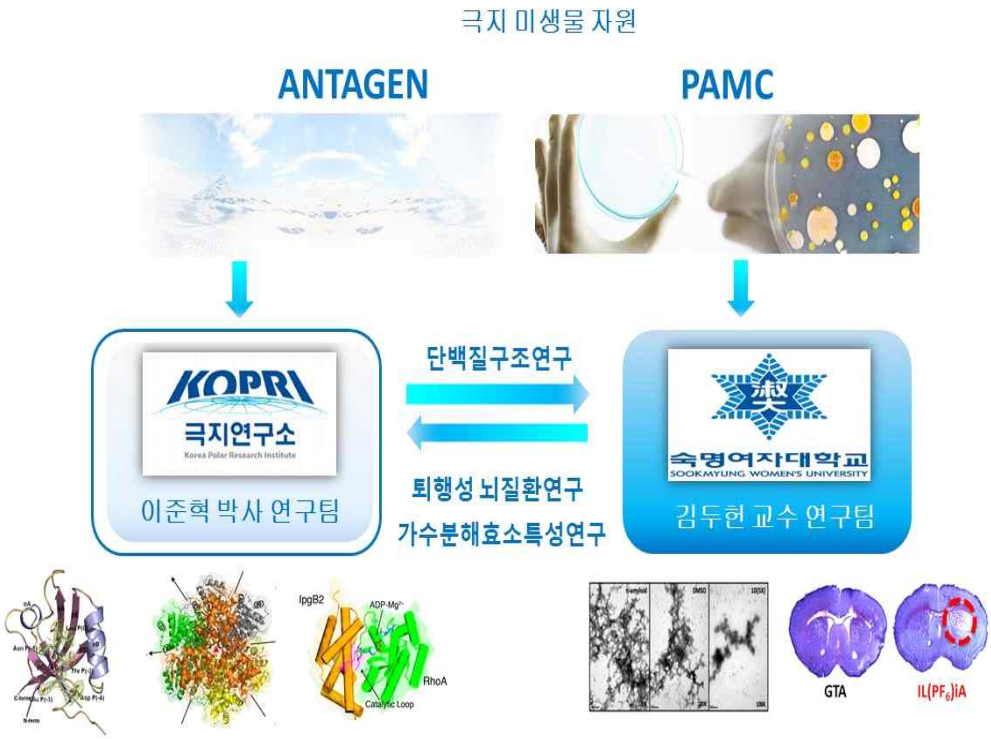

그림 3. 연구의 진행체계 및 공동연구 내용

5 절. 선행연구의 내용

본 연구진은 미생물의 유전체 및 metagenomic pool을 이용하여 가수분해효소의 라이브러리를 구축하고 있으며, 파킨슨병의 원인 물질인 알파-시누클린에 대한 생화학/분자생물학/세포생물학 실험들을 진행하고 있다. 또한, 단백질의 활성 및 안정성연구, 구조분석, 아밀로이드의 특성분석, 동물세포배양 및 세포독성연구, 실험용 쥐를 이용한 아밀로이드 독성분석에 대한 다양한 요소기술을 개발한 경험과 성과를 가지고 있으므로, 본 연구를 성공적으로 수행할 수 있을 것으로 생각되며, 주요 선행연구결과는 다음과 같다.

선행 결과 1 : 본 연구책임자는 현재까지 *Sinorhizobium melilotti 1020*과 *Listeria innocua*등으로부터 Sm23, Li22, EstA, Sm25 등의 가수분해효소들을 효과적으로 유전자분석, 단백질 발현및 대량생산하여 기능과 구조를 분석하고 해외학술지에 논문을 제출하였다. 또한, 현재, *Caluobacter crescentus*로부터 Estcc를, *Sinorhizobium melilotti*로부터 EstA1, *Streptococcus pyogenes* 로부터 EstB1을, *Streptomyces coelicolor*로부터 EstG1, EstI1, *Pseudomona fluorescens* 로부터 Est1767등을 얻어서 대장균을 이용하여 발현 및 특성분석을 진행하고 있다. 추가적으로 *Agrobacterium tumefaciens*에서 유래한 Est423, *Xanthomonas axonopodis*에서 유래한 Est411을, *Salmonella typhimurim*으로부터 Est292, *Shewanella oneidensis*로부터 Est245, *Bacillus subtilis*로부터 Est171, Est172에 해당하는 유전자 라이브러리를 구축하였다.

선행 결과 2 : 본 연구진은 이온성 액체중의 한 계열인 이미다졸리움계열의 화합물이 특히(1-butyl-3-methyl-imidazolium-based ionic liquids)가 파킨슨병과 관련한 알파-시뉴클레인의 아밀로이드 섬유의 형성을 매우 빠르게 촉진할 수 있다는 것을 보고하였다. 이러한 아밀로이드 형성 촉진 효과는 모든 이온성 액체에서 동일하게 나타나지는 않고 특정한 종류의 이온성 액체에서는 매우 효과적이며 종류에 따라 효과의 정도에 상대적인 차이가 있다. 또 다른 흥미로운 사실은, 이온성 액체에 의해 유도된 아밀로이드는 적절한 온도 및 교반조건에서 생성되는 일반적인 아밀로이드(대부분의 실험실이 채용하는 방식)와 물리적 혹은 화학적인 성격이 다르다는 점이다. 또한, 최근의 연구결과, 특정 이온성 액체를 통해 만든 알파-시뉴클레인의 아밀로이드가 마우스의 striatum에 주입되었을 때 아주 짧은 시간 내에 신경독성을 유발한다는 사실을 관찰하였다.

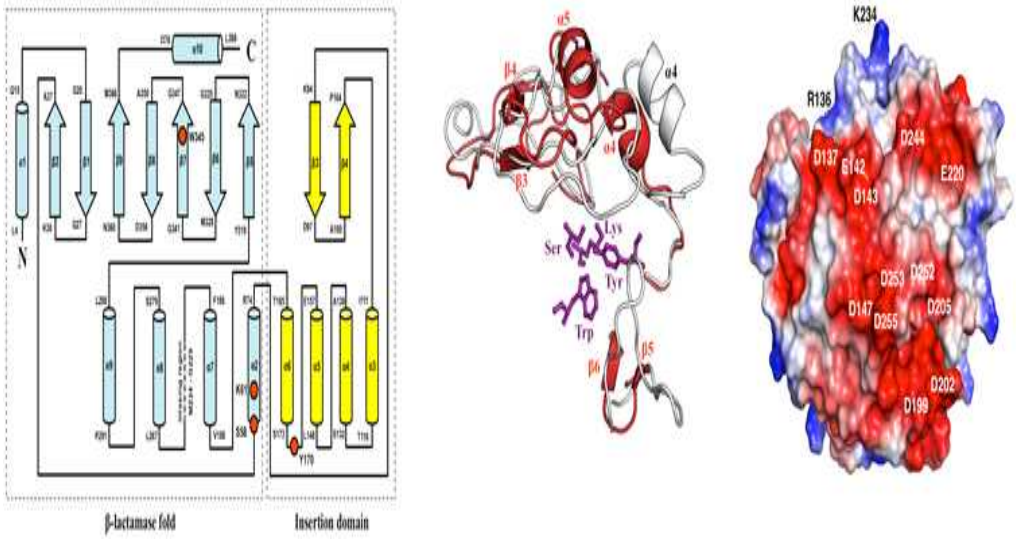

그림 4. 선행연구의 결과로 얻어진 박테리아 유래의 가수분해효소의 구조

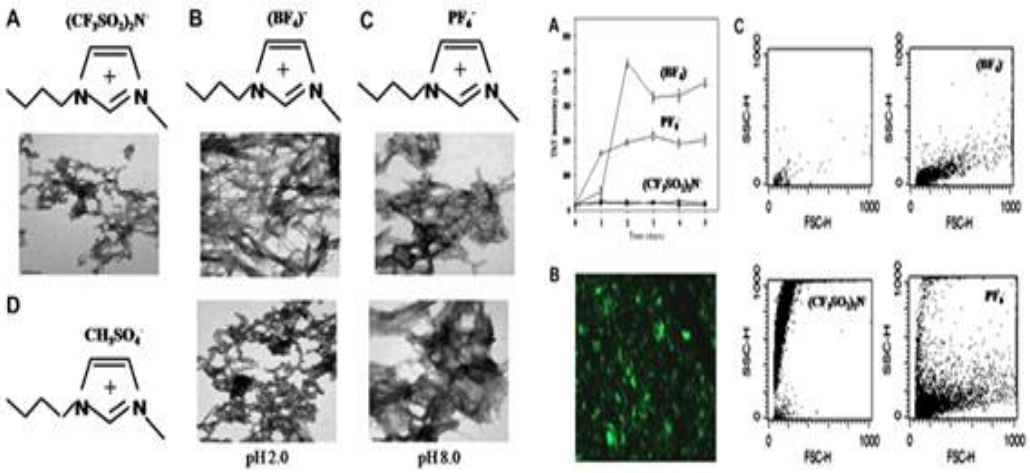

그림 5. 선행연구의 결과로 얻어진 이온성액체를 이용한 alpha-synuclein의 아밀로이드 및 올리고솜형성

선행 결과 3 : 최근의 연구결과들에 따르면 단백질/지방산 복합체는 세포독성이나 질병과 관련된 특성을 획득하는 것으로 알려져 있으며, 특히 퇴행성 뇌질환과 관련해서는 프리온 단백질과 지질의 상호작용이 신경독성을 유발한다는 것이 보고되어 있다. 본 연구진의 선행연구 결과에 따르면 알파-시뉴클레인이 aggregates나 아밀로이드를 형성하지 않는 상태에서도 올레산(Oleic acid)와 같은 지방산과 복합체 형성을 유도하였을 때 동물세포(neuroblastoma cell) 실험에서 매우 짧은 시간 내에 세포의 사멸을 일으킨다는 사실을 관찰할 수 있었다. 이러한 연구결과는 실제 질병에서 뇌세포의 퇴행(사멸)이 지방산과 상당한 연관성이 있다는 점을 시사한다. 이러한 선행연구 결과들은, 조건에 따라 특성이 서로 다른 여러 가지 종류의 아밀로이드가 생성될 수 있음을 시사한다. 따라서 다양한 방법을 통해 아밀로이드 형성 및 촉진 조건을 탐색하는 접근방식이 거꾸로 아직까지 발견되지 못한 알파-시뉴클레인의 독성 단백질종을 특정하는데 도움이 될 수 있다.

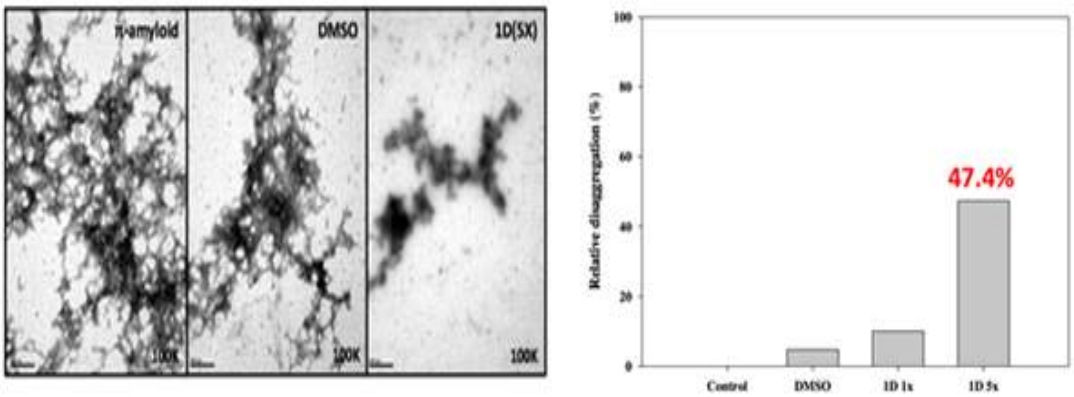

그림 6. 선행연구의 결과로 얻어진 alpha-synuclein의 아밀로이드 및 올리고솜형성에 관한 전자현미경 사진 및 세포독성결과

제 4 장 연구개발목표 달성도 및 대외 기여도

1 절. 연구개발 목표 달성도 (1년차)

연구개발목표	달성내용
○극지미생물 유래의 단백질 가수분해효소의 탐색 및 라이브러리 구축	○극지미생물 유전체 및 메타게놈으로부터 단백질 가수분해효소를 효과적으로 탐색/확인하고, 이를 이용하여 유전자 라이브러리를 구축하였음 -
○단백질가수분해효소의 생산시스템 구축 및 특성분석	○단백질 가수분해효소들을 효율적으로 생산하기 위한 시스템을 구축하고, 이의 특성을 생화학, 미생물학, 그리고 세포생물학적인 방법으로 분석하였음
○퇴행성 뇌질환의 아밀로이드형성기작 및 올리고솜 형성에 대한 메카니즘 연구	○알파-시누클린을 중심으로 단위체, 중합체, 아밀로이드복합체들의 형성과정을 체계적으로 이해하고 이를 모니터링할 수 있는 시스템을 구축하였음

2 절. 연구개발 목표 달성도(2년차)

연구개발목표	달성내용
○가수분해효소의 결정화를 통하여 3차원 구조결정을 통하여 효소의 특성 규명	○얻어진 단백질가수분해효소를 이용하여 다양한 생화학방법(CD spectroscopy, FT-IR, X-ray crystallography, Molecular modeling)등을 이용하여 및 3차원 구조를 결정하고, 개별 효소의 기질특이성, 안정성, 반응속도론적인 특성을 규명한다.
○1년차에서 얻어진 가수분해효소를 이용하여 올리고솜 분해과정의 연구	○파킨슨병에 관여하는 alpha-synuclein의 올리고솜 및 아밀로이드의 형성시스템을 구축하고 가수분해효소를 이용하는 활성분석 및 메카니즘 규명 -
○동물세포 및 마우스모델에서 신경세포의 작용기작연구	○뇌신경세포의 독성과 연관된 올리고솜을 특서오하 하고 이를 동물세포와 마우스모델에서 확인하고 효능분석

3 절. 연구개발 목표 달성의 구체적 내용

연구개발 목표	연구수행방법 (이론적・실험적 접근방법)	구체적인 내용*
극지미생물 유래의 단백질 가수분해효소의 탐색 및 라이브러리 구축	1. 유전체 및 생명공학기술	○극지미생물 유전체 및 메타게놈으로부터 단백질 가수분해효소를 효과적으로 탐색/확인하고, 이를 이용하여 유전자 라이브러리를 구축하였음
단백질가수분해효소의 생산시스템 구축 및 특성분석	2. 생화학 기술	○단백질 가수분해효소들을 효율적으로 생산하기 위한 시스템을 구축하고, 이의 특성을 생화학, 미생물학, 그리고 세포생물학적인 방법으로 분석하였음
퇴행성 뇌질환의 아밀로이드형성기작 및 올리고솜 형성에 대한 메카니즘 연구	3. 생화학 및 생물물리학 기술	○알파-시누클린을 중심으로 단위체, 중합체, 아밀로이드복합체들의 형성과정을 체계적으로 이해하고 이를 모니터링할 수 있는 시스템을 구축하였음
가수분해효소의 결정화를 통하여 3차원 구조결정을 통하여 효소의 특성 규명	4. 구조생물학 기술	○얻어진 단백질가수분해효소를 다양한 생화학방법(CD spectroscopy, FT-IR, X-ray crystallography, Molecular modeling)등을 이용하여 및 3차원 구조를 결정하고, 개별 효소의 기질특이성, 안정성, 반응속도론적인 특성을 규명하였음.
1년차에서 얻어진 가수분해효소를 이용하여 올리고솜 분해과정의 연구	5. 생화학 및 분자생물학 기술	○파킨슨병에 관여하는 alpha-synuclein의 올리고솜 및 아밀로이드의 형성시스템을 구축하고 가수분해효소를 이용하는 활성분석 및 메카니즘 규명하였음
동물세포 및 마우스모델에서 신경세포의 작용기작연구	6. 동물세포배양기술 및 및 생화학기술	○뇌신경세포의 독성과 연관된 올리고솜을 특서오하 하고 이를 동물세포와 마우스모델에서 확인하고 효능분석하였음

4 절. 연구개발의 대외 기여도

○ 본 연구진은 acetylesterase에 관한 연구를 통하여 얻어진 결과들을 유럽생화학회(Federation of European Biochemical Societies, FEBS)에서 발행하는 저널(IF 3.1)에 출판하였음. 본 연구에서는 Acetylesterase의 기본 구조 및 특성에 관한 자세한 분석을 진행하였으며 이를 바탕으로 극지미생물 유래 효소에 대한 자세한 정보를 획득하였음. 이 논문을 FEBS 홈페이지에서 주요 연구성과로 홈페이지에 게시되었음.

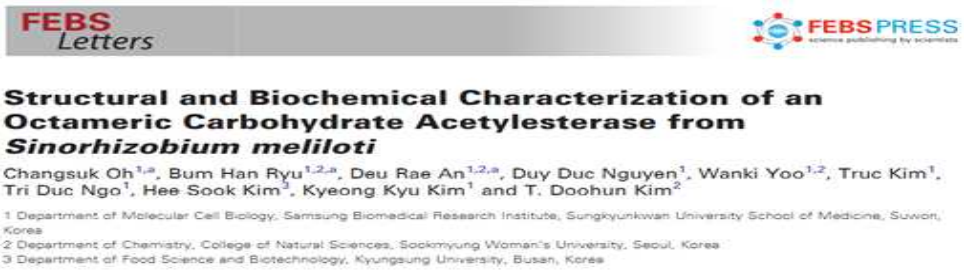

FEBS Letters

FEBS PRESS

Structural and Biochemical Characterization of an Octameric Carbohydrate Acetylesterase from *Sinorhizobium meliloti*

Changsuk Oh[1,a], Bum Han Ryu[1,2,a], Deu Rae An[1,2,a], Duy Duc Nguyen[1], Wanki Yoo[1,2], Truc Kim[1], Tri Duc Ngo[1], Hee Sook Kim[3], Kyeong Kyu Kim[1] and T. Doohun Kim[2]

1 Department of Molecular Cell Biology, Samsung Biomedical Research Institute, Sungkyunkwan University School of Medicine, Suwon, Korea
2 Department of Chemistry, College of Natural Sciences, Sookmyung Women's University, Seoul, Korea
3 Department of Food Science and Biotechnology, Kyungsung University, Busan, Korea

○ 본 연구진은 Exiguobacterium antarctium에서 esterase에 대한 구조 및 생화학 연구에 대한 논문을 세계에서 처음으로 학계에 보고하였음 (이를 PLos One에 출판됨) 이 연구성과는 현재 특허출원이 진행중에 있으며 추가적인 후속 연구가 진행중임.

PLOS | ONE

RESEARCH ARTICLE

Crystal Structure and Functional Characterization of an Esterase (*Ea*EST) from *Exiguobacterium antarcticum*

Chang Woo Lee[1,2☯], Sena Kwon[3☯], Sun-Ha Park[1☯], Boo-Young Kim[3], Wanki Yoo[3], Bum Han Ryu[3], Han-Woo Kim[1,2], Seung Chul Shin[3], Sunghwan Kim[4], Hyun Park[1,2], T. Doohun Kim[3]*, Jun Hyuck Lee[1,2]*

1 Unit of Polar Genomics, Korea Polar Research Institute, Incheon, Republic of Korea, 2 Department of Polar Sciences, University of Science and Technology, Incheon, Republic of Korea, 3 Department of Chemistry, College of Natural Science, Sookmyung Women's University, Seoul, Korea, 4 New Drug Development Center, Daegu-Gyeongpuk Medical Innovation Foundation, Daegu, Republic of Korea

☯ These authors contributed equally to this work.
* junhyucklee@kopri.re.kr (JHL); doohunkim@sookmyung.ac.kr (TDK)

Check for updates

crystals

MDPI

Communication

Identification and Crystallization of Penicillin-Binding Protein/β-Lactamase Homolog (Rp46) from *Ruegeria Pomeroyi*

Bum Han Ryu [1,2,†], Tri Duc Ngo [2,†], Wanki Yoo [1,2], Kyeong Kyu Kim [2,*] and T. Doohun Kim [1,*]

1 Department of Chemistry, College of Natural Science, Sookmyung Women's University, Seoul 04310, Korea; pseryubh@skku.edu (B.H.R.); vlqkshqlk614@skku.edu (W.Y.)
2 Department of Molecular Cell Biology, Samsung Biomedical Research Institute, Sungkyunkwan University School of Medicine, Suwon 16419, Korea; tringo@skku.edu
* Correspondence: kyeongkyu@skku.edu (K.K.K.); doohunkim@sookmyung.ac.kr (T.D.K.); Tel.: +82-31-299-6136 (K.K.K.); +82-2-2077-7806 (T.D.K.)
† These authors contributed equally to this work.

Academic Editor: Helmut Cölfen
Received: 23 November 2016; Accepted: 26 December 2016; Published: 29 December 2016

제 5 장 연구개발결과의 활용계획

1 절. 연구 성과를 통한 추가연구 및 신규분야 활성화

본 연구는 극지미생물유래의 단백질 가수분해효소를 이용하여 퇴행성 뇌질환에 대한 새로운 치료법의 제시를 목표로 한다. 본 연구과제가 2년동안 성공적으로 수행되면 그 결과물로 얻어지는 논문들은 생화학, 구조생물학 뿐만 아니라 분자/세포생물학, 미생물학 등 다양한 분야에 걸쳐 응용이 가능하며 또 이를 통해 다 학제간 연구 활성화에 기여할 수 있을 것으로 기대된다. 또한, 현재 명확하지 않은 퇴행성 뇌질환의 치료제에 대한 새로운 개념의 제시로 인하여 생명공학산업 및 보건의료산업에 대한 상당한 영향력이 있을 것으로 판단된다.

2 절. 연구 성과활용을 위한 데이터 베이스 구축

현재, 극지미생물유래의 효소에 관하여는 생화학/분자생물학/세포생물학적인 연구정보가 부족한 상황일뿐더러 체계적으로 관리되고 있지 않은 상황이므로, 본 연구진의 주도하에 (Proteases from Polar Microorganisms, PPM) 를 구축하고, 연구에서 얻어진 정보들을 널리 공유하고자 한다. 비슷한 예로써, 현재 peptidase에 관하여는 MEROPS 라 불리는 database가 영국의 Sanger center를 중심으로 구축되어, 약 3000개의 효소가 체계적으로 분류/정리되어, 이를 바탕으로 기존의 정보를 효율적으로 이용하고 새로운 효소와 응용가능성을 탐구하는 학문적인 플랫폼(platform)의 역할을 수행하고 있다. 또한, 독일의 슈트트가르트대학에는 Lipase Engineering Database가 구축되어 있어서, 학문적인 중요성과 산업적인 응용가능성이 큰 lipase 효소의 체계적인 분류/관리를 진행하고 있다.

3 절. 추가연구를 위한 국제 공동연구네트워크의 구성

본 연구과제의 핵심내용인 극지미생물 유래의 가수분해효소 및 퇴행성 뇌질환에 대한 정보들은 본 연구진뿐만 아니라 국내/외의 많은 연구기관들의 주요한 관심사항이라고 할 수 있다. 현재, 이 분야 특히 극지미생물의 효소에 대한 정보가 극히 적은 상황이므로, 본 연구과제의 결과로 얻어진 정보들은 공개적으로 제공할뿐더러, 연구과정에서 획득한 유전자와 단백질들을 국내외의 연구자들에게 제공할 예정이다. 이러한 연구 성과의 공개및 확산을 통하여 관련 연구자들의 편의를 도모하는 동시에 본 연구진들은 이 분야에 학문적인 영향력이 큰 연구 집단으로 성장하고자

한다. 따라서, 본 과제의 수행이 완료되면 본 연구진은 국내의 유수의 연구그룹으로 성장할뿐더러 국제적인 연구네트워크를 구축할 수 있을 것이다. 현재 추진을 계획하고 있는 국제공동연구네트워크는 다음과 같다.

4 절. 인력양성 기대효과

본 연구과제의 수행과정에서 얻어진 생명과학적 지식, 정보 그리고 연구 경험들은 학문적인 중요성을 바탕으로 학술논문들을 통하여 외부에 공개가 될뿐더러 본 연구과제에 참여한 대학원생들에게 유전자의 탐색, 효소의 개량, 단백질 구조의 분석, 퇴행성 뇌질환의 이해, 가수분해에 의한 퇴행성뇌질환에 새로운 치료법 제시 등에 대한 기술과 지식을 습득할 수 있는 좋은 기회가 될 것으로 생각된다. 이 연구과제를 통하여 차세대 연구인력을 양성하는 동시에 생명공학산업 및 보건의료산업에서는 다양한 영역의 지식 및 기술을 습득한 사람이 요구되고 있어 산업체에서 필요로 하는 인력을 양성할 수 있는 좋은 연구 주제이다. 본 연구책임자는 현재 생화학을 전공하는 화학과의 학부생들 및 대학원생의 생화학, 분자생물학, 구조생물학, 생명공학등의 전공교과목의 교육을 담당하고 있으며, 생화학 실험, 분자생물학 실험 등의 실험과목을 지도하고 있으므로 본 연구과제의 수행은 위에 언급한 전공교과목에서 대학원생 및 학부생들의 교육 자료로서도 널리 활용될 것이다. 본 연구과제를 수행하는 연구진에 참여한 대학원생들은 생화학 및 분자생물학, 그리고 미생물학에 대한 다양한 연구경험을 가지고 학위논문을 작성할 예정이며 본 과제와 연관된 논문의 출판등을 통하여 극지관련 연구인력으로 양성될 것을 판단된다. 또, 본 연구과제의 결과물들이 개별 대학원생들의 진로선택에 중요한 영향을 미칠 것으로 판단된다.

제 6 장 참고문헌

[1] A.S. de Miranda, L.S. Miranda, R.O. de Souza, Lipases: Valuable catalysts for dynamic kinetic resolutions. Biotechnol Adv. 33 (2015) 372-93.

[2] C.D. Anobom, A.S. Pinheiro, R.A. De-Andrade, E. C. Aguieiras, G.C. Andrade, M.V. Moura, R.V. Almeida, D.M. Freire, From structure to catalysis: recent developments in the biotechnological applications of lipases, Biomed. Res. Int. (2014) 684506

[3] G.M. Borrelli, D. Trono, Recombinant lipases and phospholipases and their use as biocatalysts for industrial applications, Int. J. Mol. Sci. 16 (2015) 20774-840

[4] T.D. Ngo, B.H. Ryu, H. Ju, E. Jang, K.K Kim, T.D. Kim, Crystallographic analysis and biochemical applications of a novel penicillin-binding protein/b-lactamase homologue from a metagenomic library. Acta Crystallogr. D. Biol. Crystallogr. 70 (2014) 2455-2466.

[5] K. Kim, B.H. Ryu, S.S. Kim, D.R. An, T.D. Ngo, R. Pandian, K.K. Kim, T.D. Kim, Structural and biochemical characterization of a carbohydrate acetylesterase from *Sinorhizobium meliloti* 1021. FEBS Lett. 589 (2015) 117-122.

[6] S.Y. Bae, B.H. Ryu, E. Jang, S. Kim, T.D. Kim, Characterization and immobilization of a novel SGNH hydrolase (Est24) from *Sinorhizobium meliloti*. Appl. Microbiol. Biotechnol. 97 (2013) 1637-1647.

[7] B.H. Ryu, T.D. Ngo, W. Yoo, S. Lee, B.Y. Kim, E. Lee, K.K. Kim, Kim TD. Biochemical and Structural Analysis of a Novel Esterase from *Caulobacter crescentus* related to Penicillin-Binding Protein (PBP). Sci. Rep. 6 (2016) 37978.

[8] C. Oh, B.H. Ryu, D.R. An, D.D. Nguyen, W. Yoo, T. Kim, T.D. Ngo, H.S. Kim, K.K Kim, T.D. Kim, Structural and Biochemical Characterization of an Octameric Carbohydrate Acetylesterase from *Sinorhizobium meliloti*, FEBS Lett. 590 (2016) 1242-1252.

[9] H. Ju, B.H. Ryu, T.D. Kim, Identification, characterization, immobilization of a novel type hydrolase (LmH) from *Listeria monocytogenes*, Int. J. Biol. Macromol. 72 (2015) 63-70.

[10] F. Sievers, A. Wilm, D. Dineen, T.J. Gibson, K. Karplus, W. Li, R. Lopez, H. McWilliam, M. Remmert, J. Söding, J.D. Thompson, D.G. Higgins, Fast, scalable generation of high-quality protein multiple sequence alignments using Clustal Omega. Mol. Syst. Biol. 7 (2011) 539.

[11] R. Gupta, N. Gupta, P. Rathi, Bacterial lipases: an overview of production, purification and biochemical properties, Appl. Microbiol. Biotechnol. 64 (2004) 763-781.

[22] K.E. Jaeger, B. W. Dijkstra, M.T. Reetz, Bacterial biocatalysts: molecular biology, three-dimensional structures, and biotechnological applications of lipases, Annu. Rev. Microbiol. 53 (1999) 315-351.

[13] Y. Chen, D.S. Black, P.J. Reilly, Carboxylic ester hydrolases: Classification and database derived from their primary, secondary, and tertiary structures. Protein Sci. 25 (2016) 1942-1953.

[14] A.S. Bommarius, M.F. Paye, Stabilizing biocatalysts, Chem. Soc. Rev. 42 (2013) 6534-6565.

[15] C.W. Lee, S. Kwon, S.H. Park, B. Y. Kim, W. Yoo, B.H. Ryu, H.W. Kim, S.C. Shin, S. Kim, H. Park, T.D. Kim, J.H. Lee, Crystal Structure and Functional Characterization of an Esterase (EaEST) from *Exiguobacterium* S1. FEBS J. 280 (2013) 6658-71.

제 7 장 출판논문

FEBS Letters

FEBS PRESS

Structural and Biochemical Characterization of an Octameric Carbohydrate Acetylesterase from *Sinorhizobium meliloti*

Changsuk Oh[1,a], Bum Han Ryu[1,2,a], Deu Rae An[1,2,a], Duy Duc Nguyen[1], Wanki Yoo[1,2], Truc Kim[1], Tri Duc Ngo[1], Hee Sook Kim[3], Kyeong Kyu Kim[1] and T. Doohun Kim[2]

1 Department of Molecular Cell Biology, Samsung Biomedical Research Institute, Sungkyunkwan University School of Medicine, Suwon, Korea
2 Department of Chemistry, College of Natural Sciences, Sookmyung Woman's University, Seoul, Korea
3 Department of Food Science and Biotechnology, Kyungsung University, Busan, Korea

Correspondence
K. K. Kim, Department of Molecular Cell Biology, Samsung Biomedical Research Institute, Sungkyunkwan University School of Medicine, Suwon 440-746, Korea
Fax: +82 31 299 6159
Tel: +82 31 299 6152
E-mail: kyeongkyu@skku.edu
T. D. Kim, Department of Chemistry, College of Natural Sciences, Sookmyung Woman's University, Seoul 140-742, Korea
Fax: +82 2 2077 7321
Tel: +82 2 2077 7906
E-mail: doohunkim@sookmyung.ac.kr

*These authors contributed equally to this study.

(Received 31 January 2016, revised 3 March 2016, accepted 9 March 2016, available online 31 March 2016)

doi:10.1002/1873-3468.12135

Edited by Miguel De la Rosa

Carbohydrate acetylesterases, which have a highly specific role among plant-interacting bacterial species, remove the acetyl groups from plant carbohydrates. Here, we determined the crystal structure of Est24, an octameric carbohydrate acetylesterase from *Sinorhizobium meliloti*, at 1.45 Å resolution and investigated its biochemical properties. The structure of Est24 consisted of five parallel β strands flanked by α helices, which formed an octameric assembly with two distinct interfaces. The deacetylation activity of Est24 and its mutants around the substrate-binding pocket was investigated using several substrates, including glucose pentaacetate and acetyl alginate. Elucidation of the structure-function relationships of Est24 could provide valuable opportunities for biotechnological explorations.

Keywords: carbohydrate acetylesterase; site-directed mutagenesis

Carbohydrate-active enzymes, which explicitly act on an extreme variety of substrates, modulate complex carbohydrates for a wide variety of biological functions. To date, the CAZy database (http://www.cazy.org) recognizes 16 carbohydrate esterase (CE) families based on sequence similarities, cofactors, and catalytic residues [1–3]. The diversity of CE family reflects intrinsic differences in molecular structures, cellular locations, substrate specificities, and biochemical properties. In general, CEs remove ester functional groups in simple or complex carbohydrates, preparing the carbohydrates for further modification by glycoside hydrolases (GHs) [4,5]. In addition to their importance in cellular functions, CEs are extensively used for biotechnological applications. Among the CE families, CE2 (acetylxylan esterases), CE3 (acetylxylan

Abbreviations
CE, carbohydrate esterase; GHs, glycoside hydrolases; NSAID, nonsteroidal anti-inflammatory drug; RGAE, rhamnogalacturonan acetylesterase.

esterases), CE12 (pectin acetylesterases, rhamnogalacturonan acetylesterases, and acetylxylan esterases), and CE13 (pectin acetylesterases) proteins are classified as SGNH family proteins (Pfam accession number CL0264), which are characterized by the presence of four conserved residues, Ser (S), Gly (G), Asn (N), and His (H) [6]. The nucleophilic Ser residue in the highly conserved GDS motif is equivalent to the classical GXSXG motif of canonical α/β hydrolases and its main chain atoms serve as the proton donors for the oxyanion hole. Catalysis in SGNH family proteins is triggered by the conserved His, and the formation of tetrahedral intermediate is supported by Gly and Asn [7,8]. Furthermore, through the deacetylation process, CE3 and CE12 of the SGNH family are involved in a wide range of biological processes including communications between plant and bacterial cells [9].

Although the SGNH family of enzymes has been extensively investigated in recent years, few studies have examined the broad substrate specificities, enzyme promiscuity, and catalytic mechanisms of these proteins at the molecular level. Recently, CEs of the SGNH family were identified from several microorganisms, including *Geobacillus stearothermophilus* [10], *Butyrivibrio proteoclasticus* [11], *Neisseria gonorrhoeae* [12], and *Escherichia coli* O157:H7 [13]. However, little information on the structures and catalytic mechanisms of these CEs is available. Furthermore, these enzymes have not been well studied in *Rhizobia* species, despite their important roles in efficient symbiosis. In previous reports, a recombinant SGNH hydrolase of 24 kDa (NCBI Reference Sequence: WP_010968046, Est24) from *Sinorhizobium meliloti*, a gram-negative nitrogen-fixing bacterium, was characterized and crystallized [14,15]. Here, we report the crystal structure of Est24 to 1.45 Å resolution, and characterize its catalytic activity using a variety of substrates. Furthermore, mutational analysis was carried out to identify functional key residues determining the substrate specificity of Est24. Since Est24 has important biotechnological potential in the biotransformation process for the production of valuable industrial compounds, current results will be beneficial for biotechnology applications.

Materials and methods

Protein expression, purification, and crystallization

The *est24* gene was amplified from chromosomal DNA of *Sinorhizobium meliloti* (Korean Collection for Type Cultures [WDCM 597], Seoul, Korea). Next, the *est24* gene was inserted into pQE30 (Qiagen, Germany) and Est24 protein was expressed with a hexa-His tag. The resulting recombinant DNA in the pQE30 vector was transformed into *Escherichia coli* XL1-Blue (Stratagene, CA, USA) as previously described [14,15]. Site-directed mutagenesis were carried out by QuickChange Site-Directed Mutagenesis Kit in accordance with the manufacturer's instructions. The PCR product was incubated with DpnI at 37 °C for 1 h, and transformed to *E. coli* DH5α. In general, three colonies were randomly selected for sequencing and the verified plasmid was then transformed into *E. coli* BL21 (DE3) using the calcium chloride transformation method for overexpression. For crystallization, 6 mg·mL^{-1} of Est24 in 20 mM Tris-HCl (pH 8.0) was incubated with 0.2 M ammonium phosphate (pH 4.6), and 20% polyethylene glycol (PEG) 3350 for 7 days.

X-ray data collection, processing, and analysis

Diffraction data (180° rotation with 0.5° oscillation and 3 s of exposure) were collected using 25% glycerol-containing mother liquor with an ADSC Quantum 315 CCD on beamline at Pohang Accelerator Laboratory (PAL, 7A, Pohang, Korea). The native data set was obtained at a wavelength of 0.9793 with 1.45 Å resolution, and all data were integrated, scaled, and processed using the HKL-3000 package [16].

Determination and analysis of the structure of Est24

The crystal structure of Est24 was determined by molecular replacement using MOLREP [17] with an arylesterase from *Mycobacterium smegmatis* (PDB ID:2Q0S) as an initial model. Model building and structural refinement were performed using the COOT program [18] and REFMAC [19] in the CCP4 package and the PHENIX program [20]. The final structure was visualized using PyMOL for graphical presentation (PyMOL Molecular Graphics System). The coordinates and structural factors of Est24 were deposited in the Protein Data Bank with the accession code 5HOE. Sequences related to Est24 were retrieval in FASTA format, and multiple sequence alignments were generated by the CLUSTALW program and then rendered with ESPript [21]. The substrate-binding pocket was analyzed with CASTp [22].

Preparation of ketoprofenyl acetate

Five grams of ketoprofen was dissolved in 50 mL THF and 1 M borane was added with constant stirring for 12 h. The mixture was then extracted using dichloromethane, and crude product was purified on silica gel with a hexane-ethyl acetate (5 : 2)-containing solution. After condensation, 0.22 g of 4-dimethylaminopyridine, 4.5 mL trimethylamine, and 1.81 mL acetyl anhydride were added and stirred for 4 h. After extraction, the final product was purified on silica gel with a hexane-ethyl acetate-containing solution. The NMR spectrum of ketoprofenyl acetate was

recorded using a Varian INOVA AS400 (Varian, CA, USA) operating at 400 MHz for ^{1}H.

Enzyme assay of Est24

The hydrolytic substrate specificity of Est24 was tested with 1-naphthyl acetate (1-NA), 1-naphthyl butyrate (1-NB), 2-naphthyl acetate (2-NB), and 1-naphthyl phosphate (1-NP) as substrates. Absorbance was determined at 310 nm using a microplate reader (BioTek, VT, USA).For pH indicator-based colorimetric assays, 4.1 μM of Est24 and its mutant proteins were added to substrate solutions containing phenol red (2 mg·mL^{-1}) [8,23]. The substrates containing acetate groups were glucose pentaacetate (25 μM), cellulose acetate (1% [w/v]), O-acetylalginate (0.5% [w/v]), glyceryl tributyrate, glyceryl trioleate, fish oil, olive oil, *tert*-butyl acetate, α-terpinyl acetate, and linalyl acetate. The standard assay solution contained 0.3 mM substrate and 4.1 μM protein in 0.9 mL buffer containing 20 mM Tris-HCl (pH 8.0). To confirm the role of each residue in the active site, mutants of Est24 including S13A, R69A, N96A, Y101A, W151A, F152A, or M155A were purified, and their activities against various substrates were investigated. The fluorescence intensity of 4-methylumbelliferone (4-MU) was used to investigate the activities of Est24 in an ultraviolet illumination box. The reaction mixture consisted of 0.5 mL of 50 mM sodium phosphate buffer (pH 7.0) containing 0.25 mM 4-MU acetate and 4-MU phosphate with purified wild-type and mutant Est24 proteins. In addition, the level of hydrolyzed acetic acids from ketoprofenyl acetate was also measured using an acetic acid determination kit (Megazyme Inc., Chicago, IL, USA).

Results and Discussion

Sequence analysis of Est24

In phylogenetic analysis, Est24 was assigned to CE family III (CE3), which was clustered with an acetylxylan esterase (CesA, Q9RLB8) from *Ruminococcus*

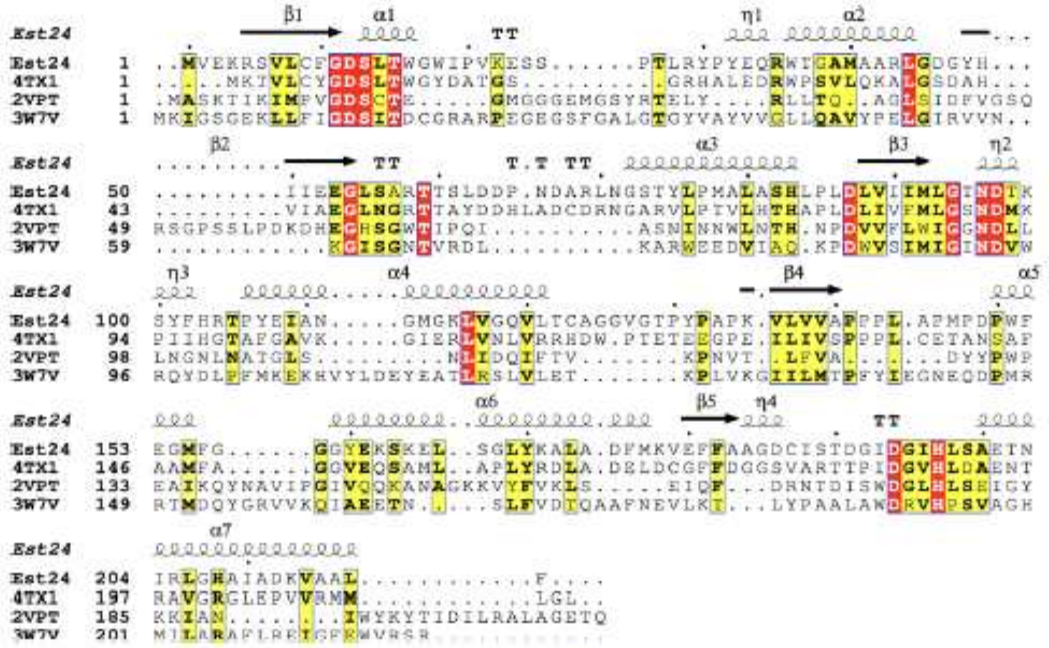

Fig. 1. Multiple sequence alignment of Est24 with three related enzymes (4TX1: a carbohydrate acetylesterase from *Sinorhizobium meliloti*, 2VPT: a carbohydrate esterase (CE10) from *Clostridium thermocellum*, and 3W7V: an acetylxylan esterase (CE10) from *Geobacillus stearothermophilus*). Sequences retrieved from the NCBI server were aligned using CLUSTAL OMEGA 1.2.1, and rendered using ESPRIPT 3.0. Secondary structure elements of Est24 are shown at the top. Identical residues are shown in red boxes, and similar residues are shown in blue boxes. 'α', 'β', 'η', and 'T' represent α helix, β strand, 3_{10} helix, and β turn, respectively. The numbers represent the positions of the amino acid residues starting from the N terminus of the protein.

flavefaciens, an acetylxylan esterase (bnaIII, O13497) from *Neocallimastix patriciarum*, or a cellulose-binding protein (Q47KJ9) from *Thermobifida fusca* (Fig. S1). Although several CE3 proteins have been identified, only two crystal structures of CE3 enzymes have been determined, including cellulosomal family 3 (CtCes3, PDB ID:2VPT) from *Clostridium thermocellum* [24] and a carbohydrate acetylesterase (Sm23, PDB ID:4TX1) from *Sinorhizobium meliloti* 1021 [8]. These two enzymes have 18.6% and 37.1% sequence identity with Est24, respectively, and only 25 residues are completely conserved among all three enzymes (Fig. 1). In addition, Est24 has limited sequence similarity (12.8%) to an acetyl-xylooligosaccharide esterase from *Geobacillus stearothermophilus* (Axe2, PDB ID:3W7V) which was recently identified as a new CE family protein [10]. Using the DALI server, two other structures with high sequence similarity to Est24 were also observed: an aryl esterase (MsAcT) from *Mycobacterium smegmatis* (PDB ID:2Q0Q; *Z*-score: 39.7) [25] and a putative aryl esterase from *Agrobacterium tumefaciens* (PDB ID:3DCI; *Z*-score: 31.7). Multiple alignments showed that Est24 contained the catalytic triad residues serine (Ser^{13}), aspartate (Asp^{194}), and histidine (His^{197}). The D-X-X-H motif was localized in the C-terminal region in the primary structure; however, it was spatially close to Ser^{13} in the GDS motif.

Overall structure of Est24

The final structure of Est24 was refined to a crystallographic *R*-factor of 17.15% (R_{free} = 21.63%) at 1.45 Å resolution. X-ray diffraction data with refinement statistics are shown in Table 1, and all amino acid residues were within the allowed regions of the Ramachandran plot. Est24 is composed of seven α helices encompassing one β sheet, in which five β strands (β2, β1, β3, β4, and β5) were aligned in parallel in a left-handed twist orientation, and the five α helices (α2, α3, α4, α6 and α7) enclosed the central β sheet (Fig. 2A). The α helices were composed of residues of 13–16 (α1), 36–44 (α2), 72–83 (α3), 106–122 (α4), 150–156 (α5), 159–177 (α6), and 200–217 (α7), whereas the central β sheet was formed by residues 5–11 (β1), 48–54 (β2), 88–92 (β3), 135–140 (β4), and 180–183 (β5). Figure 2B shows the electrostatic surface of Est24, highlighting the slightly positively charged-surface encircling the entrance of the substrate-binding site. Interestingly, two helices (α5 and α1) were located at the entrance toward the catalytic triad.

The catalytic site of Est24 was formed by the residues Ser^{13}, Asp^{194}, and His^{197}, which were situated on the C-terminal end of the central β sheet (Fig. 2C).

Table 1. Data processing and refinement statistics for Est24. The score in the bracket represents the highest resolution shell. RMSD, root mean square deviation.

	Est24
Data collection	
Space Group	C2
Cell Dimensions	
a, *b*, *c* (Å)	129.09, 88.63, 86.15
α, β, γ (°)	90, 114.30, 90
Wavelength Resolution (Å)	0.9793
R_{merge}[a]	9.4 (38.9)
$I/\sigma I$	20.3 (2.0)
Completeness (%)	93.7 (73.3)
Redundancy	2.9 (2.0)
Refinement	
Resolution (Å)	35.75–1.45
No. of reflections	145 939
R_{work}/R_{free}[b] (%)	17.17/21.64
No. of Atoms	7670
Average B-factors (Å^2)	21.24
RMSD	
Bond length (Å)	0.008
Bond angles (°)	1.027
Ramachandran statistics	
Favored (%)	96.32
Allowed (%)	3.68
Outlier (%)	0.00

[a] $R_{merge} = \Sigma_{hkl}\Sigma_i |I_i(hkl) - < I(hkl) >| / \Sigma_{hkl}\Sigma_i I_i(hkl)$, where $I_i(hkl)$ is the *i*th measurement of the intensity of the reflection (*hkl*), and $I(hkl)$ is the mean intensity measurements.
[b] R_{free} was obtained from a randomly selected set (5%) and R_{work} was obtained from a training set (95%).

Ser^{13} was situated at the N-terminal end of α1, while Asp^{194} and His^{197} were located on a loop between β5 and α7. Using site-directed mutagenesis, Ser^{13} was confirmed as a catalytic residue in Est24 [14]. The two long loops, the region between β5 and α7 (Ala^{183}–Ala^{200}), and the region between α1 and α2 (Trp^{16}–Trp^{36}) coordinated Asp^{194} and His^{197} toward Ser^{13} to form the catalytic triad (Fig. 2D). The oxygen (Oγ) of Ser^{13} formed a hydrogen bond (3.0 Å) with the nitrogen (Nε2) of His^{197}, while the oxygen (Oδ2) of Asp^{194} was within the hydrogen-bonding distance (2.7 Å) of the nitrogen (Nδ1) of His^{197}. Furthermore, the backbone atoms of Ser^{13}, Ala^{57}, and Asn^{96} were involved in the formation of an oxyanion hole to stabilize the tetrahedral intermediate during catalysis (Fig. 2C). The long loop (Gly^{54}–Gly^{72}) connecting β2 and α3 harbored an alanine (Ala^{57}), and asparagine (Asn^{96}) was situated at the loop between β3 and α4 (Met^{92}–Pro^{106}). The surface-exposed substrate-binding site formed by two α helices (α1 and α5) and four loops (Gly^{11}–Ser^{13}, Gly^{54}–Gly^{72}, Met^{92}–Pro^{106}, and Ala^{183}–Ala^{200}), is possibly involved in substrate recognition.

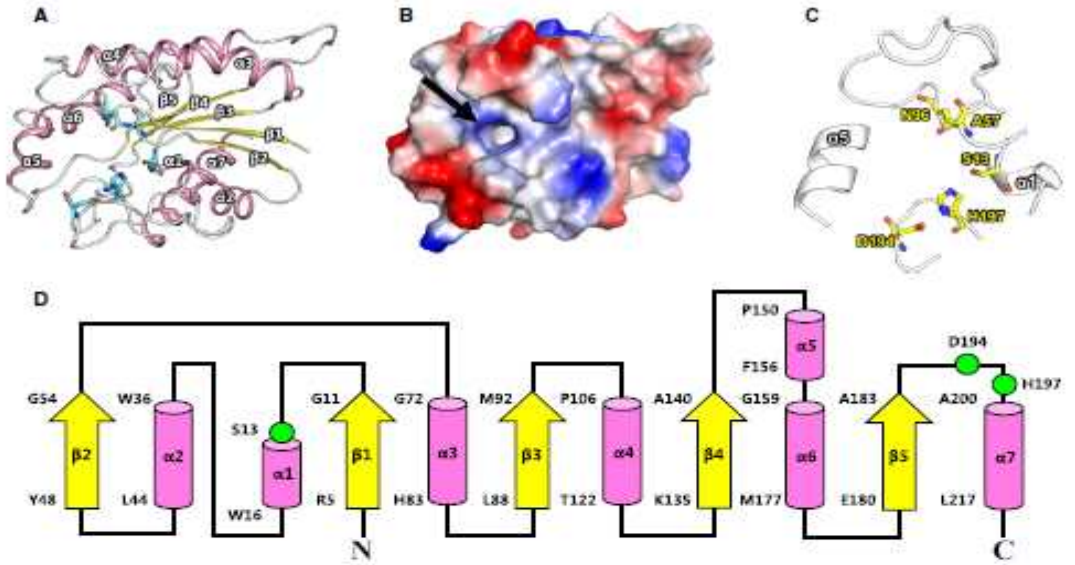

Fig. 2. Structural features of Est24. (A) Ribbon diagram of Est24. Secondary structures of α helices (pink) and β strands (yellow) with the catalytic triad (cyan, ball-and-stick models) are shown. (B) Surface electrostatic potential of Est24 (positive: blue, negative: red, and neutral: white). The substrate-binding pocket is indicated with a black arrow. (C) Highly conserved residues around the catalytic triad are depicted by ball-and-stick models with labels. Two α helices (α1 and α5), and three loops (β2/α3, β3/α4, and β5/α7) are also shown. (D) Topology diagram of Est24. Secondary structures (α helix in pink and β strand in yellow) with catalytic residues (green) are shown. Starting and ending residues in each secondary structure are also indicated.

Oligomeric nature of Est24

By oligomeric state analysis using QtPISA [25], we found that two tetramers exhibiting twofold crystallographic symmetry formed an octameric Est24. Consistent with this, the apparent molecular weight of Est24 determined by analytical size-exclusion chromatography was similar to the calculated molecular weight of the octameric form of Est24 (data not shown). Moreover, three enzymes homologous to Est24 (Sm23, CtCes3, and Axe2) have been shown to exist in an oligomeric formation [8,10,24]. In the oligomeric assembly of Est24, the central pore was almost square, with 15.7 Å for each side, and the catalytic triad faced outward, permitting the efficient binding and release of large carbohydrates. For octamer formation, four independent molecules of Est24 were arranged in two identical dimers, and each molecule was almost perfectly superimposable, with an overall RMSD value of 0–0.19 Å.

The octameric assembly of Est24 was arranged as a dimer of tetramers, and monomer-monomer interfaces of Est24 could be divided into two types: subtype 1 and subtype 2 (Fig. 3). The subtype 1 interface was formed mainly by β2, α3, α1/α2 loop, and α4/β4 loop with an interface area of 958 $Å^2$. Four salt bridges including Glu^{53} (on the β2 strand)–His^{83} (on the α3 helix) were observed. Sixteen hydrogen bonds involving Thr^{27}, Arg^{29}, and His^{83} were formed, and Trp^{16}, Tyr^{75}, Leu^{84}, and Tyr^{131} were key residues in nonpolar contacts at this interface. The subtype 2 interface (466.1 $Å^2$) contained residues mainly from α1, α4, α5, β2/α3 loop, and the α6/β5 loop as well as two long connecting loops of β2/α3 and α1/α2. Six hydrogen bonds with two salt bridges including Glu^{23} (on the α1/α2 loop)–Lys^{178} (on the α6/β5 loop) were formed in this interface. Interestingly, structural analysis revealed that the substrate-binding pocket was distant from two interfaces (subtype 1 and subtype 2), implying that these interfaces may have little impact on substrate binding (Fig. 3 bottom right).

Functional analysis of Est24

Deacetylation of carbohydrates by Est24 was investigated using glucose pentaacetate, cellulose acetate, and

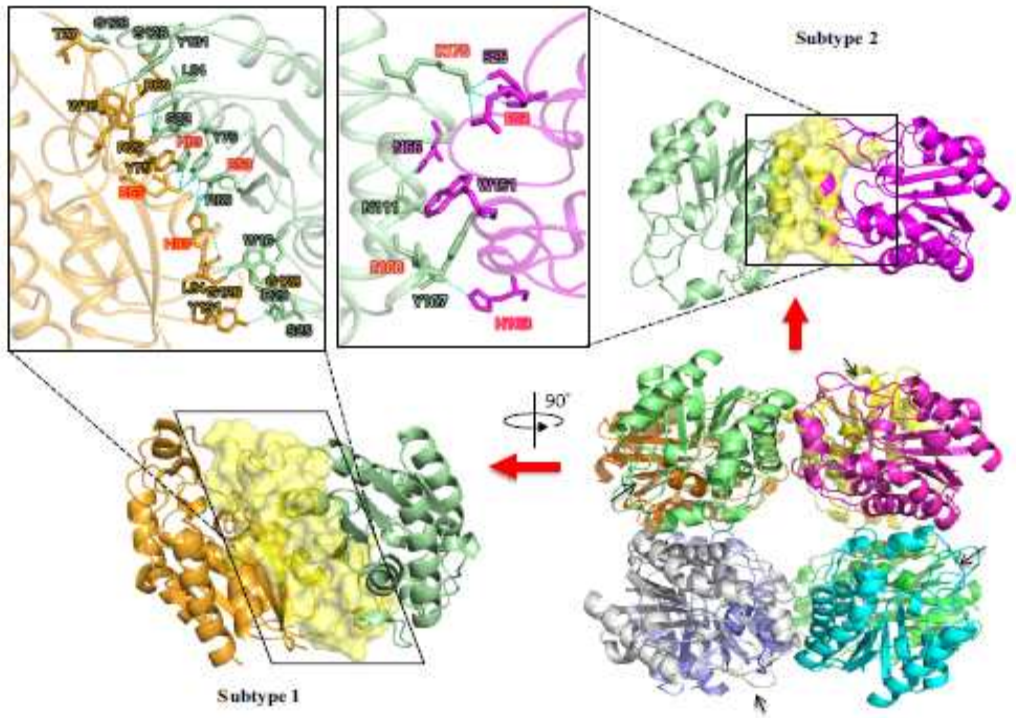

Fig. 3. Representation of the octameric structure with ribbon diagrams. Each subunit are colored differently. Two dimeric interfaces were detected from the putative octamer state of Est24: subtype 1 (bottom left) and subtype 2 (top right) interfaces are shown as surfaces presentation (yellow) with corresponding bilateral monomers. Residues involved in the formation of the dimeric surfaces are shown in insets. The residues that make salt bridges between two subunits are labeled red. The catalytic serine (Ser^{13}) of each subunit is shown as black arrows.

acetylalginate as substrates. A pH indicator-based colorimetric assay using red-to-yellow color change was employed to monitor the release of acetic acid. Est24 showed significant enzyme activity toward glucose pentaacetate, but showed little enzyme activity toward cellulose acetate (Fig. 4A). In addition, deacetylation activity toward O-acetylalginate was observed (Fig. 4B). The substrate specificity of Est24 toward naphthyl derivatives was analyzed in Tris-HCl buffer (20 mM, pH 8.0) at 25 °C. As shown in Fig. 4C, the highest activity was obtained with 1-NA, followed by 2-NA, and 1-NB. Specifically, the hydrolytic level of 1-NB was only 36% that of 1-NA. In contrast, no significant activity was observed in 1-NP (Fig. 4C).

The ability of Est24 to hydrolyze tertiary alcohol acetylesters was examined using *tert*-butyl acetate, linalyl acetate, and α-terpinyl acetate as substrates [26]. As shown in Fig. 4D, Est24 hydrolyzed only *tert*-butyl acetate, but had almost no activity toward linalyl acetate or α-terpinyl acetate. Furthermore, glyceryl tributyrate solutions became yellow gradually with the addition of Est24, suggesting that Est24 was able to hydrolyze simple lipids. However, no significant hydrolytic activities were detectable toward glyceryl trioleate, fish oil, or olive oil (Fig. 4E). A catalytic-site mutant (S13A) was shown to exhibit complete loss of activity under the same reaction conditions. Finally, Est24 was shown to effectively hydrolyze 4-methylumbelliferyl acetate (4-MU acetate), which was similar to a putative carbohydrate acetylesterase (Sm23) from *Sinorhizobium meliloti* [8]. High fluorescence due to the formation of 4-methylumbelliferone was observed in the Eppendorf tube containing 4-methylumbelliferyl acetate (4-MU acetate). However, no fluorescence sig-

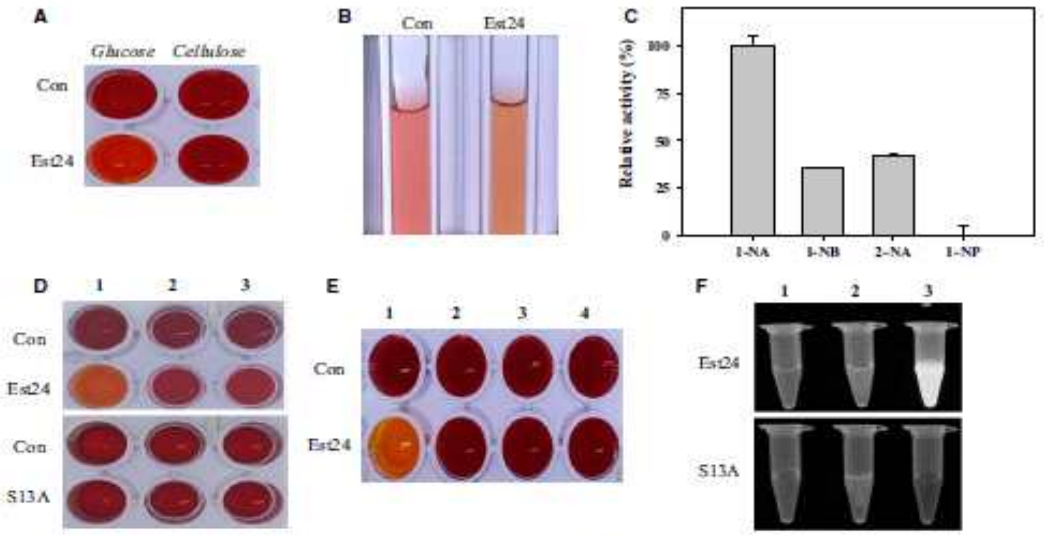

Fig. 4. Biochemical activities of Est24. (A) Hydrolysis of two simple carbohydrates (glucose pentaacetate and cellulose acetate) by Est24 was investigated using pH shift assay in which released acids change the color to yellow. (B) Hydrolysis of acetyl alginate (0.5%) by Est24 is indicated by color change. (C) Substrate specificity of Est24 toward naphthyl group esters (1-naphthyl acetate [1-NA], 1-naphthyl butyrate [1-NB], 2-naphthyl acetate [2-NA], and 1-naphthyl phosphate [1-NP]) was determined [8]. (D) Hydrolysis of tertiary alcohol esters (from left to right; tertbutyrate (1), α-terpinyl acetate [2], linalyl acetate [3]) by Est24 and its S13A mutant is indicated by pH shift assay. (E) Hydrolysis of glyceryl tributyrate (1), glyceryl trioleate (2), olive oil (3), and fish oil (4) was measured. (F) Activities of Est24 and S13A against 4-methylumbelliferyl (4-MU)-acetate were determined by measuring emitted fluorescence from 4-methylumbelliferone.

nal was observed in 4-methylumbelliferyl phosphate (4-MU phosphate) (Fig. 4F).

Substrate-binding pocket of Est24

Although the active sites of members of the carbohydrate acetylesterase family are structurally related, notable differences were observed in the orientations and shapes of the substrate-binding pockets. As shown in Fig. 5, among Est24, Sm23, CtCes3, Axe2, and rhamnogalacturonan acetylesterase (RGAE), there were significant spatial differences in the regions peripheral to the active sites, which manifests their dissimilarity in substrate specificity and regulation mechanism. Using CASTp, the areas and volumes of the substrate-binding pockets were calculated for five representative enzymes. The overall pocket structures in Est24, Sm23, and CtCes3 were similar in terms of area (A) and volume (V) (Est24: $A = 89.2$ Å^2, $V = 35.2$ Å^3, Sm23: $A = 68.4$ Å^2, $V = 34.6$ Å^3, and CtCes3: $A = 94.1$ Å^2, $V = 42.5$ Å^3, compared with those of Axe2 ($A = 12.2$ Å^2, $V = 2.2$ Å^3) and RGAE ($A = 10.4$ Å^2, $V = 2.1$ Å^3).

Specifically, the two long extended loops of β2/α3 (Gly^{54}–Gly^{72}) and β3/α4(Met^{92}–Phe^{106}) of Est24 constituted the upper region of the substrate-binding sites (Fig. 5B). These two loops, despite their length, made few contacts with the rest of Est24, which may explain the flexibility and enlargement of the substrate-binding pocket during catalysis. Specifically, the β2/α3 loop was proposed to act as a wide, flexible entrance for efficient ligand binding. In the upper regions of the binding pocket, Arg^{69} in β2/α3 and Asn^{96} in β3/α4 loop may facilitate substrate entry by electrostatic interactions and hydrogen bonds. In addition, Tyr^{101} could be used to entrap the hydrophobic part of an incoming substrate. Although these two β2/α3 and β3/α4 loops seemed to form the main entrance site for the substrate, access to the catalytic triad was also restricted by the short helix of α5 (Pro^{150}–Phe^{156}). Interestingly, other proteins seemed to have a similar helix (α5 helices in Est24 and Sm23 or α4 helices in CtCes3 and Axe2) that could limit the sizes of the substrate-binding pocket (Fig. 5C–E). Only RGAE had no corresponding regions in the substrate-binding pocket, implying that this protein may have a different mode of substrate binding (Fig. 5F).

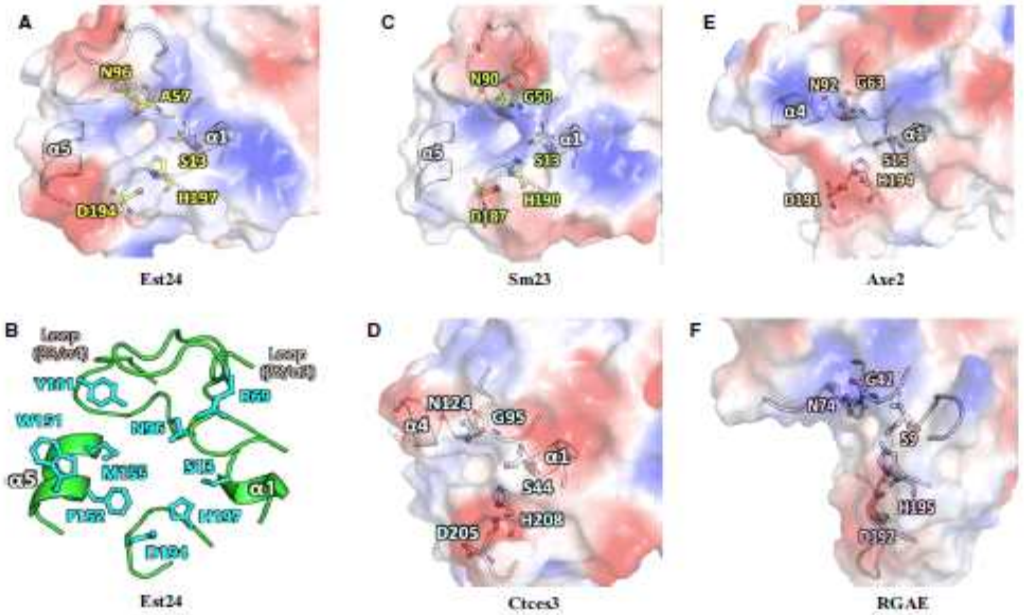

Fig. 5. Substrate-binding pockets of Est24 and other related carbohydrate acetylesterases are drawn by surface charge distribution. (A, B) Est24, (C) Sm23(4TX1), (D) CtCes3(2VPT), (E) Axe2(3W7V), and (F) RGAE(1DEO). Secondary structure is drawn by ribbon model and the residues involved in the catalytic activity are drawn by ball-and-stick models, and labeled. In (B), residues for site-directed mutagenesis are also noted. The shape of the pockets among the homologous enzymes were different, although important catalytic residues (Ser, Gly, Asn, Asp, and His) are highly conserved.

Mutational analysis of Est24

To investigate the functional role of amino acids in the substrate-binding pocket, 20 residues in this region were selected and substituted with glycine by site-directed mutagenesis. After expression and purification, the catalytic activities of seven mutants (S13A, R69A, N96A Y101A, W151A, F152A, and M155A) were tested and compared with those of wild-type Est24. As shown in Fig. 6A, W151A, F152A, and M155A had activities similar to that of wild-type Est24 for 1-NA hydrolysis. In contrast, R69A only retained ~ 25% of the activity of wild-type Est24. Similarly, for the hydrolysis of glyceryl tributyrate, W151A, F152A, and M155A did not affect the catalytic activity of Est24 (Fig. 6B). In contrast, R69A and Y101A mutants had almost no activity, suggesting that these residues in the loop regions (β2/α3 loop and β3/α4 loop) may be involved in the hydrolysis of glyceryl tributyrate. For tertiary alcohol acetylesters, only M155A showed similar activity to wild-type Est24 (Fig. 6C), although most mutants were not able to effectively hydrolyze these compounds. However, in 4-MU acetate assays, most mutants showed high fluorescence except S13A and N96A (Fig. 6D). These mutational results indicated that R69 and N96 as well as Y101 in the upper left region of the substrate-binding pocket were key residues involved in the activity of Est24.

Based on the fact that Est24 can effectively hydrolyze a wide variety of acetate-containing substrates, the hydrolysis of ketoprofenyl acetate by Est24 was investigated. Ketoprofen, (*R,S*)-2-(3-benzoylphenyl) propionic acid, is a nonsteroidal anti-inflammatory drug (NSAID), a widely drug to alleviate pain and inflammation from tissue injury. To date, several microbial esterases have been reported to be potentially useful for the preparation of ketoprofen [27,28]. Est24 showed significant ketoprofenyl acetate hydrolytic activity, although most mutants showed significantly decreased levels of enzyme activity (Fig. 7). Interestingly, the M155A mutant was shown to have activity similar to that of wild-type Est24.

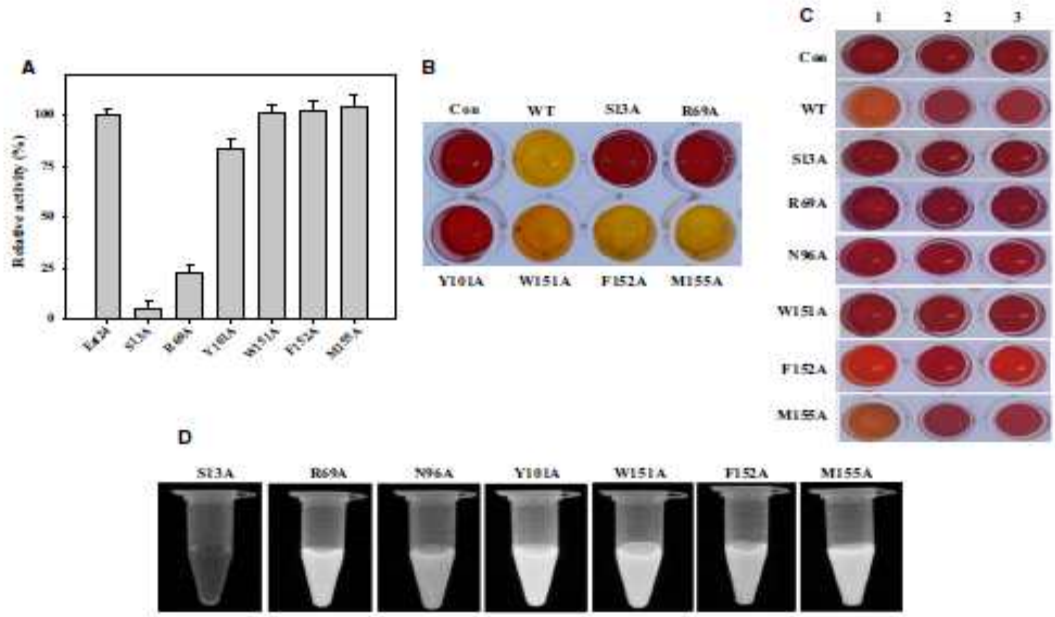

Fig. 6. Activity assay of Est24 and its mutants (A) Hydrolysis of 1-naphthyl acetate (1-NA) by Est24 and its mutants (S13A, R69A, W151A, F152A, M155A) was measured at 310 nm. (B) Hydrolysis of glyceryl tributyrate was measured using pH shift assay accompanied by color change. (C) Hydrolysis of tertiary alcohol esters by Est24 and its mutants (1: terbutyrate, 2: α-terpinyl acetate, 3: linalyl acetate) was examined by pH shift assay. (D) Hydrolysis of 4-methylumbelliferyl (4-MU)-acetate by Est24 and its mutants was detected by emitting fluorescence signal.

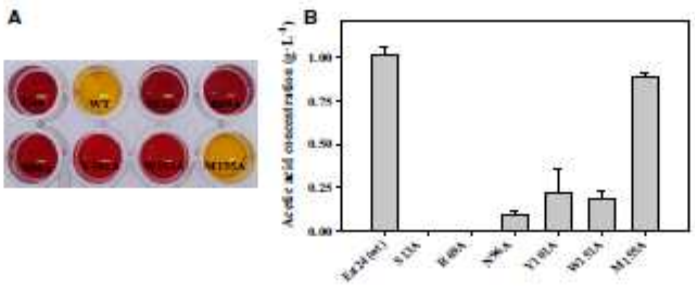

Fig. 7. Preparation of ketoprofen using Est24 and its mutants using ketoprofenyl acetate as a substrate. Ketoprofen formation was confirmed by color change to yellow (A). The amount of released acetic acids during the conversion of ketoprofenyl acetate to ketoprofen was determined using an acetic acid determination kit (B).

In conclusion, the crystal structure of Est24, an octameric carbohydrate acetylesterase from *Sinorhizobium meliloti*, was determined at 1.45 Å resolution and its catalytic properties were investigated using a wide variety of substrates. In addition, site-directed mutagenesis has been used to elucidate the structure-function relationships of Est24. Furthermore, deacetylation of ketoprofen acetate by Est24 was investigated, and Est24 was shown to be a promising biocatalyst for the preparation of ketoprofen. The results in this study may be useful for further exploration of industrial applications of carbohydrate acetylesterases.

Acknowledgements

This work was supported by the Medical Research Center Program (No. 2011-0030074) through National Research Foundation (NRF) grant funded by the

Korean government (MSIP). This work was also supported by the National Research Foundation of Korea (NRF-2014R1A1A2056859) and the Polar Academic Program (PD15010) of the Korea Polar Research Institute (KOPRI) to T.D.K. K.K.K. is supported by the Next-Generation BioGreen 21 Program (SSAC PJ001107005), and the National Research Foundation of Korea (NRF) grant (2011-0028878).

Author contributions

TDK and KKK conceived and supervised the study; CO, BHR and DRA performed experiments; DDN, WY, TK, TDN, HSK, KKK and TDK analyzed data; CO, BHR, TDK and PK wrote the manuscript.

References

1 Lombard V, Golaconda Ramulu H, Drula E, Coutinho PM and Henrissat B (2014) The carbohydrate-active enzymes database (CAZy) in 2013. *Nucleic Acids Res* **42**, D490–D495.

2 Biely P (2012) Microbial carbohydrate esterases deacetylating plant polysaccharides. *Biotechnol Adv* **30**, 1575–1588.

3 Davies GJ, Gloster TM and Henrissat B (2005) Recent structural insights into the expanding world of carbohydrate-active enzymes. *Curr Opin Struct Biol* **15**, 637–645.

4 Geisler-Lee J, Geisler M, Coutinho PM, Segerman B, Nishikubo N, Takahashi J, Aspeborg H, Djerbi S, Master E, Andersson-Gunnerås S *et al.* (2006) Poplar carbohydrate-active enzymes. Gene identification and expression analyses. *Plant Physiol* **140**, 946–962.

5 Pinard D, Mizrachi E, Hefer CA, Kersting AR, Joubert F, Douglas CJ, Mansfield SD and Myburg AA (2015) Comparative analysis of plant carbohydrate active enZymes and their role in xylogenesis. *BMC Genom* **16**, 402.

6 Akoh CC, Lee GC, Liaw YC, Huang TH and Shaw JF (2004) GDSL family of serine esterases/lipases. *Prog Lipid Res* **43**, 534–552.

7 Lesic Aslet I, Ivic N, Kovacic F, Schell S, Knorr J, Krauss U, Wilhelm S, Kojic-Prodic B and Jaeger KE (2010) Probing enzyme promiscuity of SGNH hydrolases. *ChemBioChem* **11**, 2158–2167.

8 Kim K, Ryu BH, Kim SS, An DR, Ngo TD, Pandian R, Kim KK and Kim TD (2015) Structural and biochemical characterization of a carbohydrate acetylesterase from *Sinorhizobium meliloti* 1021. *FEBS Lett* **589**, 117–122.

9 Wilhelm S, Rosenau F, Kolmar H and Jaeger KE (2011) Autotransporters with GDSL passenger domains: molecular physiology and biotechnological applications. *ChemBioChem* **12**, 1476–1485.

10 Lansky S, Alalouf O, Solomon HV, Alhassid A, Govada L, Chayen NE, Belrhali H, Shoham Y and Shoham G (2014) A unique octameric structure of Axe2, an intracellular acetyl-xylooligosaccharide esterase from *Geobacillus stearothermophilus*. *Acta Crystallogr D Biol Crystallogr* **70**, 261–278.

11 Till M, Goldstone DC, Attwood GT, Moon CD, Kelly WJ and Arcus VL (2013) Structure and function of an acetyl xylan esterase (Est2A) from the rumen bacterium *Butyrivibrio proteoclasticus*. *Proteins* **81**, 911–917.

12 Pfeffer JM, Weadge JT and Clarke AJ (2013) Mechanism of action of Neisseria gonorrhoeae O-acetylpeptidoglycan esterase, an SGNH serine esterase. *J Biol Chem* **288**, 2605–2613.

13 Rangarajan ES, Ruane KM, Proteau A, Schrag JD, Valladares R, Gonzalez CF, Gilbert M, Yakunin AF and Cygler M (2011) Structural and enzymatic characterization of NanS (YjhS), a 9-O-Acetyl N-acetylneuraminic acid esterase from Escherichia coli O157:H7. *Protein Sci* **20**, 1208–1219.

14 Bae SY, Ryu BH, Jang E, Kim S and Kim TD (2013) Characterization and immobilization of a novel SGNH hydrolase (Est24) from Sinorhizobium meliloti. *Appl Microbiol Biotechnol* **97**, 1637–1647.

15 Ryu BH, Nguyen DD, Ngo TD, Oh C, Pandian R, Kim KK and Kim TD (2014) Crystallization and preliminary X-ray analysis of a highly stable novel SGNH hydrolase (Est24) from *Sinorhizobium meliloti*. *Acta Crystallogr F Struct Biol Commun* **70**, 193–195.

16 Minor W, Cymborowski M, Otwinowski Z and Chruszcz M (2006) HKL-3000: the integration of data reduction and structure solution – from diffraction images to an initial model in minutes. *Acta Crystallogr D Biol Crystallogr* **62**, 859–866.

17 Vagin A and Teplyakov A (2010) Molecular replacement with MOLREP. *Acta Crystallogr D Biol Crystallogr* **66**, 22–25.

18 Emsley P and Cowtan K (2004) Coot: model-building tools for molecular graphics. *Acta Crystallogr D Biol Crystallogr* **60**, 2126–2132.

19 Murshudov GN, Skubak P, Lebedev A, Pannu NS, Steiner RA, Nicholls RA, Winn MD, Long F and Vagin AA (2011) REFMAC5 for the refinement of macromolecular crystal structures. *Acta Crystallogr D Biol Crystallogr* **67**, 355–367.

20 Afonine PV, Grosse-Kunstleve RW, Echols N, Headd JJ, Moriarty NW, Mustyakimov M, Terwilliger TC, Urzhumtsev A, Zwart PH and Adams PD (2012) Towards automated crystallographic structure refinement with phenix.refine. *Acta Crystallogr D Biol Crystallogr* **68**, 352–367.

21 Gouet P, Robert X and Courcelle E (2003) ESPript/ENDscript: extracting and rendering sequence and 3D information from atomic structures of proteins. *Nucleic Acids Res* **31**, 3320–3323.
22 Dundas J, Ouyang Z, Tseng J, Binkowski A, Turpaz Y and Liang J (2006) CASTp: computed atlas of surface topography of proteins with structural and topographical mapping of functionally annotated residues. *Nucleic Acids Res* **34**, W116–W118.
23 Ngo TD, Ryu BH, Ju H, Jang E, Kim KK and Kim TD (2014) Crystallographic analysis and biochemical applications of a novel penicillin-binding protein/β-lactamase homologue from a metagenomic library. *Acta Crystallogr D Biol Crystallogr* **70**, 2455–2466.
24 Correia MA, Prates JA, Bras J, Fontes CM, Newman JA, Lewis RJ, Gilbert HJ and Flint JE (2008) Crystal structure of a cellulosomal family 3 carbohydrate esterase from *Clostridium thermocellum* provides insights into the mechanism of substrate recognition. *J Mol Biol* **379**, 64–72.
25 Mathews I, Soltis M, Saldajeno M, Ganshaw G, Sala R, Weyler W, Cervin MA, Whited G and Bott R (2007) Structure of a novel enzyme that catalyzes acyl transfer to alcohols in aqueous conditions. *Biochemistry* **46**, 8969–8979.
26 Ngo TD, Ryu BH, Ju H, Jang E, Park K, Kim KK and Kim TD (2013) Structural and functional analyses of a bacterial homologue of hormone-sensitive lipase from a metagenomic library. *Acta Crystallogr D Biol Crystallogr* **69**, 1726–1737.
27 Kim S, Joo S, Yoon HC, Ryu Y, Kim KK and Kim TD (2007) Purification, crystallization and preliminary crystallographic analysis of Est25: a ketoprofen-specific hormone-sensitive lipase. *Acta Crystallogr Sect F Struct Biol Cryst Commun* **63**, 579–581.
28 Yoon S, Kim S, Ryu Y and Kim TD (2007) Identification and characterization of a novel (S)-ketoprofen-specific esterase. *Int J Biol Macromol* **41**, 1–7.

Supporting information

Additional Supporting Information may be found online in the supporting information tab for this article:
Fig. S1. Phylogenetic analysis.
Fig. S2. Analytical size-exclusion chromatography.

PLOS ONE

RESEARCH ARTICLE

Crystal Structure and Functional Characterization of an Esterase (*Ea*EST) from *Exiguobacterium antarcticum*

Chang Woo Lee[1,2☯], Sena Kwon[3☯], Sun-Ha Park[1☯], Boo-Young Kim[3], Wanki Yoo[3], Bum Han Ryu[3], Han-Woo Kim[1,2], Seung Chul Shin[1], Sunghwan Kim[4], Hyun Park[1,2], T. Doohun Kim[3]*, Jun Hyuck Lee[1,2]*

1 Unit of Polar Genomics, Korea Polar Research Institute, Incheon, Republic of Korea, 2 Department of Polar Sciences, University of Science and Technology, Incheon, Republic of Korea, 3 Department of Chemistry, College of Natural Science, Sookmyung Women's University, Seoul, Korea, 4 New Drug Development Center, Daegu-Gyeongpuk Medical Innovation Foundation, Daegu, Republic of Korea

☯ These authors contributed equally to this work.
* junhyucklee@kopri.re.kr (JHL); doohunkim@sookmyung.ac.kr (TDK)

Citation: Lee CW, Kwon S, Park S-H, Kim B-Y, Yoo W, Ryu BH, et al. (2017) Crystal Structure and Functional Characterization of an Esterase (*Ea*EST) from *Exiguobacterium antarcticum*. PLoS ONE 12 (1): e0169540. doi:10.1371/journal.pone.0169540

Editor: Eugene A. Permyakov, Russian Academy of Medical Sciences, RUSSIAN FEDERATION

Received: October 25, 2016

Accepted: December 19, 2016

Published: January 26, 2017

Data Availability Statement: The atomic coordinates and structure factors have been deposited in the Protein Data Bank (http://www.rcsb.org/) under accession code 5H3H.

Funding: This work was supported by the Antarctic organisms: Cold-Adaptation Mechanisms and its application grant (PE16070), Polar Genomics 101 Project: Genome analysis of polar organisms and establishment of application platform (PE17080) and the Polar Academic Program (PD15010) funded by the Korea Polar Research Institute (KOPRI). This study was also supported by the

Abstract

A novel microbial esterase, *Ea*EST, from a psychrophilic bacterium *Exiguobacterium antarcticum* B7, was identified and characterized. To our knowledge, this is the first report describing structural analysis and biochemical characterization of an esterase isolated from the genus *Exiguobacterium*. Crystal structure of *Ea*EST, determined at a resolution of 1.9 Å, showed that the enzyme has a canonical α/β hydrolase fold with an α-helical cap domain and a catalytic triad consisting of Ser96, Asp220, and His248. Interestingly, the active site of the structure of *Ea*EST is occupied by a peracetate molecule, which is the product of perhydrolysis of acetate. This result suggests that *Ea*EST may have perhydrolase activity. The activity assay showed that *Ea*EST has significant perhydrolase and esterase activity with respect to short-chain p-nitrophenyl esters (≤C8), naphthyl derivatives, phenyl acetate, and glyceryl tributyrate. However, the S96A single mutant had low esterase and perhydrolase activity. Moreover, the L27A mutant showed low levels of protein expression and solubility as well as preference for different substrates. On conducting an enantioselectivity analysis using R- and S-methyl-3-hydroxy-2-methylpropionate, a preference for R-enantiomers was observed. Surprisingly, immobilized *Ea*EST was found to not only retain 200% of its initial activity after incubation for 1 h at 80˚C, but also retained more than 60% of its initial activity after 20 cycles of reutilization. This research will serve as basis for future engineering of this esterase for biotechnological and industrial applications.

Introduction

Esterases (E.C. 3.1.1.X) are members of the α/β-hydrolase family that catalyze the hydrolysis of a variety of substrates containing ester linkages, such as aryl esters, acylglycerols, and carboxylic esters. These enzymes are widely distributed in bacteria, fungi, plants, insects, and animals,

National Research Foundation of Korea, which is funded by the Korean Government (MSIP), (NRF-2016M1A5A1901770) (PN16082, KOPRI). The funders had no role in study design, data collection and analysis, decision to publish, or preparation of the manuscript.

Competing Interests: The authors have declared that no competing interests exist.

many of which are thought to play important physiological roles in lipid metabolism and detoxification of xenobiotics [1–5]. Carboxylesterases (carboxylester hydrolases, E.C. 3.1.1.1) and lipases (triacylglycerol acylhydrolases, E.C. 3.1.1.3) from microbial origin have increasingly gained interest in research, and a considerable number of novel enzymes have been discovered and characterized [6–8]. Many of them show substrate promiscuity and high regio- and stereoselectivity, as well as stability, in organic solvents; this makes them attractive biocatalysts for industrial processes including food modification, detergent formulation, and synthesis of fine chemicals and pharmaceuticals [9, 10].

Several crystal structures of microbial esterases have been described recently, such as those from the *Bacillus subtilis* strain 168, *B. subtilis* Thai I-8, and *Rhodopseudomonas palustris* [11, 12]. According to structural studies, esterases have a canonical α/β-hydrolase fold, which is composed of a central β-sheet surrounded by α-helices. The active site contains a catalytic triad formed by Ser-Asp-His residues, which is also found in other esterases and serine proteases. In addition, their enzymatic reaction mechanisms using this catalytic triads have been well studied [13, 14].

Over the last few years, many esterases with different enzymological properties and substrate specificities have been isolated from psychrophilic microorganisms including *Psychrobacter cryohalolentis* $K5^T$, *Pseudomonas mandelii*, *Psychrobacter pacificensis*, and *Thalassospira* sp. GB04J01 [15–18]. Psychrophilic organisms living in a permanently cold environment produce enzymes adapted to function and display high catalytic efficiency at low temperatures [19, 20]. The relatively high activity of cold-active enzymes in low temperatures can be explained by two factors. The first is a decrease in the enthalpy of these enzymes due to a reduction in protein-ligand interactions. Thus, this may allow for substrate-binding and product-release with a low energy barrier at low temperatures. The second factor is an increase in the entropy difference between the apo-enzyme and the enzyme-substrate complex, due to the conformational flexibility of cold-active enzymes during substrate binding. It is known that these two factors cooperatively induce favorable reactions in cold-active enzymes at low temperatures [21, 22]. With ongoing demand for reducing energy consumption, cold-adapted esterases have great commercial potential and offer efficient catalytic alternatives for industrial applications [23]. Thus far, relatively fewer esterases from psychrophilic organisms have been studied compared with those from their mesophilic counterparts.

In this study, we report on the detailed structural and biochemical characteristics of an esterase (*Ea*EST) from a psychrophilic bacterium *Exiguobacterium antarcticum* B7 [24]. This organism was isolated from a microbial biofilm at Ginger Lake on King George Island, Antarctic Peninsula. We determined the crystal structure of *Ea*EST complexed with a peracetate molecule, which indicates that *Ea*EST has perhydrolase activity. Perhydrolysis may be a side activity of esterases and lipases [25–27]. However, it can be useful in industry and organic synthesis. In our activity assay, *Ea*EST demonstrated significant perhydrolysis activity with a k_{cat} value of $0.24 \pm 0.01\ s^{-1}$, which is higher than that of the wild-type esterase ($0.12 \pm 0.01\ s^{-1}$) from *Pseudomonas fluorescens* (*Pf*EST). Recent studies on *Pf*EST revealed that a single mutation, L29P, increased the perhydrolase activity to $5.1 \pm 0.4\ s^{-1}$ [27]. Therefore, *Ea*EST can also provide a good template for constructing a perhydrolase with a higher activity via protein engineering.

The crystal structure of peracetate-bound *Ea*EST was resolved at high resolution, revealing that *Ea*EST retains the characteristic α/β-hydrolase fold with a cap domain and has a catalytic triad of Ser96, Asp220, and His248. The optimal pH and temperature of *Ea*EST, as well as its substrate profiles and enantioselectivity, were investigated through mutational analysis. We found that *Ea*EST has broad substrate profiles including short-chain p-nitrophenyl esters (≤C8), naphthyl derivatives, and glyceryl tributyrate. Furthermore, the resulting immobilization of *Ea*EST showed significantly enhanced stability and reusability. Our results will provide a platform for the rational design and engineering of more robust biocatalysts.

Materials and Methods

Cloning and protein expression of *Ea*EST

The *Ea*EST gene (GenBank Accession CP003063) was amplified from chromosomal DNA of *E. antarcticum* B7 (Korea Collection for Type Cultures (KCTC), Republic of Korea) by PCR (hot start at 94˚C (10 min) followed by 94˚C (1 min), 58˚C (45 sec), and 72˚C (1 min), for 30 cycles with appropriate primers). The resulting PCR product was inserted into a pET-21a vector (Novagen, WI, USA), and the recombinant construct (pET-*Ea*EST) was transformed in *E. coli* BL21 (DE3). A single colony was inoculated into LB medium containing ampicillin (100 mg/ml) until the optical density at 600 nm (OD_{600}) reached 0.4–0.6. Then, induction was done with the addition of 1 mM isopropyl-β-D-1-thiogalactoside (IPTG) for 3 h. The resulting cells were harvested, sonicated, and resuspended in a lysis buffer containing 20 mM Tris-HCl, pH 8.0, 10 mM imidazole, and 100 mM NaCl. After centrifugation at 18,000 rpm for 1 h, cell lysates were loaded onto a His-Trap Ni-NTA column using an AKTA Prime Plus (GE Healthcare, Little Chalfont, U.K.). Finally, after extensive washing with a buffer containing 20 mM imidazole, the bound *Ea*EST was eluted with an elution buffer containing 250mM imidazole. The eluted proteins were desalted using PD-10 column with 20 mM Tris-HCl (pH8.0) containing 100 mM NaCl. The protein purity of *Ea*EST was confirmed by SDS-PAGE and one liter of culture of the transformed *E. coli* usually resulted in approximately 8 mg of *Ea*EST.

Crystallization of *Ea*EST

*Ea*EST was purified and concentrated to 24.4 mg/mL in a buffer consisting of 20 mM Tris-HCl pH 8.0 and 100 mM NaCl. A preliminary crystallization screen was performed with a mosquito robot (TTP Labtech, UK) using commercially available screening kits such as MCSG1-4 (Microlytic) and Index (Hampton Research). Initial screening was performed using sitting-drop vapor-diffusion method in 96-well crystallization plates at 293K. Two-hundred nanoliters of *Ea*EST was mixed with an equal volume of reservoir solution and equilibrated against 80 μL of reservoir solution. Initial crystals were obtained after 1 day under several different conditions. The hexagonal shaped single crystal was obtained from 0.2 M ammonium acetate, 0.1 M HEPES:NaOH pH 7.5, and 25% (w/v) PEG 3350 (MCSG2 #27). For further optimization, hanging-drop vapor-diffusion method was used in 24-well crystallization plates. Drops consisting of 1 μL of *Ea*EST and 1 μL of reservoir solution were equilibrated against 500 μL of reservoir solution. Optimized single crystals appeared after 1 day of incubation with 0.2 M ammonium acetate, 0.1 M HEPES:NaOH pH 7.5, and 27% (w/v) PEG 3350 at 293K.

Data collection and structure determination of *Ea*EST

A single crystal of *Ea*EST was harvested and transferred to Pratone-N oil for cryoprotection. A data set containing 180 images at the resolution of 1.90 Å was collected on a 7A beam line at Pohang Accelerator Laboratory (PAL; Pohang, Korea) at 100K. The diffraction data were indexed, integrated, and scaled using the program HKL-2000 [28]. An *Ea*EST crystal belongs to the trigonal space group *P*3, with unit cell parameters of a = 76.765 Å, b = 76.765 Å, c = 68.161 Å, and α = β = 90˚, γ = 120˚. The volume of the asymmetric unit allows the presence of two copies with a Matthews coefficient of 1.83 $Å^3Da^{-1}$ and a solvent content of 32.84% [29]. The structure of *Ea*EST was determined by molecular replacement using the program MOLREP [30]. The coordinates of an esterase from *P. fluorescens* (PDB cold 3HI4) [27], which has 39% identity to *Ea*EST, was used as a model for molecular replacement. The resulting coordinate was rebuilt and refined manually based on electron-density maps using the programs REFMAC5 and COOT [31, 32]. After multiple rounds of structural refinement, the final structure of *Ea*EST has

the R_{work} and R_{free} of 0.185 and 0.238, respectively, with a total of 542 amino acid residues and 191 water molecules. The statistics of data collection and structure refinement are listed in Table 1. The atomic coordinates and structure factors have been deposited in the Protein Data Bank (http://www.rcsb.org/) under accession code 5H3H.

Analytical ultracentrifugation (AUC)

Sedimentation velocity data were obtained at 20˚C using a XL-A analytical ultracentrifuge (Beckman Coulter). *Ea*EST protein (2 mg/ml) in 25mM Tris-HCl pH 8.0, 200mM NaCl, 5 mM $MgCl_2$ and 2 mM dithiothreitol (DTT) and the reference butter were loaded into a dual sector Epon centerpiece. *Ea*EST was spun at 45,000 rpm and the movement of a boundary formed by high centrifugal force was monitored over time at the wavelength of 280 nm. The obtained data was analyzed and calculated $c(s)$ using the program SEDFIT [33, 34].

Enzyme assay and immobilization of *Ea*EST

For esterase activity of *Ea*EST, *p*-nitrophenyl esters of different acyl chain lengths including *p*-nitrophenyl acetate (C_2, *p*-NA), butyrate (C_4, *p*-NB), hexanoate (C_6, *p*-NH), octanoate (C_8, *p*-NO), decanoate (C_{10}, *p*-NDec), dodecanoate (C_{12}, *p*-NDo), and phosphate (*p*-NP) were used

Table 1. X-ray diffraction data collection and refinement statistics.

Data set	*Ea*EST complexed with peracetate
X-ray source	Beam line 7A, PAL
Space group	*P*3
Wavelength (Å)	0.97933
Range of resolution (Å)	50.00–1.90 (1.93–1.90)
No. of observed reflections	172600
No. of unique reflections	35239 (1760)
R_{merge} [a]	0.096 (0.500)
$CC_{1/2}$	0.97(0.88)
Average I/σ	43.0 (16.0)
Completeness (%)	99.3 (100.0)
Redundancy	4.9 (5.5)
Refinement	
Resolution (Å)	50.01–1.90 (1.95–1.90)
No. of reflections in working set	33487 (2463)
No. of reflections in test set	1768 (120)
No. of residues	542
No. of water molecules	191
R_{cryst} [b] total	0.185 (0.200)
R_{free} [c] total	0.238 (0.282)
R.m.s. bond length (Å)	0.018
R.m.s. bond angle (˚)	2.00
Average B value (Å^2) (protein)	28.432
Average B value (Å^2) (solvent)	32.753

[a] $R_{sym} = \sum | <I> - I | / \sum <I>$.
[b] $R_{cryst} = \sum | |Fo| - |Fc| | / \sum |Fo|$.
[c] R_{free} calculated using high-resolution data with 10% of all reflections excluded from refinement stages.
Values in parentheses refer to shells at highest resolution.

doi:10.1371/journal.pone.0169540.t001

as substrates. The release of *p*-nitrophenol was measured at 405 nm using an EPOCH2 microplate reader (Biotek, USA). Regioselectivity of *Ea*EST was also studied by using 1-naphthyl phosphate (1-NP), 1-naphthyl acetate (1-NA), 1-naphthyl butyrate (1-NB), and 2-naphthyl acetate (2-NA). The absorbance was measured at 310 nm.

The kinetic constants of *Ea*EST toward acetic acid perhydrolysis were measured using a monochlorodimedone (MCD) assay at 25˚C. All reactions contained 0.047 mM of MCD, 149 mM of potassium bromide, and appropriated amounts of the enzyme. The concentrations of acetic acid were varied to 1.4 M. The reaction was initiated with the addition of 9.9 mM of hydrogen peroxide. Enzyme activity was determined by the halogenation of MCD (ε = 19.9 mM^{-1} cm^{-1} at 290 nm) as described previously [35]. The data were fit to the Michaelis-Menten equation using nonlinear regression (GraphPad Prism 5 Software, San Diego, CA, USA).

The optimal temperature and pH were investigated in the assay mixture containing 20 mM Tris-HCl, 100 mM NaCl (pH 8.0), 0.5 mM *p*-NA, and 10 μg of *Ea*EST. The optimal pH was studied by measuring enzyme activity of *Ea*EST from pH 3.0 to pH 10.0 at 25˚C. Following buffers were used including 50 mM citrate-NaOH (pH 3.0–6.0), 100 mM phosphate-NaOH (pH 7.0), 50 mM Tris-HCl (pH 8.0), and 20 mM glycine-NaOH (pH 9.0–10.0). The optimal temperature was examined at 20, 40, 45, 50, 55, 60, and 80˚C. Thermostability of *Ea*EST was measured by incubating the enzyme at 0, 20, 40, 50, and 60˚C for 1 h. Each aliquot was taken every 15 min for measuring the residual activity.

The effects of NaCl and glycerol additions on *Ea*EST were determined by incubating the enzyme with various concentrations of NaCl (0–5 M) or glycerol (0–5 M) at 25˚C for 1 h. For chemical stability of *Ea*EST, the effects of ethanol, isopropanol (i-PrOH), SDS, Tween 20, Triton X-100, and phenylmethylsulfonyl fluoride (PMSF) were determined. For enantioselectivity analysis, a pH shift-colorimetric assay was carried out with (*R*)- and (*S*)-methyl-3-hydroxy-2-methylpropionate in 20 mM Tris-HCl (pH 8.0), 100 mM NaCl in 100 μl reaction mixture. The absorbance spectra were recorded from 350 nm to 600 nm. This pH shift-colorimetric assay was also used for the hydrolysis of phenyl acetate, 2-phenylethyl acetate, and 2-methylbutyl acetate. In addition, the hydrolysis of glyceryl tributyrate, glyceryl trioleate, olive oil, and fish oil were measured with this assay. Fluorescence analysis was executed using a Jasco FP-8200 spectrofluorometer (MD, USA). *Ea*EST samples were incubated with different concentration urea (0–5 M) for 1 h. After excitation at 280 nm, emission spectra were recorded from 300 nm to 400 nm using a 5 nm slit width and a scan speed of 250 nm/min.

To prepare immobilized forms of *Ea*EST, a purified *Ea*EST (2 mg) was precipitated with 80% ammonium sulfate and crosslinked with 50 mM glutaraldehyde with gentle inverting for 12 h. Then, suspension was centrifuged at 13,000 rpm at 4˚C for 30 min and the resulting immobilized *Ea*ESTs were washed 3 times with 20 mM Tris-HCl (pH 8.0), 100 mM NaCl. Activity of immobilized *Ea*EST was monitored by measuring the hydrolysis of *p*-nitrophenyl acetate (C_2, *p*-NA). Thermal stability of immobilized *Ea*EST was investigated at 80˚C and the activity of soluble *Ea*EST was set to 100%. To examine reusability, immobilized *Ea*EST was retrieved by simple centrifugation after each reaction. After repeated washing steps (usually 3 times), new substrate was added for another cycle and the activity of immobilized *Ea*EST was measured. For surface morphology of immobilized *Ea*EST, a scanning electron microscope (SUPRA 55VP, Carl Zeiss, Jena, Germany) was used. Samples were prepared by fixation process with 0.05 M cacodylate buffer (pH 7.2) containing 1% osmium tetraoxide (OsO_4) at 4˚C and consecutive cycles of dehydration by ethanol solutions. After drying with hexamethyldisilazane solution, samples were mounted on metal stubs and sputtered with gold.

Results and Discussion

Overall structure of *Ea*EST

The crystal structure of an esterase (*Ea*EST) from *Exiguobacterium antarcticum* was determined in a *P*3 space group. As a search model, we used the structure of aryl esterase (*Pf*EST, PDB code 3HI4) from *Pseudomonas fluorescens* with a molecular replacement (MR) method. The final model was refined up to 1.9 Å and produced R_{work} and R_{free} values of 0.185 and 0.235, respectively (Table 1). The structure of an *Ea*EST monomer is composed of 11 α-helices and eight β-strands with dimensions of 45 × 42 × 40 Å. The structure shows a typical αβ-hydrolase fold with an α-helical cap domain. The central eight β-strands are surrounded by seven side α-helices (α1-α3 and α8-α11) and an α-helical cap domain (α4-α7 helices) (Fig 1). The asymmetric unit of an *Ea*EST crystal contains two protomers. The results of analytical ultracentrifugation demonstrated that the purified *Ea*EST protein is a stable trimer in solution (Fig 2A). Additionally, a crystallographic symmetry operator generates a tight trimeric arrangement, as shown in Fig 2B. The trimer interface in *Ea*EST is formed by α1, the β4-α2 loop region, α4, α5, α6, and an α7-helix (Figs 1 and 2B). Using mainly hydrogen bonds and hydrophobic interactions, the trimer interface obscures 466 $Å^2$ of the total monomer surface area (3176 $Å^2$).

A search of structural homologs using the DALI server identified an aryl esterase (PDB code 3HEA and 3HI4) as the closest structural homolog of *Ea*EST; additionally, bromoperoxidase (PDB code 3FOB), haloperoxidase (PDB code 1A8S), chloroperoxidase (PDB code 4DGQ), and esterase (PDB code 1ZOI) were included in the top five hits (Table 2) [36]. The top solution structure was the *Pf*EST structure used in the MR search; the *Pf*EST structure was aligned to the *Ea*EST structure with 0.96 Å r.m.s. deviation for 307 C_α atoms. Notably, all of the listed proteins in DALI result from trimer in solution; the exception to that is haloperoxidase (PDB code 1A8S), the oligomeric state of which has not yet been experimentally resolved.

During the process of structure determination, unknown electron-density maps were found near the active sites of both molecules in the asymmetric unit (Fig 3A). Even if no specific ligands were added to *Ea*EST at purification and crystallization, the unknown electron density was initially interpreted as an acetate because of crystallization conditions containing 0.2 M ammonium acetate. After building and refining the model, additional electron density was clearly observed in the hydroxyl group of acetic acid, indicating that *Ea*EST has perhydrolysis activity via acetic acid. Therefore, peracetic acid could be located. Using repetitive refinement, the peracetate molecule was perfectly fitted into the electron-density map (Fig 3B). The active site of *Ea*EST is comprised of a conserved catalytic triad (Ser96, Asp220, and His248) and the neighboring hydrophobic pocket, which is composed of the hydrophobic residues Trp30, Phe127, Met137, Leu145, Met156, Phe160, Ile163, Leu199, Phe164, and Val 222. The hydrophobic pocket may play a role in portal substrate entry and initial binding. The hydroxyl group of peracetic acid forms hydrogen bonds with the O atom of Ser96, the NE2 atom of His248, and main-chain oxygen atom of Trp30. Additionally, methyl group of peracetic acid toward the hydrophobic pocket of active site (Fig 3B and 3C).

Comparison of *Ea*EST structure with that of *Pf*EST

Structural comparison using superimposition between *Ea*EST and *Pf*EST (PDB code 3HI4, acetate-bound form) shows that the overall monomer structures, as well as trimeric structures, are very similar, but the local orientation of the loop region between β6 and α4 (residues 123–141) differs slightly. In the *Ea*EST structure, the β6-α4 loop protrudes inward, toward the center of the hydrophobic pocket, located at the vicinity of the active site. The Met137 residue,

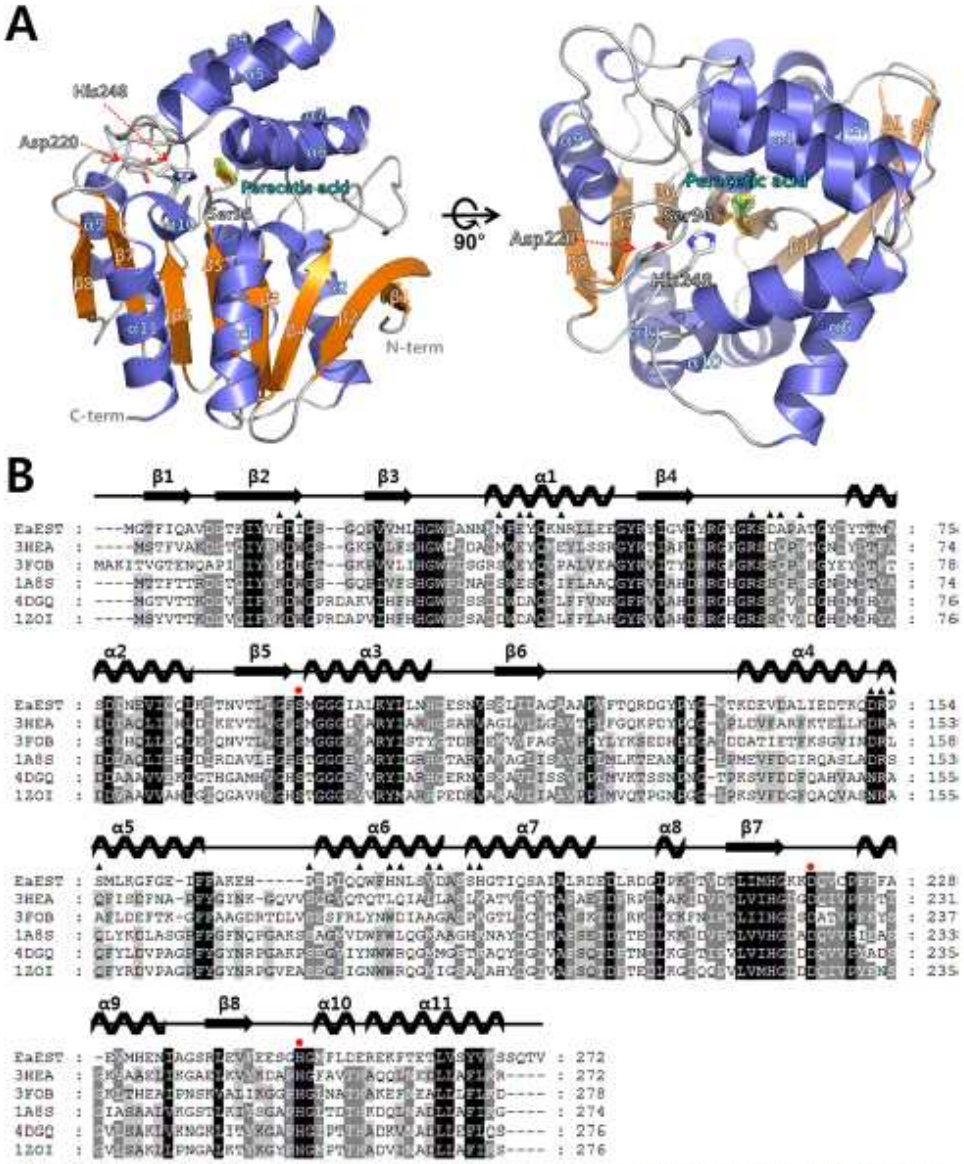

Fig 1. Crystal structure of peracetate-bound *Ea*EST. (**A**) Overall structure of monomeric *Ea*EST is shown in front view (left panel) and top view (right panel) rotated at 90˚. The structure of *Ea*EST was drawn as a ribbon diagram with α-helices colored slate blue and β-strands colored orange. Bound peracetate molecule (cyan) is shown as a stick model with a 2Fo-Fc electron-density map (green) at 1.0 σ. The catalytic triad residues (Ser96, Asp220, and His248) are shown as stick models. *N*- and *C*-termini are labeled in gray letters and indicated

with a red dashed arrow. (**B**) Multiple sequence alignment of *Ea*EST (NCBI reference sequence number WP_014970431.1), aryl esterase (PDB code 3HEA; UniProtKB code P22862), bromoperoxidase (PDB code 3FOB; UniProtKB code Q81NM3), haloperoxidase (PDB code 1A8S; UniProtKB code O31158), chloroperoxidase (PDB code 4DGQ; UniProtKB code B4EA96), and esterase (PDB code 1ZOI; UniProtKB code Q3HWU8). Secondary structural elements in the crystal structure of *Ea*EST are represented above the multiple sequence alignment. The catalytic triad residues (Ser96, Asp220, and His248) are indicated with red circles and the residues involved in the trimer interaction are indicated by black triangles. The multiple sequence alignment was performed with *ClustalX* and edited with *GeneDoc*.

doi:10.1371/journal.pone.0169540.g001

located on the β6-α4 loop, enables hydrophobic interactions with Ile163, Leu145, Phe127, and Phe160. Similarly, the Phe127 residue, located on the β6-α4 loop, is also oriented toward the hydrophobic pocket, more than is the Phe125 of *Pf*EST. These interactions also induce further movement of the α5-helix toward the β6-α4 loop region. The α5-helix is directly involved in substrate interactions (Fig 3C). A comparison of binding sites revealed that the β6-α4 loop region also plays an important role in substrate binding. The catalytic triad of Ser96, Asp220, and His 248 (Ser94, Asp222, and His251 in *Pf*EST) is conserved, but the residues of the neighboring hydrophobic pocket show clear distinctions. Notably, the Met137 residue (Val135 in *Pf*EST), located on the β6-α4 loop region, shows the largest structural difference (Figs 3D and 4A). In *Pf*EST, the Val135 residue, located on the β6-α4 loop region, shows a relatively open state of its active site. In *Ea*EST, however, The Met137 residue extends to the hydrophobic pocket and shows a closed state compared with that of *Pf*EST. Because of these interactions, peracetate may bind to the active site of *Ea*EST more tightly and deeply than acetate binds to the active site of *Pf*EST. Peracetate interacts with Trp30, Ser96, and His248 directly. In *Pf*EST, acetate interacts with Trp28 and His251 via mediation by a water molecule. The protruding hydroxyl group of peracetic acid substitutes for a water molecule (Fig 4B and 4C). Therefore, these investigations suggest that the β6-α4 loop region may be critical for controlling ligand recognition and may function as a selective substrate filter.

Functional analysis of *Ea*EST

The substrate profiles of *Ea*EST were investigated using *p*-nitrophenyl esters such as *p*-NA, *p*-NB, *p*-NH, *p*-NO, *p*-NDec, and *p*-NDo. The enzyme showed considerable activity toward all tested substrates except for *p*-NDo (Fig 5A). The highest activity was observed with *p*-NA, *p*-NB, and *p*-NO, whereas the hydrolytic level of *p*-NDo was 90% lower than that of *p*-NA (set at 100%). We also analyzed substrate profiles of *Ea*EST using naphthyl derivatives. As shown in Fig 5B, *Ea*EST showed the highest activity toward 1-NA, followed by 1-NB and 2-NA, but showed low activity toward 1-NP.

Previously, *Pf*EST and its mutant showed perhydrolase activity, the reversible formation of peracetic acids from acetic acids and hydrogen peroxide, as well as esterase activity [26, 27]. The findings of our structural study led us to hypothesize that peracetate can bind to the active site of *Ea*EST. Thus, in order to clarify whether *Ea*EST also had perhydrolase activity, kinetic constants for acetic acid perhydrolysis were measured using the MCD assay with varied concentrations of acetic acid and 9.9 mM hydrogen peroxide. We found that *Ea*EST is a good catalyst for perhydrolysis of acetic acid, showing a high k_{cat} value of 0.24 ± 0.01 s^{-1} compared with that of *Pf*EST (0.12 ± 0.02 s^{-1}) (Fig 5C). Mutant S96A showed very low perhydrolase activity toward acetic acid (Fig 5D).

The optimum pH and temperature of *Ea*EST was monitored at the pH range of 3.0 to 10.0 and temperature range of 20 to 80˚C using *p*-NA as substrate. *Ea*EST exhibited maximum activity at pH 8.0–9.0. However, the enzyme was rapidly inactivated at below pH 6.0, with less than 10% of its maximum activity remaining (Fig 5E). The optimum temperature for the activity of *Ea*EST was 40˚C (Fig 5F). The effect of temperature on the stability of *Ea*EST was investigated by measuring the residual activity of *Ea*EST at 15 min intervals using a temperature range of 0

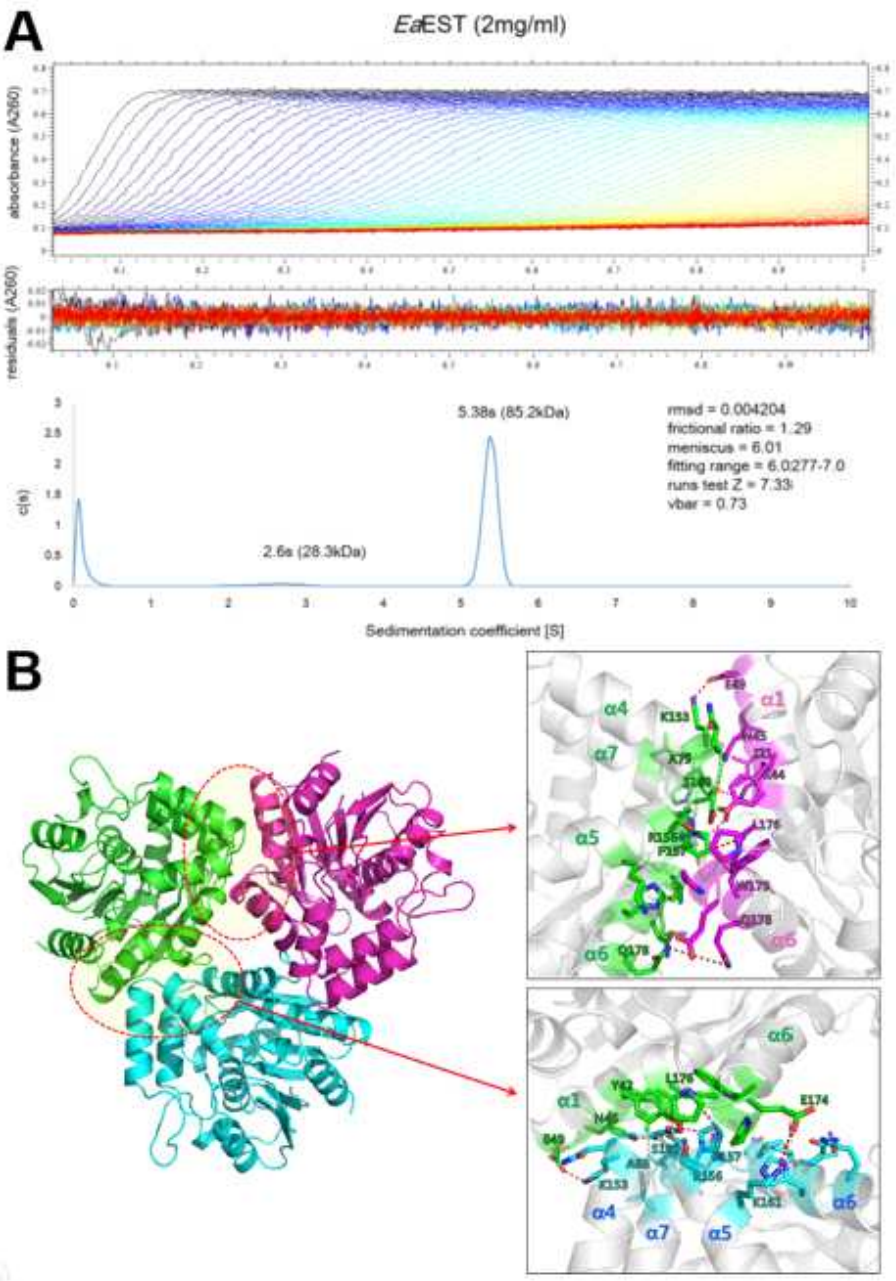
A
*Ea*EST (2mg/ml)
absorbance (A260)
residuals (A260)
c(s)
5.38s (85.2kDa)
2.6s (28.3kDa)
rmsd = 0.004204
frictional ratio = 1.29
meniscus = 6.01
fitting range = 6.0277-7.0
runs test Z = 7.33
vbar = 0.73
Sedimentation coefficient [S]
B
α1
α4
α5
α6
α7

Fig 2. Trimeric structure of *Ea*EST. (A) Analytical ultracentrifugation (AUC) experiments using 2 mg/mL *Ea*EST give a mass of 85.2 kDa (sedimentation coefficient of 5.38 S and a frictional ratio of 1.29), indicating that *Ea*EST is a stable trimer in solution. (B) *Ea*EST trimer has a triangular shape. Each protomer has two binding interfaces for trimerization.

doi:10.1371/journal.pone.0169540.g002

to 50˚C. There was a gradual reduction in activity as temperature increased. *Ea*EST retained more than 50% of its initial activity after incubation at 45˚C for 30 min, while a significant loss of activity occurred after only 15 min when the enzyme was incubated at 50˚C (Fig 5C).

Next, we investigated the effects of NaCl and glycerol on the function of *Ea*EST. The enzyme was most active in the presence of 2 M NaCl, but concentration of NaCl did not significantly affect enzyme activity (Fig 6A). Although, the activity decreased with increasing glycerol concentration, more than 60% of maximal activity was retained in the presence of 5 M glycerol (Fig 6B). To examine the effects of detergents and organic solvents on the stability of *Ea*EST, the enzyme was incubated with each chemical compound, and then residual activities were measured. The results show that all the chemicals used inhibited the activity of *Ea*EST, with less than 40% of its original activity remaining. Among these chemicals, sodium dodecyl sulfate (SDS) at 1.0% (w/v) completely inhibited the activity of *Ea*EST (Fig 6C).

Enantioselectivity analysis and activity assay of *Ea*EST and S96A mutant

Carboxylesterase has become increasingly attractive due to its ability to perform enantioselective biotransformation in the production of chiral pharmaceuticals. Thus, we conducted an enantioselectivity analysis of *Ea*EST using a pH shift assay with (*R*)- and (*S*)-methyl-3-hydroxy-2-methylpropionate. Hydrolytic activity was detected based on color and changes in absorbance. As shown in Fig 7A and 7B, a change of color to yellow was observed only in the mixture containing the (*R*)-enantiomer, which indicates that *Ea*EST prefers the (*R*)-enantiomer of the chiral ester to the (*S*)-enantiomer. The result was confirmed by measuring the absorbance spectra. When we performed these assays using the catalytic-site mutant S96A, the mutant showed no detectable enzymatic activity toward either the (*R*)- or the (*S*)-enantiomer. In addition to phenyl-substituted substrates, phenyl acetate, 2-phenylethyl acetate, and 2-methylbutyl acetate were also used to characterize *Ea*EST and the S96A mutant. The hydrolytic activity of *Ea*EST is limited to phenyl acetate. Only the reaction mixture containing phenyl acetate was observed to turn yellow, which is consistent with the results of the absorbance spectra (Fig 7C and 7D). Additionally, the enzymes were investigated for their ability to hydrolyze glyceryl esters and oils. We determined that *Ea*EST could hydrolyze glyceryl tributyrate but showed little or no activity toward glyceryl trioleate, olive oil, or fish oil. The S96A mutant had a severely reduced ability to hydrolyze the tested substrates (Fig 7E and 7F).

Table 2. Selected structural homologs of *Ea*EST obtained using DALI search (DALI-Lite server).

Protein	PDB code	DALI score	Biological unit	Sequence % ID with *Ea*EST (aligned residue number/total number of residues)	Reference
aryl esterase	3HEA	42.7	Trimer	38% (266/271)	[27]
bromoperoxidase	3FOB	41.3	Trimer	34% (267/276)	It has not yet been published
haloperoxidase	1A8S	41.3	*ND	33% (266/273)	[37]
chloroperoxidase	4DGQ	40.5	Trimer	38% (266/271)	It has not yet been published
esterase	1ZOI	39.8	Trimer	25% (268/275)	[38]

*ND means not determined experimentally.

doi:10.1371/journal.pone.0169540.t002

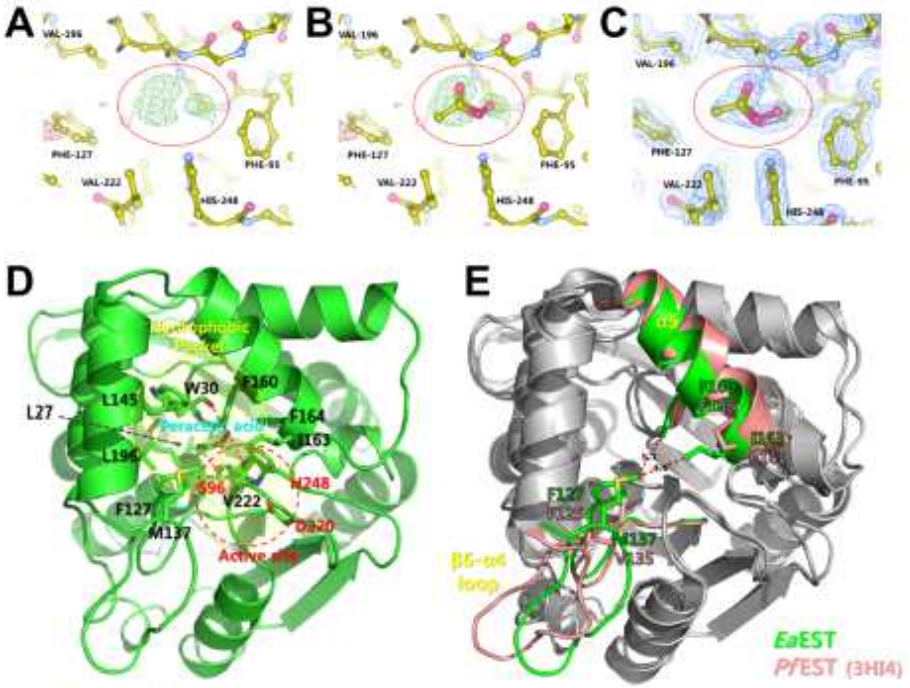

Fig 3. Peracetate-binding in *Ea*EST. (A) The positive electron density (green) was observed in the Fo-Fc omit map (contoured at 2.0 σ). (B) The peracetate model was overlaid on the Fo-Fc omit map (green, contoured at 2.0 σ). (C) The 2Fo-Fc electron-density map at 1.0 σ is shown after peracetate model building and refinement. (D) Peracetate-binding site is shown. Side chains of residues near ligand recognizing hydrophobic pocket (yellow circle) and active site (red circle) are indicated by sticks. (E) Conformational changes between peracetate-bound *Ea*EST and acetate-bound *Pf*EST (PDB code 3HI4). The β5-α4 loop region of *Ea*EST may undergo conformational change to open the entrance hydrophobic channel for ligand exchange.

doi:10.1371/journal.pone.0169540.g003

Effect of urea on activity and conformation of *Ea*EST

To explore the effects of urea on the activity of *Ea*EST, enzyme activity with respect to *p*-NA was measured in the presence of various concentrations of urea (Fig 8A). There was a significant reduction in activity at mildly denaturing condition of 1 M urea, with only 27% of the original activity retained. *Ea*EST activity decreased gradually with increasing urea concentrations, indicating that urea induced conformational changes at the active site of *Ea*EST. Further, to clarify the results of the activity assays, we monitored the intrinsic fluorescence emission spectra of *Ea*EST in the presence of different urea concentrations (Fig 8B). The conformational changes in *Ea*EST during urea-induced unfolding were monitored using fluorescence properties of tryptophan residues, which are highly sensitive to the environment. Under native conditions, the maximum fluorescence emission wavelength (λmax) of *Ea*EST is 327 nm. In 1 M urea, fluorescence intensity rapidly increased and λmax was red-shifted. However, increasing urea concentrations higher than 2 M caused a progressive decrease in fluorescence intensity, with accompanying red-shifted emission maximum ranging from 338 to 349 nm. The results

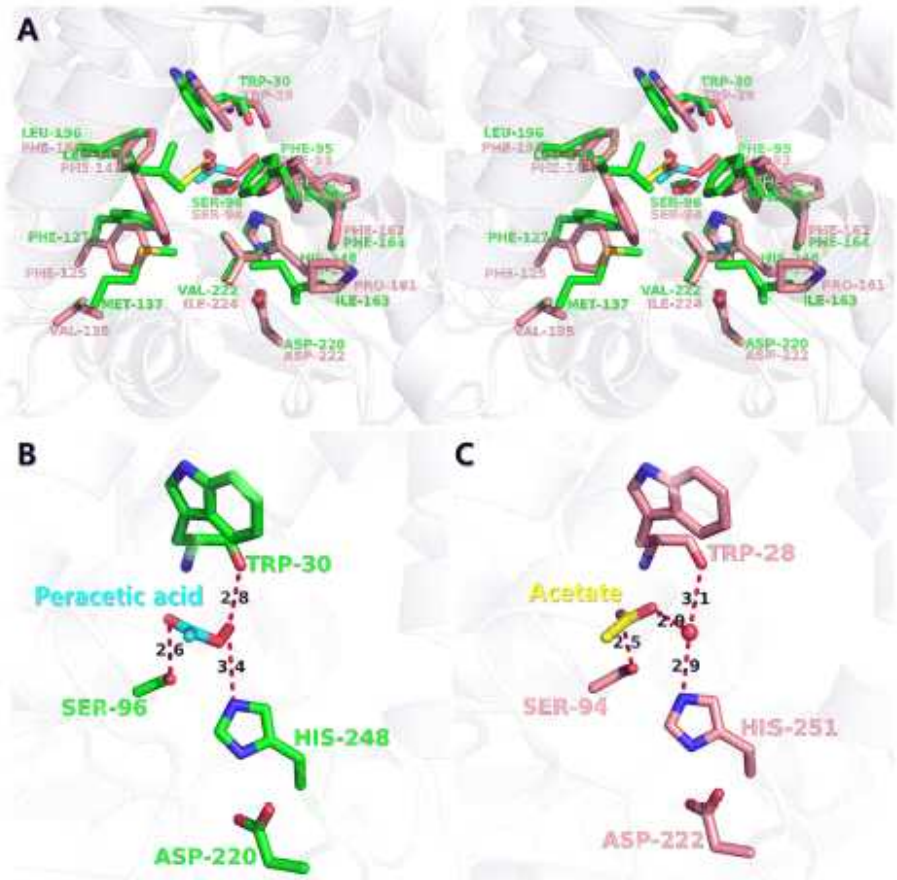

Fig 4. Structural comparisons of ligand-binding site between peracetate-bound *Ea*EST and acetate-bound *Pf*EST. (A) Stereo view of the superimposed structure of peracetate (cyan)-bound *Ea*EST (green) and acetate (yellow)-bound *Pf*EST (PDB code 3HI4, acetate-bound form, salmon). The residues comprising the active and ligand-binding sites are shown in a stick representation. (B) Peracetate-binding mode and its interactions in *Ea*EST structure. (C) Acetate-binding mode and its interactions in *Pf*EST structure.

doi:10.1371/journal.pone.0169540.g004

can be attributed to the gradual exposure of Trp residues upon urea-induced unfolding of *Ea*EST.

Biochemical analysis of the L27A mutant of *Ea*EST

For the mutagenesis study, we investigated substrate profiles and enantioselectivity of S96A and L27A, located in the catalytic site of *Ea*EST. Native gel analysis with purified wild-type and mutated *Ea*EST proteins indicated that L27A did not separate on the gel in contrast to wild-

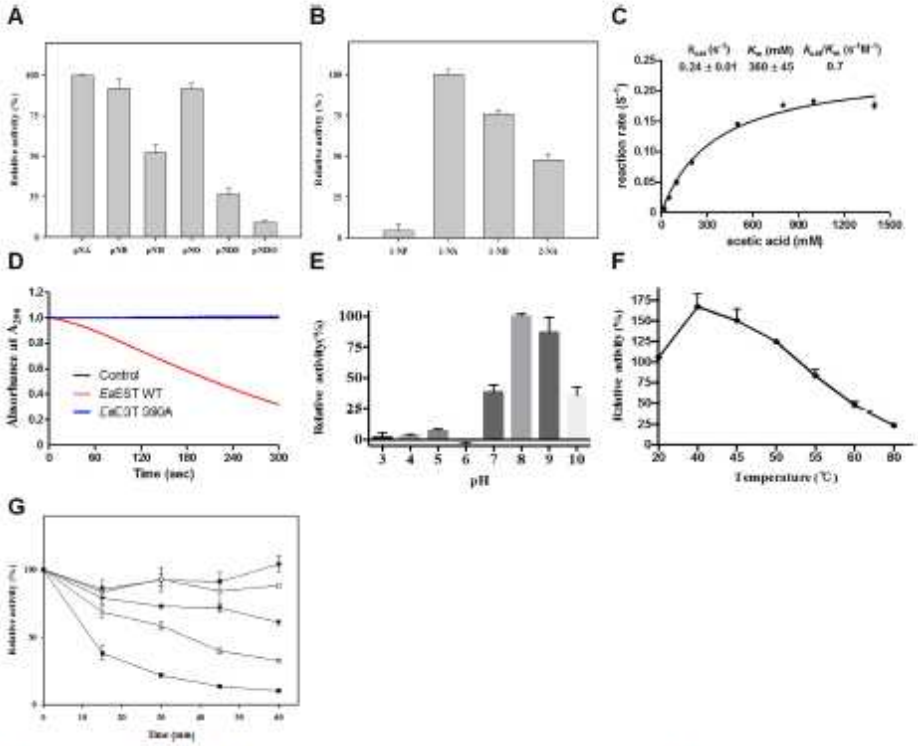

Fig 5. Enzyme activity of *Ea*EST. (A) The substrate profiles of *Ea*EST were determined using different *p*-NP esters (A) and naphthyl derivatives (B). (C) The reaction rate of acetic acid perhydrolysis catalyzed by wild-type *Ea*EST. Perhydrolase activities were measured at pH 5.5 at 25˚C. Kinetic constants were obtained by varying the concentration of acetic acid. (D) Specific activities for acetic acid perhydrolysis catalyzed by wild-type *Ea*EST and the S96A mutant. (E) pH stability of *Ea*EST. The pH dependence of hydrolysis of *p*-NA by *Ea*EST was measured at 25˚C. (F) Effect of temperature on the residual activity of *Ea*EST. (G) Thermostability of *Ea*EST. Residual activities are expressed relative to the original activity during incubation at 0, 20, 40, 45, and 50˚C. The results are the mean of three individual experiments.

doi:10.1371/journal.pone.0169540.g005

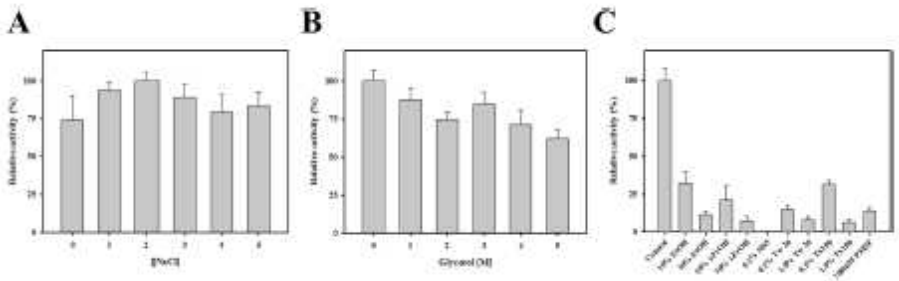

Fig 6. Effect of NaCl (A) and glycerol (B) on the activity of *Ea*EST. Relative activity was determined by incubating the enzyme with different concentrations of NaCl and glycerol (0 to 5 M). The maximum activity value obtained was set to 100%. (C) Chemical stability of *Ea*EST. Residual activity after 1 h of incubation is expressed relative to the original activity obtained without the addition of chemical compounds (100%).

doi:10.1371/journal.pone.0169540.g006

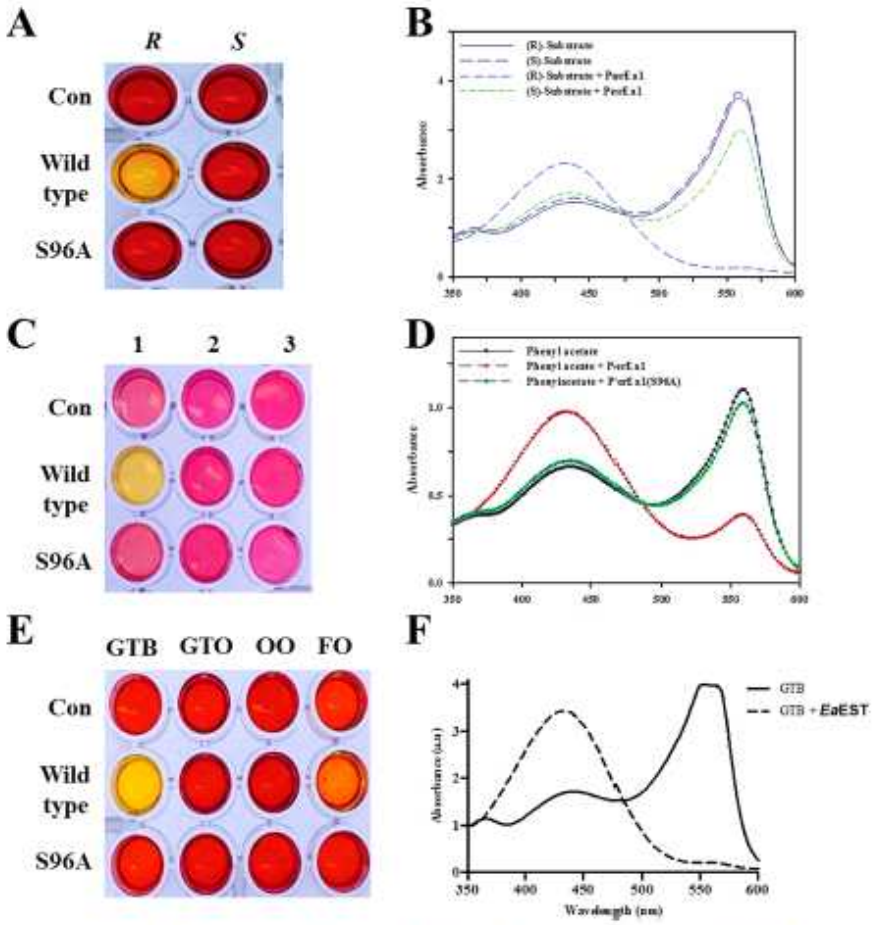

Fig 7. (A) pH shift assay for enantioselectivity analysis of *Ea*EST and S96A mutant conducted with (*R*)- and (*S*)-methyl-3-hydroxy-2-methylpropionate. (B) Absorbance spectra of the reaction mixtures in (A). (C) Hydrolysis of phenyl-substituted substrates: 1, phenyl acetate; 2, 2-phenylethyl acetate; 3, 2-methylbutyl acetate. (D) Absorbance spectra of 1 from (C) were measured. (E) Hydrolysis of glyceryl esters (glyceryl tributyrate [GTB] and glyceryl trioleate [GTO]) and oils (olive oil [OO] and fish oil [FO]) by *Ea*EST was investigated. (F) Absorbance spectra of GTB hydrolysis by wild-type *Ea*EST were measured.

doi:10.1371/journal.pone.0169540.g007

type and S96A. Moreover, the L27A mutant of *Ea*EST was expressed at a low level and this single mutation results in reduced solubility compared to the wild-type protein, suggesting that Leu27 may be important for protein solubility. Fig 9A shows substrate profiles of L27A for *p*-nitrophenyl esters. Interestingly, the replacement of Leu27 by Ala considerably changed the catalytic pattern of wild-type *Ea*EST. L27A showed the greatest preference for *p*-NDo and low-level activities toward *p*-NA and *p*-NB. Conversely, the wild-type was most active toward *p*-NA and *p*-NB, and did not prefer *p*-NDo. Substrate profiles of L27A for naphthyl derivatives

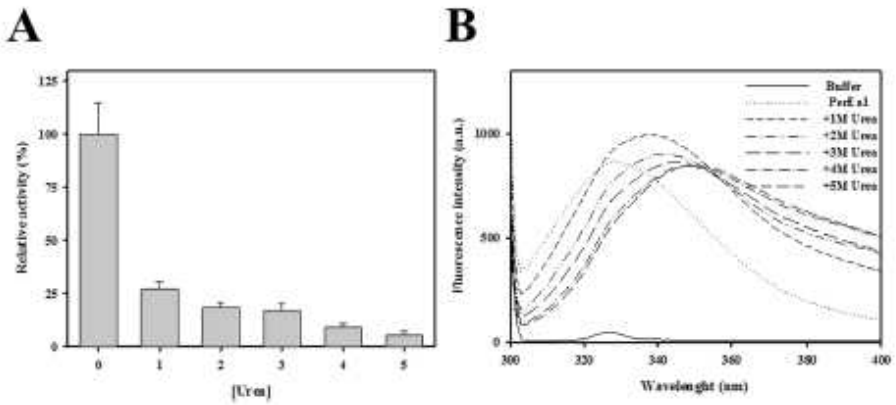

Fig 8. (A) Effect of concentration of urea on the activity of *Ea*EST. (B) Intrinsic fluorescence spectra were recorded with increasing concentrations of urea (0 to 5 M).

doi:10.1371/journal.pone.0168540.g008

were also investigated. Although L27A showed the highest activity against 1-NB, less than 20% of activity was obtained with 1-NP, 1-NA, and 2-NA relative to that of 1-NB. Wild-type *Ea*EST demonstrated substrate preference for 1-NA rather than for 1-NB, which is different from the preference of L27A (Fig 9B). Additionally, to examine whether this mutation can modulate enantioselectivity of *Ea*EST, pH shift assays were performed with (*R*)- and (*S*)-methyl-3-hydroxy-2-methylpropionate. As shown in Fig 9C, wild-type *Ea*EST showed preference for (*R*)-enantiomers, but the L27A mutant showed no activity toward either enantiomer. These results indicate that the Leu27 residue is critical for catalytic activity, as well as for protein solubility, of *Ea*EST.

Immobilization of *Ea*EST

Enzyme immobilization is an effective strategy to improve the stability and recyclability of free enzymes. Immobilization of *Ea*EST was characterized for biotechnological and industrial applications. *Ea*EST was immobilized as a cross-linked enzyme aggregate (CLEA) via precipitation with ammonium sulfate and cross-linking with glutaraldehyde. Scanning electron

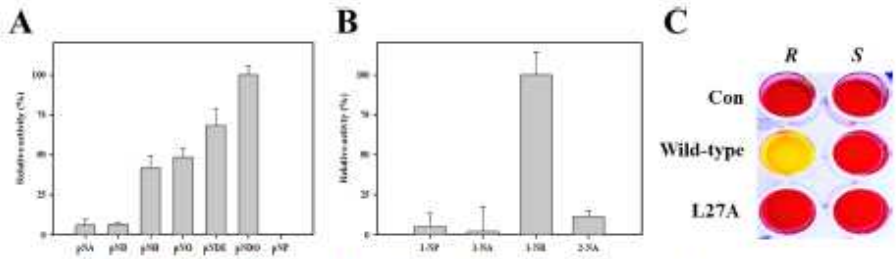

Fig 9. Analysis of substrate profiles and enantioselectivity of the L27A mutant. Substrate profiles of L27A were investigated toward different *p*-nitrophenyl esters (A) and naphthyl derivatives (B). (C) pH shift assay was conducted in the presence of (*R*)- or (*S*)-methyl-3-hydroxy-2-methylpropanoate.

doi:10.1371/journal.pone.0168540.g009

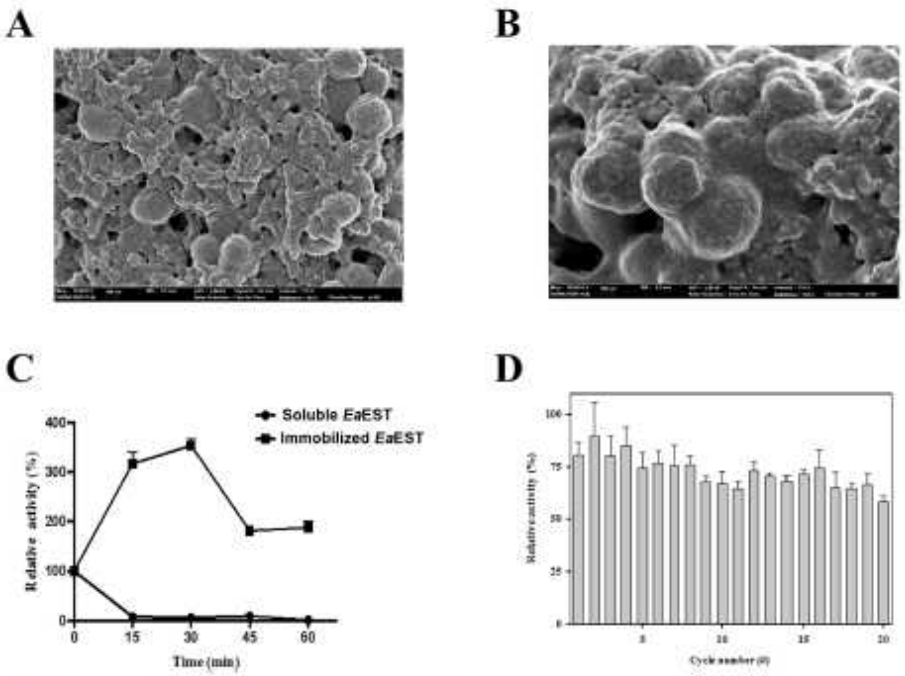

Fig 10. Immobilization of *Ea*EST. Scanning electron microscope (SEM) image of cross-linked enzyme aggregates (*Ea*EST-CLEAs). Representative images at 50 kX (A) and 100 kX (B) are shown. (C) Thermostability of immobilized *Ea*EST (▪) and soluble *Ea*EST (•) at 80˚C. Activity was measured every 15 min. (D) Reusability of immobilized *Ea*EST was compared to the soluble enzyme for 20 reaction cycles. Residual activities were expressed relative to those of free Sm23 (100%).

doi:10.1371/journal.pone.0169540.g010

microscopy (SEM) images of CLEAs show the morphological structure of the amorphous aggregate of *Ea*EST (Fig 10A and 10B). The thermostability of soluble and immobilized *Ea*EST was determined by pre-incubating at 80˚C for various time intervals. Surprisingly, immobilized *Ea*EST exhibited significantly enhanced activity and stability. Approximately 350% of its initial activity was retained after exposure to 80˚C for 30 min; even after incubating for 1 hour, immobilized *Ea*EST showed 200% of its initial activity. However, all of its soluble enzymatic activity was lost after only 15 min. The thermostability of the immobilized *Ea*EST was higher than that of the soluble enzyme (Fig 10C). Fig 10D shows reusability of immobilized *Ea*EST with *p*-NA hydrolysis. Immobilized *Ea*EST retained more than 60% of its initial activity after 20 reutilization cycles. The results suggest that immobilized *Ea*EST could be effectively reutilized for potential industrial applications.

Conclusion

In this study, we characterized the *Ea*EST enzyme using structural analysis based on crystal diffraction and biochemical data and activity analysis. Using an analytical ultracentrifugation (AUC) analysis, we also confirmed that the purified *Ea*EST protein forms a stable trimer in solution. These studies provide insight into an unusual enzymatic feature, the dual catalytic role

of *Ea*EST as a typical esterase and perhydrolase. The crystal structure of *Ea*EST in peracetate-bound form provides the first structural insights into the final product-bound state during perhydrolysis. A comparison of the structure of *Ea*EST with that of *Pf*EST (PDB code 3HI4) revealed that the bound peracetate has different interactions compared with the bound acetate in *Pf*EST. As a result, peracetate-binding induced rearrangements of the active site residues and conformational changes in β6-α4 loop region and the α-helix. In its esterase activity, *Ea*EST displays the broad substrate profiles for short-chain *p*-nitrophenyl esters (≤C8), naphthyl derivatives, phenyl acetate, and glyceryl tributyrate. Additionally, immobilized *Ea*EST showed approximately 200% of its initial activity and 60% activity after 20 reutilization cycles. Given that wild-type *Ea*EST has the dual activity of esterase and perhydrolase, it can be used as template in structure-based protein engineering for developing modified enzymes having different substrate specificities or a single robust activity. For example, our L27A mutant *Ea*EST showed different substrate preference and stereo selectivity compared with those of wild-type *Ea*EST.

Acknowledgments

We would like to thank the staff at the X-ray core facility of the Korea Basic Science Institute (KBSI; Ochang, Korea) and the BL-7A of the Pohang Accelerator Laboratory (Pohang, Korea) for their kind help with data collection. This work was supported by the Antarctic organisms: Cold-Adaptation Mechanisms and its application grant (PE16070), Polar Genomics 101 Project: Genome analysis of polar organisms and establishment of application platform (PE17080) and the Polar Academic Program (PD15010) funded by the Korea Polar Research Institute (KOPRI). This study was also supported by the National Research Foundation of Korea, which is funded by the Korean Government (MSIP), (NRF-2016M1A5A1901770) (PN16082, KOPRI).

Author Contributions

Conceptualization: TDK JHL.

Data curation: CWL S. Kwon S-HP.

Formal analysis: BHR H-WK SCS.

Funding acquisition: HP TDK JHL.

Investigation: B-YK WY H-WK SCS S. Kwon.

Methodology: S. Kim.

Project administration: TDK JHL.

Resources: HP TDK.

Writing – original draft: CWL S. Kwon S-HP S. Kim TDK JHL.

Writing – review & editing: HP.

References

1. Liu P, Ewis HE, Tai PC, Lu C-D, Weber IT. Crystal structure of the *Geobacillus stearothermophilus* carboxylesterase Est55 and its activation of prodrug CPT-11. J Mol Biol. 2007; 367: 212–223. doi: 10.1016/j.jmb.2006.12.067 PMID: 17239398
2. Legler PM, Kumaran D, Swaminathan S, Studier FW, Millard CB. Structural characterization and reversal of the natural organophosphate resistance of a D-type esterase, *Saccharomyces cerevisiae* S-

formylglutathione hydrolase. Biochemistry. 2008; 47: 9592–9601. doi: 10.1021/bi800100t PMID: 18707125

3. Ileperuma NR, Marshall SD, Squire CJ, Baker HM, Oakeshott JG, Russell RJ, et al. High-resolution crystal structure of plant carboxylesterase AeCXE1, from *Actinidia eriantha*, and its complex with a high-affinity inhibitor paraoxon. Biochemistry. 2007; 46: 1851–1859. doi: 10.1021/bi062046w PMID: 17256879
4. Jackson CJ, Liu J-W, Carr PD, Younus F, Coppin C, Meirelles T, et al. Structure and function of an insect α-carboxylesterase (αEsterase7) associated with insecticide resistance. Proc Natl Acad Sci. 2013; 110: 10177–10182. doi: 10.1073/pnas.1304097110 PMID: 23733941
5. Bencharit S, Morton CL, Hyatt JL, Kuhn P, Danks MK, Potter PM, et al. Crystal structure of human carboxylesterase 1 complexed with the Alzheimer's drug tacrine: from binding promiscuity to selective inhibition. Chem Biol. 2003; 10: 341–349. PMID: 12725862
6. Arpigny JL, Jaeger K-E. Bacterial lipolytic enzymes: classification and properties. Biochem J. 1999; 343: 177–183. PMID: 10493927
7. Sharma R, Chisti Y, Banerjee UC. Production, purification, characterization, and applications of lipases. Biotechnol Adv. 2001; 19: 627–662. PMID: 14550014
8. Bornscheuer UT. Microbial carboxylesterases: classification, properties and application in biocatalysis. FEMS Microbiol Rev. 2002; 26: 73–81. PMID: 12007643
9. Panda T, Gowrishankar B. Production and applications of esterases. Appl Microbiol Biotechnol. 2005; 67: 160–169. doi: 10.1007/s00253-004-1840-y PMID: 15630579
10. Sharma S, Kanwar SS. Organic solvent tolerant lipases and applications. Sci World J. 2014; 2014:15–29.
11. Rozeboom HJ, Godinho LF, Nardini M, Quax WJ, Dijkstra BW. Crystal structures of two *Bacillus* carboxylesterases with different enantioselectivities. Biochim Biophys Acta, Proteins Proteomics. 2014; 1844: 567–575.
12. Hajighasemi M, Nocek BP, Tchigvintsev A, Brown G, Flick R, Xu X, et al. Biochemical and structural insights into enzymatic depolymerization of polylactic acid and other polyesters by microbial carboxylesterases. Biomacromolecules. 2016; 17: 2027–2039. doi: 10.1021/acs.biomac.6b00223 PMID: 27087107
13. Nardini M, Dijkstra BW. α/β Hydrolase fold enzymes: the family keeps growing. Curr Opin Struct Biol. 1999; 9: 732–737. PMID: 10607665
14. Bornscheuer UT, Kazlauskas RJ. Hydrolases in organic synthesis: regio-and stereoselective biotransformations. 2nd ed. New York: John Wiley & Sons Press; 2006.
15. Novototskaya-Vlasova K, Petrovskaya L, Yakimov S, Gilichinsky D. Cloning, purification, and characterization of a cold-adapted esterase produced by *Psychrobacter cryohalolentis* K5T from Siberian cryopeg. FEMS Microbiol Ecol. 2012; 82: 367–375. doi: 10.1111/j.1574-6941.2012.01385.x PMID: 22486752
16. Lee C, Kim J, Hong S, Goo B, Lee S, Jang S-H. Cloning, expression, and characterization of a recombinant esterase from cold-adapted *Pseudomonas mandelii*. Appl Biochem Biotechnol. 2013; 169: 29–40. doi: 10.1007/s12010-012-9947-6 PMID: 23117417
17. Wu G, Wu G, Zhan T, Shao Z, Liu Z. Characterization of a cold-adapted and salt-tolerant esterase from a psychrotrophic bacterium *Psychrobacter pacificensis*. Extremophiles. 2013; 17: 809–819. doi: 10.1007/s00792-013-0562-4 PMID: 23868329
18. De Santi C, Leiros H-KS, Di Scala A, de Pascale D, Altermark B, Willassen N-P. Biochemical characterization and structural analysis of a new cold-active and salt-tolerant esterase from the marine bacterium *Thalassospira* sp. Extremophiles. 2016; 20: 323–336. doi: 10.1007/s00792-016-0824-z PMID: 27016194
19. Georlette D, Blaise V, Collins T, D'Amico S, Gratia E, Hoyoux A, et al. Some like it cold: biocatalysis at low temperatures. FEMS Microbiol Rev. 2004; 28: 25–42. doi: 10.1016/j.femsre.2003.07.003 PMID: 14975528
20. Struvay C, Feller G. Optimization to low temperature activity in psychrophilic enzymes. Int J Mol Sci. 2012; 13:11643–11665. doi: 10.3390/ijms130911643 PMID: 23109875
21. Santiago M, Ramírez-Sarmiento CA, Zamora RA, Parra LP. Discovery, molecular mechanisms, and industrial applications of cold-active enzymes. Front Microbiol. 2016; 7:1408–1439. doi: 10.3389/fmicb.2016.01408 PMID: 27667987
22. Lonhienne T, Gerday C, Feller G. Psychrophilic enzymes: revisiting the thermodynamic parameters of activation may explain local flexibility. Biochim Biophys Acta, Protein Struct Mol Enzymol. 2000; 1543: 1–10.

23. Luisa Tutino M, di Prisco G, Marino G, de Pascale D. Cold-adapted esterases and lipases: from fundamentals to application. Protein Pept Lett. 2009; 16:1172–1180. PMID: 19508185

24. Carneiro AR, Ramos RTJ, Dall'Agnol H, Pinto AC, de Castro Soares S, Santos AR, et al. Genome sequence of *Exiguobacterium antarcticum* B7, isolated from a biofilm in Ginger Lake, King George Island, Antarctica. J Bacteriol. 2012; 194(23):6689–90. doi: 10.1128/JB.01791-12 PMID: 23144424

25. Carboni-Oerlemans C, de Maria PD, Tuin B, Bargeman G, van Gemert R. Hydrolase-catalysed synthesis of peroxycarboxylic acids: Biocatalytic promiscuity for practical applications. J Biotechnol. 2006; 126: 140–151. doi: 10.1016/j.jbiotec.2006.04.008 PMID: 16730828

26. Bernhardt P, Hult K, Kazlauskas RJ. Molecular basis of perhydrolase activity in serine hydrolases. Angew Chem. 2005; 117: 2802–2806.

27. Yin DL, Bernhardt P, Morley KL, Jiang Y, Cheeseman JD, Purpero V, et al. Switching catalysis from hydrolysis to perhydrolysis in *Pseudomonas fluorescens* esterase. Biochemistry. 2010; 49: 1931–1942. doi: 10.1021/bi9021268 PMID: 20112920

28. Otwinowski Z, Minor W. Processing of X-ray diffraction data collected in oscillation mode. Macromol Crystallogr Part A. 1997; 276: 307–326.

29. Kantardjieff KA, Rupp B. Matthews coefficient probabilities: improved estimates for unit cell contents of proteins, DNA, and protein–nucleic acid complex crystals. Protein Sci. 2003; 12: 1865–1871. doi: 10.1110/ps.0350503 PMID: 12930986

30. Vagin A, Teplyakov A. MOLREP: an automated program for molecular replacement. J Appl Crystallogr. 1997; 30: 1022–1025.

31. Emsley P, Cowtan K. Coot: model-building tools for molecular graphics. Acta Crystallogr, Sect D: Biol Crystallogr. 2004; 60: 2126–2132.

32. Murshudov GN, Skubák P, Lebedev AA, Pannu NS, Steiner RA, Nicholls RA, et al. REFMAC5 for the refinement of macromolecular crystal structures. Acta Crystallogr, Sect D: Biol Crystallogr. 2011; 67: 355–367.

33. Schuck P. Size-distribution analysis of macromolecules by sedimentation velocity ultracentrifugation and lamm equation modeling. Biophys J. 2000; 78: 1606–1619. doi: 10.1016/S0006-3495(00)76713-0 PMID: 10692345

34. Schuck P, Rossmanith P. Determination of the sedimentation coefficient distribution by least-squares boundary modeling. Biopolymers. 2000; 54: 328–341. doi: 10.1002/1097-0282(20001015)54:5<328::AID-BIP40>3.0.CO;2-P PMID: 10935973

35. Yamada H, Itoh N, Murakami S, Izumi Y. New bromoperoxidase from coralline algae that brominates phenol compounds. Agric Biol Chem. 1985; 49: 2961–2967.

36. Holm L, Rosenström P. Dali server: conservation mapping in 3D. Nucleic Acids Res. 2010; 38(Suppl 2): W545–W549.

37. Hofmann B, Tölzer S, Pelletier I, Altenbuchner J, Van Pee K, Hecht H. Structural investigation of the cofactor-free chloroperoxidases. J Mol Biol. 1998; 279: 889–900. doi: 10.1006/jmbi.1998.1802 PMID: 9642069

38. Elmi F, Lee H-T, Huang J-Y, Hsieh Y-C, Wang Y-L, Chen Y-J, et al. Stereoselective esterase from *Pseudomonas putida* IFO12996 reveals α/β hydrolase folds for D-β-acetylthioisobutyric acid synthesis. J Bacteriol. 2005; 187: 8470–8476. doi: 10.1128/JB.187.24.8470-8476.2005 PMID: 16321951

crystals

MDPI

Communication

Identification and Crystallization of Penicillin-Binding Protein/β-Lactamase Homolog (Rp46) from *Ruegeria Pomeroyi*

Bum Han Ryu [1,2,†], Tri Duc Ngo [2,†], Wanki Yoo [1,2], Kyeong Kyu Kim [2,*] and T. Doohun Kim [1,*]

1 Department of Chemistry, College of Natural Science, Sookmyung Women's University, Seoul 04310, Korea; psryubh@skku.edu (B.H.R.); vlqkshqk61@skku.edu (W.Y.)

2 Department of Molecular Cell Biology, Samsung Biomedical Research Institute, Sungkyunkwan University School of Medicine, Suwon 16419, Korea; tringo@skku.edu

* Correspondence: kyeongkyu@skku.edu (K.K.K.); doohunkim@sookmyung.ac.kr (T.D.K.); Tel.: +82-31-299-6136 (K.K.K.); +82-2-2077-7806 (T.D.K.)

† These authors contributed equally to this work.

Academic Editor: Helmut Cölfen

Received: 23 November 2016; Accepted: 26 December 2016; Published: 29 December 2016

Abstract: In spite of the enormous biological and clinical significance of penicillin-binding protein (PBP)/β-lactamase (βL), few of their many homologs (PBP)/βLs homologs) have been studied crystallographically, and have known functions. Herein, X-ray crystallographic study of a PBP/βL homolog (Rp46) from *Ruegeria pomeroyi* is described. Multiple sequence alignments indicate that Rp46 has a conserved serine residue within the S^{70}-X-X-K^{73} motif (Motif I), acting as the catalytic nucleophile. Moreover, an invariant tyrosine residue (Tyr^{185}) and a Trp^{365}-X-Gly motif (Motif III) were also identified. The recombinant Rp46 protein was expressed in *Escherichia coli* and purified to homogeneity judging from the SDS-PAGE analysis. Rp46 was crystallized using a solution consisting of 20% (*w*/*v*) PEG 3000, 0.1 M Tris-HCl, pH 7.0, 0.2 M calcium acetate, and the X-ray diffraction data were collected to a resolution of 1.90 Å with an R_{merge} of 7.4%. The crystals of Rp46 belong to the space group *I*422, with unit cell parameters $a = b = 141.26$ Å, and $c = 119.75$. The structure determination and biochemical characterization are in progress. (Synopsis: A penicillin-binding protein/β-lactamase homolog (Rp46) from *Ruegeria pomeroyi* was identified and crystallized in the space group *I*4, and the diffraction data were collected to a resolution of 1.90 Å.)

Keywords: penicillin-binding protein; lactamase; protein crystal

1. Introduction

Bacterial penicillin-binding proteins (PBPs) and β-lactamases (βLs) form a large family of serine proteases [1,2]. These enzymes are characterized by phylogenetic analysis, primary sequences, functional properties, and structural similarities. Interestingly, this PBP/βL family has the nucleophilic serine located within a conserved S-X-X-K motif in the N-terminal region, although most bacterial hydrolases have a highly conserved catalytic motif of G-X-S-X-G in α/β-hydrolase fold [3,4]. To date, the bacterial PBP/βL family is composed of three classes including low-molecular-weight penicillin-binding proteins (class A to C), high-molecular-weight penicillin-binding proteins (class A to C), and β-lactamases (class A to D) [5–7]. Interestingly, several bacterial enzymes with similar active sites to PBP/βL proteins, namely PBP-βL homologs, were identified from bacterial organisms including *Klebsiella pneumoniae* [8], *Burkholderia gladioli* [9], *Arthrobacter nitroguajacolicus* [10], *Staphylococcus aureus* [11], *Marinobacter lipolyticus* [12], *Caulobacter crescentus* [13], and *Pseudomonas fluorescens* [14]. Furthermore, these PBP-βL homologs have also been identified from metagenomic

libraries [15–18]. Although physiological roles of these PBP-βL homolog proteins are largely unknown, some of them seem to be involved in the hydrolysis of diverse substrates including DD-peptides [19].

To date, a very limited number of crystal structures of PBP-βL homologs is known including an esterase (EstB) from *Burkholderia gladioli* [20], a simvastatin synthase (LovD) from *Aspergillus terreus* [21], a family VIII carboxylesterase (EstU1) [22], Est-Y29 from a metagenomic library [23], and a PBP-like esterase (CcEstA) [24]. Furthermore, the catalytic mechanisms and physiological functions of this enzyme family remain mainly unclear. In this study, we report the characterization, crystallization, and preliminary crystallographic analysis of a penicillin-binding protein/β-lactamase homolog (Rp46) from *Ruegeria pomeroyi*. *Ruegeria pomeroyi* is a heterotrophic marine organism essential for understanding the physiology and ecology of *Roseobacter* clade, which consists of ~20% of bacteria in coastal and ocean waters [25]. The crystal structure of Rp46 will provide molecular understanding on the catalytic mechanism and structural features of PBP/βL homologs.

2. Experimental Procedures

2.1. Cloning, Expression, and Purification of Rp46

The gene coding for Rp46 (GenBank I.D.: AAV95236) was amplified by Polymerase chain reaction (PCR) from the chromosomal DNA of *Ruegeria pomeroyi* (Microbank of Microbial Genomics and Application Center, Daejon, South Korea). The following primers were used: forward (5′-CAGGATCC ATGCCCGACCCCGGTTAC-3′; BamHI) and reverse (5′-CCAAGCTTCTAAGGAGTCCAAGCTCA-3′; HindIII). This amplification yielded a ~1.2 kb product, including the full length of Rp46 gene. The PCR product was inserted into the pQE30 vector (Qiagen, Hilden, Germany), and the recombinant plasmid (pQE30-Rp46) was used to express the recombinant protein with an N-terminal His-tag (MRGSHHHHHHGS) in *Escherichia coli* XL1-Blue (Stratagene, La Jolla, CA, USA). After DNA sequencing, transformed *E. coli* were grown in an LB medium containing 100 μg/mL of ampicillin at 310 K and 0.1 mM isopropyl-β-D-1-thiogalactoside (IPTG) for the overexpression of Rp46 protein when the OD_{600} reached 0.5. The bacterial culture was grown at 310 K for 4.5 h before centrifugation at 5000 rpm for 20 min at 277 K. The cell pellet was then resuspended in a lysis buffer (50 mM sodium phosphate, pH 8.0, 300 mM NaCl, and 10 mM imidazole), followed by sonication. The cell lysate was centrifuged at 15,000 rpm for 20 min, and the supernatant was filtered through a 0.22 μm syringe filter. The supernatants were applied to a Ni-NTA affinity column in an AKTA prime plus system (GE healthcare, Piscataway, NJ, USA), which was previously equilibrated with lysis buffer. After an extensive washing step with lysis buffer containing 40 mM imidazole, the bound Rp46 protein was eluted with elution buffer (50 mM sodium phosphate, pH 8.0, 300 mM NaCl, and 250 mM imidazole). The fractions of the purified Rp46 were desalted on a PD-10 column (GE healthcare, Piscataway, NJ, USA) using phosphate-buffered saline (PBS) pH 7.4. The purity of Rp46 was confirmed by SDS-PAGE and the concentration was determined using a Bio-Rad assay kit (Bio-Rad Laboratories, Hercules, CA, USA). The purified protein was concentrated to 5 mg/mL using Vivaspin concentrators (Vivascience, Westford, MA, USA). The final sample was stored at 253 K without further modification.

2.2. Biochemical Characterization

To identify the hydrolytic activity of Rp46, overlay assay using 4-methylumbelliferyl acetate (4-MU acetate) was performed [26,27]. At first, native-PAGE was performed, followed by staining with Coomassie Brilliant Blue (R-250) to confirm the position of the intact Rp46. Next, the gel was washed with double distilled water for 15 min and next immersed several times in 50 mM sodium phosphate buffer, pH 7.0. Afterwards, 250 μM 4-MU acetate was added as the substrate. The activity of Rp46 was estimated under UV illumination by measuring the fluorescence generated by the enzyme product 4-methylumbelliferone.

2.3. Crystallization

Crystallization trials of Rp46 were performed by the microbatch method [28] under AI's oil using commercial screening kits Wizard I and II crystallization screening solutions (Emerald BioSystems, Bainbridge Island, WA, USA) at 298 K. A drop (1 µL screening solution and 1 µL protein solution) was placed into each well of a Nunc 96-well Mini Tray (Nalge Nunc International, New York, NY, USA). A single crystal grown from the condition of Wizard II No. 18 [20% (*w*/*v*) PEG 3000, 0.1 M Tris-HCl, pH 7.0, 0.2 M calcium acetate] was used for X-ray diffraction analysis.

2.4. X-ray Data Collection and Data Processing

The Rp46 crystals were then transferred to a cryosolution consisting of the screening solution supplemented with 25% glycerol and flash-frozen in a cold nitrogen gas stream at 100 K prior to data collection. High quality diffraction data were collected using an ADSC Quantum 315 CCD detector (Beamline PAL 4A, Pohang Accelerator Laboratory, Pohang, Korea) at 100 K. The wavelength of the synchrotron X-rays was 1.000 Å and the crystal-to-detector distance was 220 mm. The crystal was rotated through a total of 180° with 0.5° oscillation range at an exposure time of 3 s per frame. The data were processed using the HKL2000 package [29]. The data collection and processing statistics are listed in the Table 1.

Table 1. X-ray data collection and processing statistics values in parentheses are for the highest resolution shell.

Space Group	I422
Unit cell parameters (Å)	$a = b = 141.26$, $c = 119.75$
Wavelength (Å)	1.000
Resolution (Å)	50.00–1.90 (1.93–1.90)
Unique reflections	92,068 (4589)
Completeness (%)	99.9 (100)
Redundancy	7.6 (7.2)
R_{merge} [1] (%)	7.4 (34.5)
Mean I/σ (I)	44.1 (7.0)

[1] $R_{merge} = \sum_{hkl} |I - \langle I \rangle| / \sum_{hkl} I$

3. Results and Discussion

Rp46 consists of a single 411-amino-acid polypeptide chain with a pI of 5.63. Sequence similarities to Rp46 were annotated mostly as β-lactamases or penicillin-binding proteins (PBPs) in the Conserved Domain Search database (CD search) [30]. Multiple sequence alignments of Rp46 with four sequentially-related hydrolases in the Protein Data Bank (PDB) database [31] indicate that they share the sequence motifs essential for their functionality with low sequence identities (Figure 1). Specifically, Rp46 showed significant sequence identity with EstB from *Burkholderia gladioli* (1CI8, 29.4%), EstU1 from a metagenomic library (4IVI, 32.5%), and Est-Y29 from a metagenomic library (4P6B, 30.1%) (Figure 1). Three highly conserved motifs (Motifs I, II, and III) including the S-X-X-K motif have been previously identified in low-molecular-weight class B penicillin-binding proteins or class C β-lactamases (Figure 2). Rp46 also presents these conserved motifs, indicating that Rp46 shares common structural features with these proteins. In these proteins, a Ser residue (Ser^{70} in Rp46) and a Lys residue (Lys^{73} in Rp46) from the S-X-X-K motif act as a nucleophile and a general base, and both of them are involved in the formation of oxyanion holes at the active site [32]. The hydroxyl group of tyrosine (Tyr^{185} in Rp46) in Motif II is essential for acylation steps [3,33].

Interestingly, there are sequence variations in Motif III among these proteins. In class C β-lactamases, the triad Lys-Thr-Gly is found in the center of Motif III, whereas His-Xaa-Gly is observed in low Molecular weight (MW) class B PBPs [2,3,34]. Therefore, Motif III, unlike the other two motifs, is not highly conserved between low MW class B PBPs and class C β-lactamases. Moreover, Rp46, in common with EstB, EstU1, LovD, and Est-Y29, presents a Trp residue (Trp^{365}) in Motif III, whereas this position is occupied by a His residue in low MW class B PBPs or a Lys residue in class C β-lactamases (Figure 2). Collectively, only a glycine (Gly^{367} in Rp46) in Motif III among these proteins is strictly conserved. It is interesting to speculate that the sequence differences of Motif III among these proteins could be related to biological functions of this protein family.

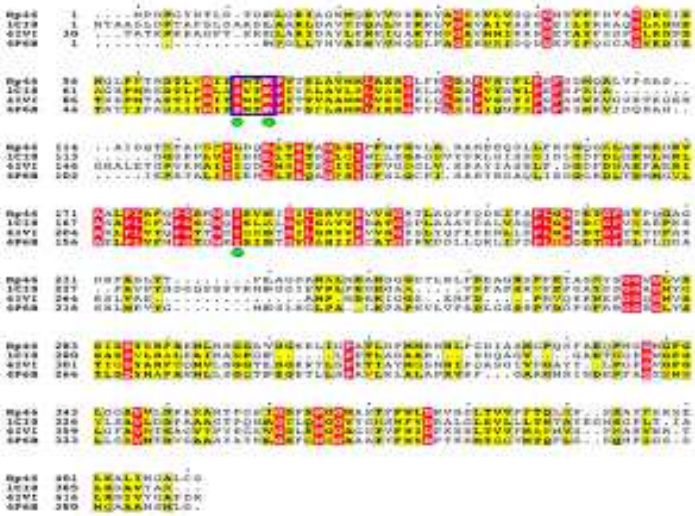

Figure 1. Multiple sequence alignment including Rp46 and three related hydrolases found in the PDB database [31] (1C18: EstB from *B. gladioli* [20]; 4IV1: Family VIII carboxylesterase from uncultured bacterium [22]; 4P6B: PBP-βL homolog from uncultured bacterium [23]). Sequences retrieved from the NCBI server were aligned with *CLUSTAL O* [35], and the output was rendered using ESPript [36]. Identical and highly conserved residues are shown in red and yellow boxes, respectively. The three catalytic residues (Ser, Lys, and Tyr) are labeled with a green circle.

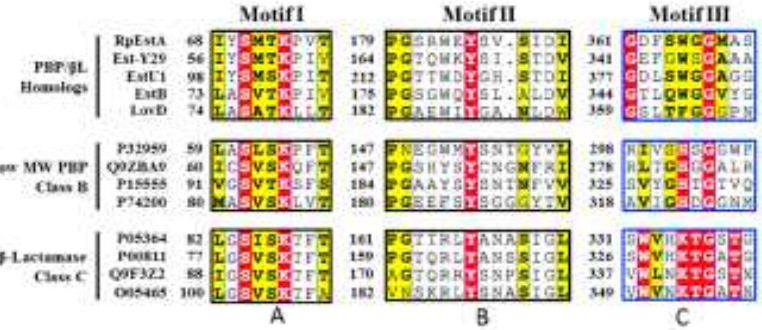

Figure 2. Motifs I, II, and III belonging to PBP-βL homologs, low-molecular-weight class B PBPs, and class C β-Lactamase. Completely conserved residues are shown in red and highly conserved residues are shown in yellow. Note that the catalytic residues of Motifs I and II are highly conserved compared to those of Motif III.

The recombinant Rp46 with an N-terminal His-tag was expressed in *Escherichia coli* and purified to electrophoretic homogeneity for crystallization (Figure 2A). As shown in Figure 3A, the molecular mass of the Rp46 was estimated to be 46 kDa (Figure 2C), which was consistent with the calculated molecular mass (45.98 kDa). The biochemical activity of Rp46 was confirmed on a native Polyacrylamide Gel Electrophoresis (PAGE) gel by zymogram analysis in the presence of 4-MU acetate (Figure 2B).

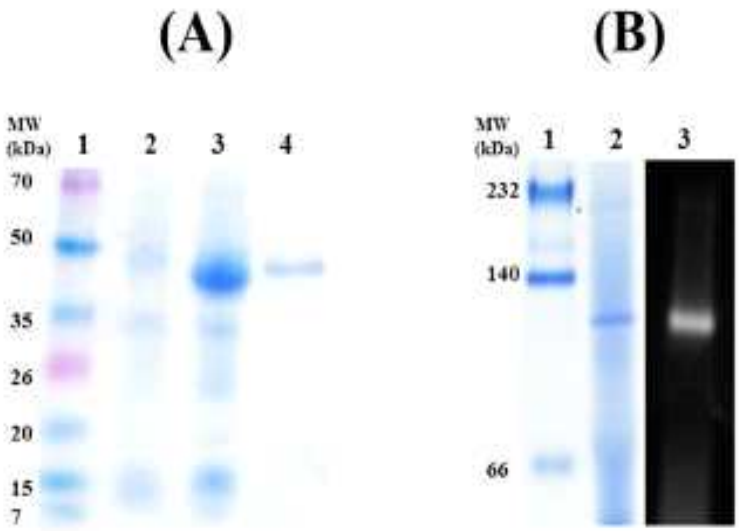

Figure 3. SDS-PAGE and zymography of Rp46. (**A**) SDS-PAGE analysis of protein samples during purification. From left to right, molecular weight markers (1), *E. coli* crude extracts before (2) and after IPTG induction (3), and purified Rp46 (4). (**B**) Zymographic analysis of Rp46. Molecular weight markers (1), Coomassie Brilliant Blue staining after Native-PAGE (2), and overlay activity assay with 4-MU acetate after Native-PAGE (3).

A diffraction-quality crystal of tetragonal shape was obtained under Wizard II-18 condition [20% (*w*/*v*) PEG 3000, 0.1 M Tris-HCl, pH 7.0, 0.2 M calcium acetate] within two weeks, and grew to final dimensions of 0.3 × 0.3 × 0.2 mm^3 (Figure 4). The crystals belonged to the space group *I*4 with unit cell parameters $a = b = 141.26$ Å, and $c = 119.75$ Å. The diffraction data set was processed to 1.90 Å resolution with 99.9% completeness, and R_{merge} value of 7.4%. The data collection statistics are listed in Table 1. Assuming the presence of one molecule per asymmetric unit, Matthews coefficient (V_M) is calculated to be 3.12 $Å^3$/Da. This V_M value is within the range commonly observed for protein crystals, and corresponds to 60.6% solvent content [37]. The structure of Rp46 was searched by molecular replacement using Phenix Phaser-MR [38]. The crystal structure of recently-solved Est-Y29 (PDB ID 4P6B), which has 30.1% sequence identity to Rp46, was used as the search model. The best solution generated by Phaser-MR has LLG = 190.0. Early refinement of this solution by Phenix gives R_{work}/R_{free} = 22.5%/24.9%, indicating the solution is correct. However, manual model building and further refinement are still needed for structural analyses. The biochemical characterization of Rp46 is under progress, and structural and functional studies will elucidate the substrate specificity and the catalytic mechanism of Rp46 in the near future.

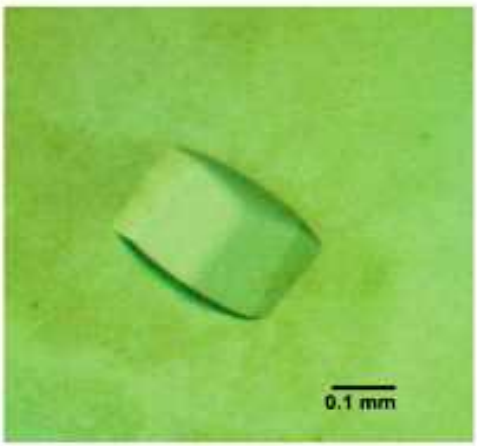

Figure 4. Rp46 crystal was obtained using Wizard II condition No. 18 [20% (*w*/*v*) PEG 3000, 100 mM Tris-HCl, pH 7.0, 200 mM calcium acetate]. The crystal dimensions were 0.3 × 0.3 × 0.2 mm. The scale bar represents 0.1 mm.

Acknowledgments: This work was supported by the Sookmyung Women's University Research Grant (1-1503-0020). This work was also supported by the Polar Academic Program (PD15010) of the Korea Polar Research Institute (KOPRI) to T. Doohun Kim.

Author Contributions: Bum Han Ryu and T. Doohun Kim identified the gene from the chromosome of *Ruegeria pomeroyi*. Bum Han Ryu, Tri Duc Ngo, and Kyeong Kyu Kim overexpressed and crystallized the protein. The protein was biochemically characterized by Bum Han Ryu, Wanki Yoo, and Tri Duc Ngo. T. Doohun Kim and Kyeong Kyu Kim coordinated the project and wrote the manuscript. All authors reviewed the results and approved the final version of the manuscript.

Conflicts of Interest: The authors declare no competing financial interests.

References

1. Macheboeuf, P.; Contreras-Martel, C.; Job, V.; Dideberg, O.; Dessen, A. Penicillin binding proteins: Key players in bacterial cell cycle and drug resistance processes. *FEMS Microbiol. Rev.* **2006**, *30*, 673–691. [CrossRef] [PubMed]
2. Zapun, A.; Contreras-Martel, C.; Vernet, T. Penicillin-binding proteins and beta-lactam resistance. *FEMS Microbiol. Rev.* **2008**, *32*, 361–385. [CrossRef] [PubMed]
3. Sauvage, E.; Kerff, F.; Terrak, M.; Ayala, J.A.; Charlier, P. The penicillin-binding proteins: Structure and role in peptidoglycan biosynthesis. *FEMS Microbiol. Rev.* **2008**, *32*, 234–258. [CrossRef] [PubMed]
4. Carr, P.D.; Ollis, D.L. α/β Hydrolase Fold: An Update. *Protein Pept. Lett.* **2009**, *16*, 1137–1148. [PubMed]
5. Pérez-Llarena, F.J.; Bou, G. Design and Synthesis of Mimics of the T7-loop of FtsZ. *Curr. Med. Chem.* **2009**, *16*, 3740–3765. [PubMed]
6. Meroueh, S.O.; Minasov, G.; Lee, W.; Shoichet, B.K.; Mobashery, S. Structural Aspects for Evolution of β-Lactamases from Penicillin-Binding Proteins. *J. Am. Chem. Soc.* **2003**, *125*, 9612–9618. [CrossRef] [PubMed]
7. Hall, B.G.; Barlow, M. Structure-based phylogenies of the serine beta-lactamases. *J. Mol. Evol.* **2003**, *57*, 255–260. [CrossRef] [PubMed]
8. Bauernfeind, A.; Schneider, I.; Jungwirth, R.; Sahly, H.; Ullmann, U. A Novel Type of AmpC β-Lactamase, ACC-1, Produced by a *Klebsiella pneumoniae* Strain Causing Nosocomial Pneumonia. *Antimicrob. Agents Chemother.* **1999**, *43*, 1924–1931. [PubMed]
9. Petersen, E.I.; Valinger, G.; Sölkner, B.; Stubenrauch, G.; Schwab, H. A novel esterase from *Burkholderia gladioli* which shows high deacetylation activity on cephalosporins is related to beta-lactamases and DD-peptidases. *J. Biotechnol.* **2001**, *89*, 11–25. [CrossRef]
10. Schütte, M.; Fetzner, S. EstA from *Arthrobacter nitroguajacolicus* Rü61a, a thermo- and solvent-tolerant carboxylesterase related to class C beta-lactamases. *Curr. Microbiol.* **2007**, *54*, 230–236. [CrossRef] [PubMed]

11. Fan, X.; Liu, Y.; Smith, D.; Konermann, L.; Siu, K.W.; Golemi-Kotra, D. Diversity of penicillin-binding proteins. Resistance factor FmtA of *Staphylococcus aureus*. *J. Biol. Chem.* **2007**, *282*, 35143–35152. [CrossRef] [PubMed]
12. Pérez, D.; Kovacic, F.; Wilhelm, S.; Jaeger, K.E.; García, M.T.; Ventosa, A.; Mellado, E. Identification of Amino Acids Involved in the Hydrolytic Activity of Lipase LipBL From Marinobacter Lipolyticus. *Microbiology* **2012**, *158*, 2192–2203. [CrossRef] [PubMed]
13. Ryu, B.H.; Ngo, T.D.; Jang, E.; Kim, S.; Ju, H.; Kim, K.K.; Kim, T.D. Identification, crystallization and preliminary X-ray diffraction analysis of esterase A from *Caulobacter crescentus* CB15, a family VIII lipolytic enzyme. *Acta Crystallogr. Sect. F Struct. Biol. Cryst. Commun.* **2012**, *68*, 560–564. [CrossRef] [PubMed]
14. Kim, S.; Ngo, T.D.; Kim, K.K.; Kim, T.D. Characterization, crystallization and preliminary X-ray diffraction analysis of an (*S*)-specific esterase (*pf* EstA) from *Pseudomonas fluorescens* KCTC 1767: Enantioselectivity for potential industrial applications. *Acta Crystallogr. Sect. F Struct. Biol. Cryst. Commun.* **2012**, *68*, 1374–1377. [CrossRef] [PubMed]
15. Yoon, S.; Kim, S.; Ryu, Y.; Kim, T.D. Identification and characterization of a novel (*S*)-ketoprofen-specific esterase. *Int. J. Biol. Macromol.* **2007**, *41*, 1–7. [CrossRef] [PubMed]
16. Rashamuse, K.; Magomani, V.; Ronneburg, T.; Brady, D. A novel family VIII carboxylesterase derived from a leachate metagenome library exhibits promiscuous beta-lactamase activity on nitrocefin. *Appl. Microbiol. Biotechnol.* **2009**, *83*, 491–500. [CrossRef] [PubMed]
17. Jeon, J.H.; Kim, S.J.; Lee, H.S.; Cha, S.S.; Lee, J.H.; Yoon, S.H.; Koo, B.S.; Lee, C.M.; Choi, S.H.; Lee, S.H.; et al. Novel Metagenome-Derived Carboxylesterase That Hydrolyzes β-Lactam Antibiotics. *Appl. Environ. Microbiol.* **2011**, *77*, 7830–7836. [CrossRef] [PubMed]
18. Mokoena, N.; Mathiba, K.; Tsekoa, T.; Steenkamp, P.; Rashamuse, K. Functional Characterisation of a Metagenome Derived Family VIII Esterase with a Deacetylation Activity on β-Lactam Antibiotics. *Biochem. Biophys. Res. Commun.* **2013**, *437*, 342–348. [CrossRef] [PubMed]
19. Pratt, R.F. β-Lactamases: Why and How. *J. Med. Chem.* **2016**, *59*, 8207–8220. [CrossRef] [PubMed]
20. Wagner, U.G.; Petersen, E.I.; Schwab, H.; Kratky, C. EstB from *Burkholderia gladioli*: A novel esterase with a β-lactamase fold reveals steric factors to discriminate between esterolytic and β-lactam cleaving activity. *Protein Sci.* **2002**, *11*, 467–478. [CrossRef] [PubMed]
21. Gao, X.; Xie, X.; Pashkov, I.; Sawaya, M.R.; Laidman, J.; Zhang, W.; Cacho, R.; Yeates, T.O.; Tang, Y. Directed evolution and structural characterization of a simvastatin synthase. *Chem. Biol.* **2009**, *16*, 1064–1074. [CrossRef] [PubMed]
22. Cha, S.S.; An, Y.J.; Jeong, C.S.; Kim, M.K.; Jeon, J.H.; Lee, C.M.; Lee, H.S.; Kang, S.G.; Lee, J.H. Structural basis for the β-lactamase activity of EstU1, a family VIII carboxylesterase. *Proteins* **2013**, *81*, 2045–2051. [CrossRef] [PubMed]
23. Ngo, T.D.; Ryu, B.H.; Ju, H.; Jang, E.J.; Kim, K.K.; Kim, T.D. Crystallographic analysis and biochemical applications of a novel penicillin-binding protein/β-lactamase homologue from a metagenomic library. *Acta Crystallogr. D Biol. Crystallogr.* **2014**, *70*, 2455–2466. [CrossRef] [PubMed]
24. Ryu, B.H.; Ngo, T.D.; Yoo, W.; Lee, S.; Kim, B.Y.; Lee, E.; Kim, K.K.; Kim, T.D. Biochemical and Structural Analysis of a Novel Esterase from *Caulobacter crescentus* related to Penicillin-Binding Protein (PBP). *Sci. Rep.* **2016**, *6*, 37978. [CrossRef] [PubMed]
25. Buchan, A.; Gonzalez, J.M.; Moran, M.A. Overview of the Marine *Roseobacter* Lineage. *Appl. Environ. Microbiol.* **2005**, *71*, 5665–5677. [CrossRef] [PubMed]
26. Ju, H.; Ryu, B.H.; Kim, T.D. Identification, characterization, immobilization of a novel type hydrolase (LmH) from *Listeria monocytogenes*. *Int. J. Biol. Macromol.* **2015**, *72*, 63–70. [CrossRef] [PubMed]
27. Jang, E.; Ryu, B.H.; Shim, H.W.; Ju, H.; Kim, D.W.; Kim, T.D. Adsorption of microbial esterases on *Bacillus subtilis*-templated cobalt oxide nanoparticles. *Int. J. Biol. Macromol.* **2014**, *65*, 188–192. [CrossRef] [PubMed]
28. Chayen, N.E.; Shaw Steward, P.D.; Maeder, D.L.; Blow, D.M. An automated system for micro-batch protein crystallization and screening. *J. Appl. Cryst.* **1990**, *23*, 297–302. [CrossRef]
29. Otwinowski, Z.; Minor, W. Processing of X-ray Diffraction Data Collected in Oscillation Mode. *Methods Enzymol.* **1997**, *276*, 307–326. [PubMed]
30. Marchler-Bauer, A.; Bryant, S.H. CD-Search: Protein domain annotations on the fly. *Nucleic Acids Res.* **2004**, *32*, 327–331. [CrossRef] [PubMed]

31. Berman, H.M.; Henrick, K.; Nakamura, H. Announcing the worldwide Protein Data Bank. *Nat. Struct. Biol.* **2003**, *10*, 980. [CrossRef] [PubMed]
32. Frère, J.M.; Page, M.G. Penicillin-binding proteins: Evergreen drug targets. *Curr. Opin. Pharmacol.* **2014**, *18*, 112–119. [CrossRef] [PubMed]
33. Silvaggi, N.R.; Anderson, J.W.; Brinsmade, S.R.; Pratt, R.F.; Kelly, J.A. The crystal structure of phosphonate-inhibited D-Ala-D-Ala peptidase reveals an analogue of a tetrahedral transition state. *Biochemistry* **2003**, *42*, 1199–1208. [CrossRef] [PubMed]
34. Peltsaro, N.; Poliansky te, Z.; Tuimala, J.; Pörn-Ares, I.; Liobikas, J.; Speer, O.; Lindholm, D.; Thompson, J.; Eriksson, O. Evolution of a family of metazoan active-site-serine enzymes from penicillin-binding proteins: A novel facet of the bacterial legacy. *BMC Evol. Biol.* **2008**, *8*, 26. [CrossRef] [PubMed]
35. Sievers, F.; Wilm, A.; Dineen, D.; Gibson, T.J.; Karplus, K.; Li, W.; Lopez, R.; McWilliam, H.; Remmert, M.; Söding, J.; et al. Fast, scalable generation of high-quality protein multiple sequence alignments using Clustal Omega. *Mol. Syst. Biol.* **2011**, *7*, 539. [CrossRef] [PubMed]
36. Gouet, P.; Robert, X.; Courcelle, E. ESPript/ENDscript: Extracting and rendering sequence and 3D information from atomic structures of proteins. *Nucleic Acids Res.* **2003**, *31*, 3320–3323. [CrossRef] [PubMed]
37. Matthews, B.W. Solvent content of protein crystals. *J. Mol. Biol.* **1968**, *33*, 491–497. [CrossRef]
38. Adams, P.D.; Afonine, P.V.; Bunkoczi, G.; Chen, V.B.; Davis, I.W.; Echols, N.; Headd, J.J.; Hung, L.W.; Kapral, G.J.; Grosse-Kunstleve, R.W.; et al. *PHENIX*: A comprehensive Python-based system for macromolecular structure solution. *Acta Crystallogr. D Biol. Crystallogr.* **2010**, *66*, 213–221. [CrossRef] [PubMed]

주 의

1. 이 보고서는 극지연구소 PAP사업 연구결과 보고서입니다.
2. 이 보고서 내용을 발표할 때에는 반드시 극지연구소에서 PAP 사업으로 수행한 연구결과임을 밝혀야 합니다.
3. 국가과학기술 기밀유지에 필요한 내용은 대외적으로 발표 또는 공개하여서는 안됩니다.